DESIGN AND CONTROL OF ROBOTIC SYSTEMS FOR UPPER EXTREMITY REHABILITATION FOLLOWING STROKE

By

Furui Wang

Dissertation

Submitted to the Faculty of the

Graduate School of Vanderbilt University

in partial fulfillment of the requirements

for the degree of

DOCTOR OF PHILOSOPHY

in

Mechanical Engineering

December, 2011

Nashville, Tennessee

Approved:

Dr. Nilanjan Sarkar

Dr. Derek Kamper

Dr. George Cook

Dr. Michael Goldfarb

Dr. Robert Webster

ACKNOWLEDGEMENTS

I would like to express sincere appreciation to my advisor, Dr. Nilanjan Sarkar. I would like to thank him for his invaluable support and continuous guidance. Without his advice and encouragement, this work will never happen. I would also like to thank my co-advisor, Dr. Derek Kamper. He is always willing to share his knowledge in biomedical field. His insights in stroke rehabilitation gave me lots of inspirations in my project.

I would like to express my appreciation to my committee members Dr. George E. Cook, Dr. Michael Goldfarb and Dr. Robert Webster for their helpful suggestions and comments, which guided and challenged my thinking, substantially improving this work.

I would like to thank my collaborators in the exoskeleton project, Christopher Jones, Milind Shastri and Vikash Gupta. Our good collaboration makes this challenging project more interesting. I enjoyed working with all of them.

I am grateful to be a member of the Robotics and Autonomous Systems Laboratory. I would like to thank Yu Tian, Jadav Das, Duygun Erol Barkana, Changchun Liu, Esubalew Bekele and other members in RASL for their kindly help and support. People in RASL are always willing to help each other when needed.

My deepest gratitude, appreciation, and thanks go to my mom and my dad. Thanks for their belief in me all the time, for their understanding and encouragement from far away. Without their boundless love and encouragement, I would never have come to this point in my career. I would like to give my very special thanks to my soul mate, Jia Bai, for her invaluable support, continuous encouragement and patience throughout these years. She is the motivation and inspiration of my research and life.

TABLE OF CONTENTS

Page

LIST OF TABLES

LIST OF FIGURES

CHAPTER I

INTRODUCTION

The purpose of this research work is to explore how to improve robot-assisted rehabilitation of upper extremity impairment following stroke. The background, literature survey, scope and summary of current research work will be presented in this chapter.

Stroke & Stroke Rehabilitation

Upper extremity impairment is a prevalent outcome for a variety of neuromuscular disorders, such as stroke. According to the American Stroke Association, each year about 795,000 Americans experience a new or recurrent stroke; i.e., every 40 seconds in the United States, someone suffers a stroke [1]. 60-75% of these patients will live beyond one year after the incidence, resulting in an estimated stroke population of 7 million [1-3]. Arm function is acutely impaired in a large majority of those diagnosed with stroke [4-6]. Furthermore, acute hemiparesis presages chronic hemiparesis in over 40% of individuals [5, 6] suffering from stroke. Chronic deficits are prevalent in the distal upper extremities, especially with regard to finger extension [7]. Anything that could help patients regain useful functions of upper limbs, help with activities of daily living, and make them more independent, would be useful.

Clinical results have indicated that movement assisted therapy can have a significant beneficial impact on a large segment of the population affected by stroke. In recent years, new techniques adopting a task-oriented approach have been developed to encourage

active training of the affected limb, which assume that control of movement is organized around goal-directed functional tasks [8, 9]. “Shaping” is one of the task oriented behavioral training techniques employed in Constraint-Induced Movement (CI) therapy [8-10], which has the effect of placing optimal adaptive task practice procedures into a systematic, standardized and quantified format. The availability of such training techniques, however, is limited by the amount of costly therapist’s time they involve, and the ability of the therapist to provide controlled, quantifiable and repeatable assistance to complex arm and hand motion.

Consequently, robot assisted rehabilitation could be used to automate labor-intensive training technique, to provide programmable levels of assistance to the patients, and to quantitatively monitor and adapt to the patient’s progress during rehabilitation.

State-of-the-Art in Robotic Systems and Devices for Upper Extremity Rehabilitation

Robot-assisted physical rehabilitation has been an active research area for the last few years to assist, enhance and quantify rehabilitation. The robot-assisted therapies provide autonomous training where patients are engaged in repeated and intense practice of goal-directed tasks leading to improvements in motor function. Rehabilitation robotic devices and systems are being developed to automate therapy for the arm, wrist and hand following stroke. The MIT-Manus (Massachusetts Institute of Technology Manus) [11, 12] (Figure I-1.a), Assisted Rehabilitation and Measurement (ARM) Guide [13, 14] (Figure I-1.b), Mirror Image Movement Enabler (MIME) [15-17] (Figure I-1.c) and GENTLE/s [18] (Figure I-1.d) are developed to facilitate the arm movement of stroke patients. Robotic devices designed for wrist rehabilitation have been reported in [19-21].

New rehabilitation therapy environments are developed to permit the training of real-life functional tasks involving reaching and grasping [22]. In recent years, a number of devices have been developed expressly for or applied to hand rehabilitation. These include both commercial products, such as CyberGrasp (Immersion Corporation, San Jose, CA) [23], the Hand Mentor (Kinetic Muscles Inc., Tempe, AZ) [24], and the Amadeo Hand System (Tyromotion GmbH, Graz, Austria) [25]. Experimental devices include Rutgers Master II-ND [26], HWARD [27], and HandCARE [28], among others [29-31].

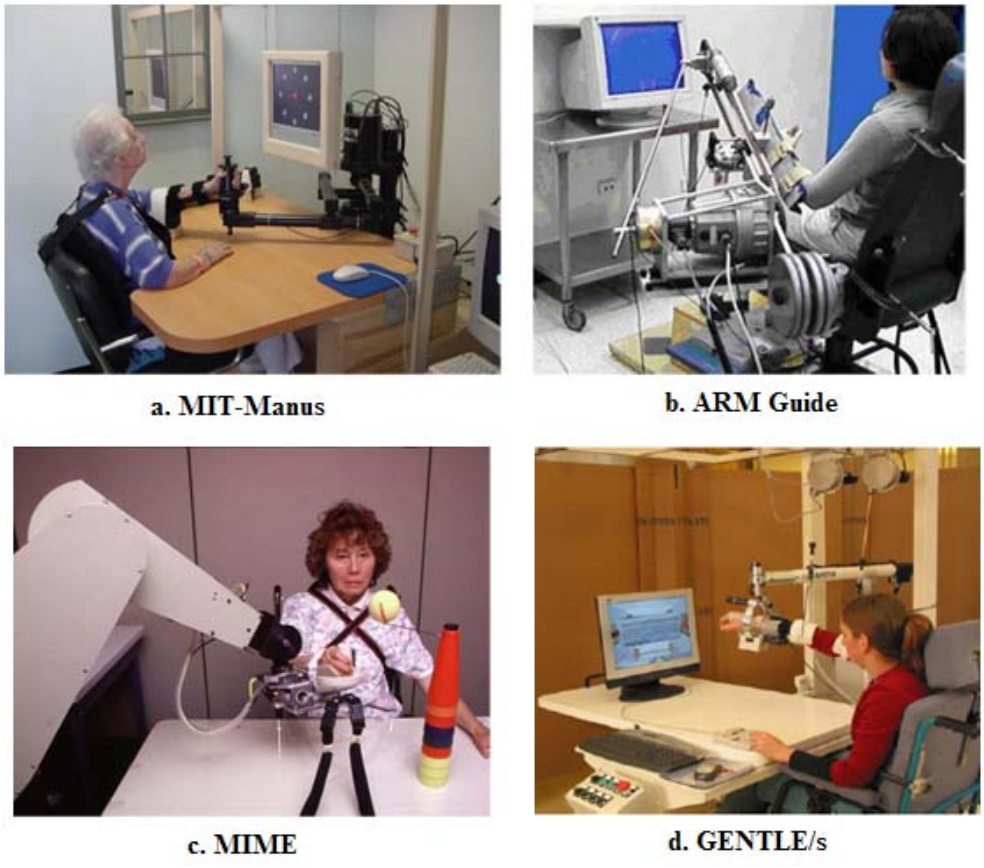

a. MIT-Manus b. ARM Guide

c. MIME d. GENTLE/s

Figure I-1 Robotic Systems for Arm Rehabilitation

The CyberGrasp [23] is a commercial hand assistive device which is built to provide extension forces to the tips of the fingers and the thumb for grasping (Figure I-2). However, this device cannot provide flexion forces. The CyberGrasp is developed as part of a CyberGlove for interactions with virtual environments, and has been successfully used in medical applications and remote handling of hazardous materials.

Figure I-2 CyberGrasp

The Hand Mentor [24] (Figure I-3) is an exercise therapy device that encourages the patient to extend their wrist and fingers as much as possible on their own. When maximum self extension is achieved the Mentor engages a pneumatic actuator and assists the movement of the wrist and fingers to full extension. In addition to recruitment of hand function, the Mentor actively stretches the hand in an effort to reduce spasticity.

Figure I-3 Hand Mentor

The Amadeo Hand System [25] (Figure I-4) is the only mechatronic finger rehabilitation device available on the market that allows each individual finger, including the thumb, to move independently and separately (Figure I-4). It moves the fingers and thumb according to a given pattern determined by the software. The finger carriages can be adjusted to make either a consecutive or simultaneous movement of flexion and extension.

Figure I-4 The Amadeo Hand System

The Rutgers Master II-ND (Figure I-5) is one of the hand assistive devices designed for dexterous interactions with virtual environments [26] developed at Rutgers University in New Jersey. It has a unique design to actuate the tips of three fingers as well as the thumb (Figure I-5) and uses custom-made pneumatic cylinders to push the fingertips out from the palm. The Rutgers Master II-ND is an example of a lightweight and palm-mounted finger manipulator. It is still not clear whether it is possible to pull the fingers in toward the palm.

Figure I-5 The Rutgers Master II-ND

The Hand-Wrist Assisting Robotic Device (HWARD), shown in Figure I-6, has been developed to assist repetitive grasping and releasing movements while allowing the patient to feel real objects during therapy [27]. HWARD is a pneumatically-actuated back-drivable robotic device with 3 degrees-of-freedom (DOF).

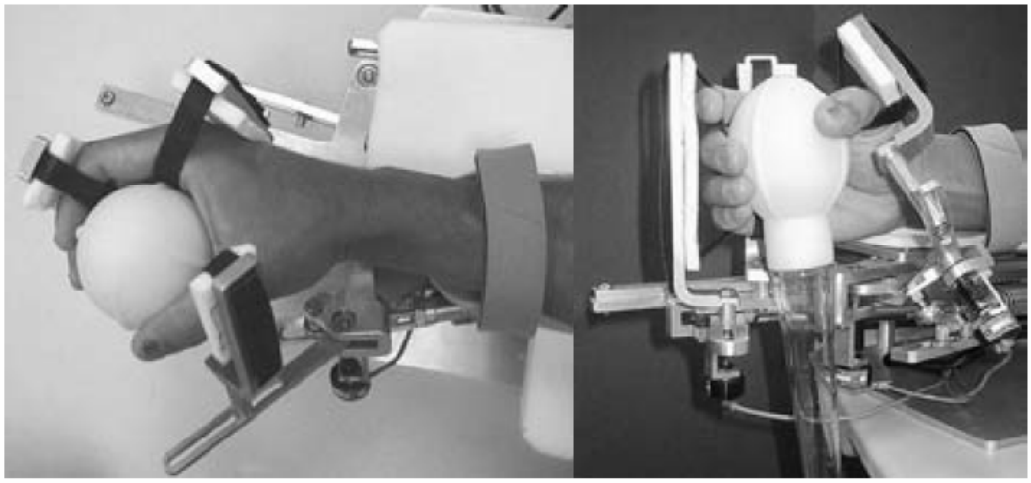

Figure I-6 The HWARD

The HandCARE [28] is a cable-actuated rehabilitation system (Figure I-7), in which each finger is attached to an instrumented cable loop allowing force control and a predominantly linear displacement. This device can assist the subject in both opening and closing movements. Main features of the interface include a differential sensing system, and a clutch system which allows independent movement of the five fingers with only one actuator.

Figure I-7 The HandCARE System

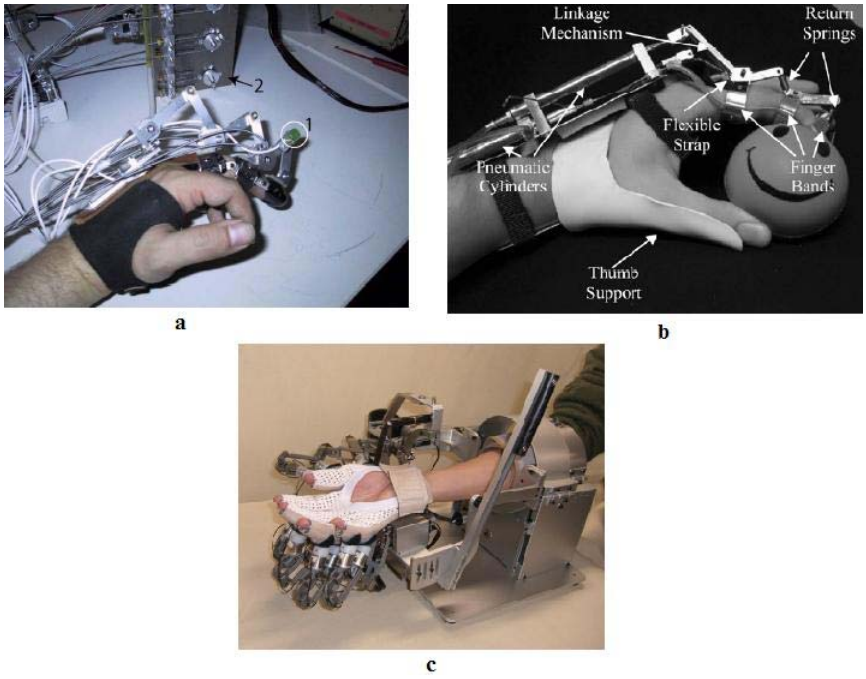

Figure I-8 Other Hand Devices

State-of-the-Art in Robot-Assisted Rehabilitation Strategies

There are significant research activities in the development of new methodologies for robot-assisted rehabilitation in the last few years. The promising results of the above-

mentioned rehabilitation robotic systems indicate that the robots could be used as effective rehabilitation tools. Those with the most success to date tend to focus on intense and repetitive practice of the affected limb with cognitive processing as a means for motor program reorganization, during which patients not only make repetitive movement but also pay attention to tracking accuracy. However, the patients may not be able to track the desired motion because of their impairments during the task execution. Thus robotic assistance is provided to help the patients complete the task in different manners.

Several strategies for robot-assisted rehabilitation therapies have been developed, including passive [32, 33], active-assistance [13, 14, 19, 32-35], active-constrained [33], counterpoise control [36], resistive [35], error-amplifying [36-39], and bimanual modes [33, 40, 41] . Of these strategies, the primary therapy strategies tested so far is **active assistance** [13, 14, 19, 32-35], a clinical term that refers to exercises in which the patient attempts a movement (**active**) and in which a therapist manually helps complete the movement if the patient is unable (**assistance**) [42]. Such active assistance may improve recovery by enhancing proprioceptive input, reducing spasticity, restoring soft tissue suppleness, improving self-confidence, or by simply making exercise psychologically more tolerable, but it is labor intensive and time consuming. It was a logical target when engineers and clinicians were presented with weak patients and force-generating robots. Meanwhile, it has been suggested that in robot-assisted rehabilitation, assisting every movement of a patient is not as beneficial compared to assistance as needed [43]. Performance-based therapies have showed better results in improving patients' impairment scores than conventional therapies [13, 14, 44]. Thus, a robot-assisted rehabilitation system could be more efficient if the robotic assistance provided to the

patient is given as and when needed based on the performance of the patient, which is called **assist-as-needed** training in this manuscript.

Meanwhile, recent research has demonstrated that movement tracking training that requires cognitive processing achieved greater gains in performance than that of movement training that did not require cognitive processing [45]. Moreover, recent research in many models and artificial learning systems such as neural networks suggest that error drives sensorimotor learning of a person, so that one can learn adaptation more quickly if the error is augmented to a certain degree [46]. Such error-driven learning processes are believed to be central to adaptation and the acquisition of skill in human movement [44, 47]. It has been shown that **visual error augmentation** can improve the rate and extent of motor learning in healthy participants [38] and elicit functional improvements in patients with chronic stroke and traumatic brain injury [39]. Thus, it is desirable to integrate the visual feedback and visual error augmentation strategy in rehabilitation training.

Scope and Summary of the Dissertation

The purpose of my research work is to explore how to improve robot-assisted rehabilitation for upper extremity disability following stroke. We have probed this question in three different approaches including system enhancement (Manuscript I), evaluation of novel training strategies (Manuscript II) and design of new hardware (Manuscript III and IV). The dissertation is organized as follows:

First in Chapter II, development of a robotic system incorporating verbal feedback for arm rehabilitation is described. This robotic system is able to recognize the participant's

verbal commands and adjust the rehabilitation training online accordingly. A high-level supervisory controller is designed to monitor the task execution, make task adjustment according to the recognized verbal feedback from the participant during the task execution to impart effective therapy to the participant in an automated manner. This enhancement will keep the patients in the loop and reduce the intervention and workload of the therapists.

Next in Chapter III, an investigation of a novel rehabilitation strategy in improving the efficacy of robot-assisted arm rehabilitation is presented. Two rehabilitation training strategies, assist-as-needed and visual error augmentation, are implemented on the existing robotic system. A crossover study is designed to assess the impact of the integrated training method of these two strategies on robot-assisted arm rehabilitation. The experimental results show that the integrated training method has improved the rehabilitation training efficacy compared to the assist-as-needed method. This improvement is statistically significant.

While existing robotic systems may be able to provide the hardware platforms for arm rehabilitation, the same is not currently true for the hand. There are several technical challenges, such as designing an articulated system to accommodate the many joints of the hand and controlling these joints independently, while providing the necessary levels of power, speed, and reliability. Existing hand devices do not provide the complete range of speed, force, and independence of joint control to thoroughly explore the space of different training algorithms and environments [23]-[31].

Thus, in Chapter IV and V, the design of an actuated hand exoskeleton (AHX) is presented. The AHX, consisting of an actuated finger exoskeleton (AFX) and an actuated

thumb exoskeleton (ATX), has the potential to serve as a test-bed to facilitate hand rehabilitation and motor control study for stroke patients. In Chapter IV, the performance of a real-time control system for the AFX with both position and torque control is shown. The AFX exhibited high speed and torque capacity with good backdrivability. Then, in Chapter V, the design and control of an ATX with 5 active degree-of-freedoms (DOF) and 3 passive DOF that allows individual actuation of each DOF for the human thumb are described. The ATX showed independent actuation of each thumb joint with high speed and torque capacity and good backdrivability.

The proposed research work is presented in 4 manuscripts as follows:

Manuscript 1: Incorporating Verbal Feedback into a Robot-Assisted Rehabilitation System

Background

In the last few years, robot-assistance for physical rehabilitation of stroke survivors has been an active area of research [11]-[31]. There are two important roles that a robotic rehabilitation system needs to fulfill. First, robotic rehabilitation systems need to monitor the task and safety issues, provide assessment of progress, and alter the task parameters to impart effective therapy. Second, robotic rehabilitation systems need to alter the presentation of the rehabilitation therapy task based on patients' feedback. A robotic system that is able to monitor the task and safety, recognize the patients' feedback and alter the presentation of the rehabilitation therapy in an automated manner will greatly facilitate robot-assisted rehabilitation.

Summary of Contribution

The main contributions of this work are to augment the capabilities of a robotic rehabilitation system by enabling it to: 1) comprehensively monitor the task and safety issues, provide assessment of the progress, and alter the task parameters to impart effective therapy during the execution of the task in an automated manner; and 2) recognize patient's verbal feedback such that it can address his/her concern. This work is built upon the preliminary work [48, 49] on an intelligent control framework for robotic rehabilitation to incorporate patient feedback within the overall control architecture. My main contributions to this work are: 1) to establish the real-time communication interface between the robotic system and voice recognition system, and 2) to develop the high-level supervisory controller for the robotic system that monitors the task execution and safety, provides assessment of the progress, alters the rehabilitation therapy according to the recognized voice feedback of the subjects.

- Barkana, D.E.; Wang, F.; Das, J.; Sarkar, N.; Groomes, T.E., "A step toward increasing automation in robot-assisted rehabilitation," Biomedical Robotics and Biomechatronics, 2008. BioRob 2008. 2nd IEEE RAS & EMBS International Conference on, pp.930-935, 19-22 Oct. 2008.
- Duygun Erol Barkana, Jadav Das, Furui Wang, Thomas E. Groomes and Nilanjan Sarkar, "Incorporating verbal feedback into a robot-assisted rehabilitation system". Robotica, 2011, vol. 29, issue 3, pp 433-443.

Manuscript 2: Impact of Visual Error Augmentation When Integrated with Assist-as-needed Training Method in Robot-assisted Rehabilitation

Background

Robot-assisted rehabilitation has been an active research topic in recent years [11]-[31]. Various rehabilitation training strategies have been proposed to improve the efficacy of robot-assisted rehabilitation training [42]. Two novel strategies, assist-as-needed and visual error augmentation, have been individually investigated in literatures and suggested to be beneficial for upper-limb rehabilitation [11, 36]. However, none of the work has investigated the combination of these two training strategies, which could be integrated in robot-assisted rehabilitation, with the potential to take the advantages of both training strategies.

Summary of Contribution

There are two contributions in this work. The first contribution is to enhance the functionality of the existing robotic system for arm rehabilitation with the assist-as-needed and visual error augmentation training method, and design a controller that could execute the two training methods in an integrated manner. The second contribution is to design a crossover study to investigate the assist-as-needed only and the integrated training methods, and to conduct statistical analysis to compare the training efficiency of these two methods. The experimental results show that: 1) the robotic system is able to provide the designed training methods; and 2) the integrated training method shows improved training efficiency compared to the assist-as-needed only training method.

- Furui Wang; Barkana, D.E.; Sarkar, N., "Impact of Visual Error Augmentation When Integrated With Assist-as-Needed Training Method in Robot-Assisted Rehabilitation," Neural Systems and Rehabilitation Engineering, IEEE Transactions on , vol.18, no.5, pp.571-579, Oct. 2010.
- Furui Wang; Barkana, D.E.; Sarkar, N., "Integration of error augmentation training method to an assistive controller for rehabilitation robotic systems," Rehabilitation Robotics, 2009. ICORR 2009. IEEE International Conference on, pp.463-468, 23-26 June 2009.
- Furui Wang; Barkana, D.E.; Sarkar, N., "Evaluation of a robot-assisted rehabilitation system with assist-as- needed and visual error augmentation training methods," Intelligent Robots and Systems, 2009. IROS 2009. IEEE/RSJ International Conference on, pp.3555-3560, 10-15 Oct. 2009.

Manuscript 3: Design and Development of an Actuated Finger Exoskeleton for Hand Rehabilitation following Stroke

Background

Finger impairment following stroke results in significant deficits in hand manipulation and the performance of everyday tasks. Recent advances in rehabilitation robotics have shown improvement in efficacy of rehabilitation [50], [51]. Current devices [23]-[31], however, lack the capacity to accurately interface with the human finger at levels of velocity and torque comparable to the performance of everyday hand manipulation tasks.

Summary of Contribution

The main contributions of this work are the design and control of the Actuated Finger Exoskeleton (AFX), a three DOF robotic exoskeleton for the index finger. The AFX improves on current rehabilitation robotics solutions by providing a versatile framework with high performance, real-time control, and forces and speeds comparable to normal human function. The AFX will allow for normal task execution in a rehabilitation or motor study environment. My main contributions to this work are to analyze the kinematics of the AFX model and to develop and implement the position and torque control system in real-time.

- Jones, C.L.; Furui Wang; Robert Morrison; Sarkar, N.; Kamper, D.G., "Design and development of an Actuated Finger Exoskeleton for hand rehabilitation following stroke,", submitted to IEEE/ASME Transaction on Mechatronics.
- Jones, C.L.; Furui Wang; Osswald, C.; Xuan Kang; Sarkar, N.; Kamper, D.G., "Control and kinematic performance analysis of an Actuated Finger Exoskeleton for hand rehabilitation following stroke," Biomedical Robotics and Biomechatronics (BioRob), 2010 3rd IEEE RAS and EMBS International Conference on, pp.282-287, 26-29 Sept. 2010.

Manuscript 4: Design and Development of an Actuated Thumb Exoskeleton for Hand Rehabilitation following Stroke

Background

Hand impairment is a prevalent outcome for a variety of neuromuscular disorders, such as stroke. Loss of hand function due to neuromuscular disorders frequently prevents

effective self-care and limits employment opportunities. A number of devices have been developed expressly for or applied to hand rehabilitation [23]-[31]. As such, they typically do not allow for independent control of the joints, especially for the thumb with five degrees-of-freedom (DOF). Others may insufficient torque or overly restrict thumb movement. Thus, these devices are not suitable to serve as a test-bed for studying the thumb motor control and thumb rehabilitation.

Summary of Contribution

The main contributions of this work are to design and develop an actuated thumb exoskeleton (ATX), with five active DOF and 3 passive DOF, which allows independent actuation of each DOF of the thumb. The ATX is able to provide individual actuation for each thumb DOF, while possessing sufficient torque to overcome possibly excessive coactivation and increased stiffness in the affected thumb and high speed joint motion comparable to the natural motion of the human thumb joints. This ATX has the potential to serve as a test bed to evaluate thumb rehabilitation therapies and motor learning paradigms. My contributions in this work are the mechanical design, kinematics analysis, actuation and sensory systems development, instrumentation and real-time control system design and implementation.

- Wang, Furui; Shastri, Milind; Jones, Christopher L.; Kamper, Derek G.; Sarkar, Nilanjan, "Design and control of an actuated thumb exoskeleton for hand rehabilitation following stroke," Robotics and Automation (ICRA), 2011 IEEE International Conference on , pp.3688-3693, 9-13 May 2011.

- Wang F, Jones C, Shastri M, Gupta V, Osswald C, Kang X, Kamper D, Sarkar N, "Design and development of an actuated thumb exoskeleton for hand rehabilitation following stroke," in preparation for submission to IEEE/ASME Transaction on Mechatronics.

References

[1] *American Heart Association, Heart and Stroke Statistical Update, 2010*. Available: http://www.Americanheart.org/statistics/stroke.htm

[2] R Bonita, A Stewart, *et al.*, "International trends in stroke mortality: 1970-1985.," *Stroke,* vol. 21, pp. 989-92, Jul 1990.

[3] JP Broderick, SJ Phillips, *et al.*, "Incidence rates of stroke in the eighties: the end of the decline in stroke?," *Stroke,* vol. 20, pp. 577-82, May 1989.

[4] CS Gray, JM French, *et al.*, "Motor recovery following acute stroke.," *Age Ageing,* vol. 19, pp. 179-84, May 1990.

[5] H Nakayama, HS Jørgensen, *et al.*, "Recovery of upper extremity function in stroke patients: the Copenhagen Stroke Study.," *Arch Phys Med Rehabil,* vol. 75, pp. 394-8, Apr 1994.

[6] VM Parker, DT Wade, *et al.*, "Loss of arm function after stroke: measurement, frequency, and recovery.," *Int Rehabil Med,* vol. 8, pp. 69-73, 1986.

[7] CA Trombly, MV Radomski, *et al.*, "Stroke," in *Occupational therapy for physical dysfunction*, ed: Williams & Wilkins Baltimore, MD, 1989.

[8] E Taub, NE Miller, *et al.*, "Technique to improve chronic motor deficit after stroke.," *Arch Phys Med Rehabil,* vol. 74, pp. 347-54, Apr 1993.

[9] BT Volpe, ""Stroke, stroke": a coxswain's call for more work and more innovation.," *J Rehabil Res Dev,* vol. 41, pp. vii-x, May 2004.

[10] E Taub, G Uswatte, *et al.*, "Constraint-Induced Movement Therapy: a new family of techniques with broad application to physical rehabilitation--a clinical review.," *J Rehabil Res Dev,* vol. 36, pp. 237-51, Jul 1999.

[11] H. I. Krebs, J. J. Palazzolo, *et al.*, "Rehabilitation Robotics: Performance-Based Progressive Robot-Assisted Therapy," *Autonomous Robots,* vol. 15, pp. 7-20, 2003.

[12] HI Krebs, M Ferraro, *et al.*, "Rehabilitation robotics: pilot trial of a spatial extension for MIT-Manus.," *J Neuroeng Rehabil,* vol. 1, p. 5, Oct 2004.

[13] LE Kahn, ML Zygman, *et al.*, "Robot-assisted reaching exercise promotes arm movement recovery in chronic hemiparetic stroke: a randomized controlled pilot study.," *J Neuroeng Rehabil,* vol. 3, p. 12, 2006.

[14] LE Kahn, PS Lum, *et al.*, "Robot-assisted movement training for the stroke-impaired arm: Does it matter what the robot does?," *J Rehabil Res Dev,* vol. 43, pp. 619-30, 2006 Aug-Sep 2006.

[15] PS Lum, CG Burgar, *et al.*, "Quantification of force abnormalities during passive and active-assisted upper-limb reaching movements in post-stroke hemiparesis.," *IEEE Trans Biomed Eng,* vol. 46, pp. 652-62, Jun 1999.

[16] CG Burgar, PS Lum, *et al.*, "Development of robots for rehabilitation therapy: the Palo Alto VA/Stanford experience.," *J Rehabil Res Dev,* vol. 37, pp. 663-73, 2000 Nov-Dec 2000.

[17] PS Lum, CG Burgar, *et al.*, "MIME robotic device for upper-limb neurorehabilitation in subacute stroke subjects: A follow-up study.," *J Rehabil Res Dev,* vol. 43, pp. 631-42, 2006 Aug-Sep 2006.

[18] Rui Loureiro, Farshid Amirabdollahian, *et al.*, "Upper Limb Robot Mediated Stroke Therapyâ ”GENTLE/s Approach," *Autonomous Robots,* vol. 15, pp. 35-51, 2003.

[19] S Hesse, G Schulte-Tigges, *et al.*, "Robot-assisted arm trainer for the passive and active practice of bilateral forearm and wrist movements in hemiparetic subjects.," *Arch Phys Med Rehabil,* vol. 84, pp. 915-20, Jun 2003.

[20] S. K. Charles, H. I. Krebs, *et al.*, "Wrist rehabilitation following stroke: initial clinical results," in *Rehabilitation Robotics, 2005. ICORR 2005. 9th International Conference on*, 2005, pp. 13-16.

[21] Abhishek Gupta, Marcia K. O'Malley, *et al.*, "Design, Control and Performance of RiceWrist: A Force Feedback Wrist Exoskeleton for Rehabilitation and Training," *The International Journal of Robotics Research,* vol. 27, pp. 233-251, February 1, 2008 2008.

[22] M. J. Johnson, K. J. Wisneski, *et al.*, "Development of ADLER: The Activities of Daily Living Exercise Robot," in *Biomedical Robotics and Biomechatronics, 2006. BioRob 2006. The First IEEE/RAS-EMBS International Conference on*, 2006, pp. 881-886.

[23] SV Adamovich, GG Fluet, *et al.*, "Design of a complex virtual reality simulation to train finger motion for persons with hemiparesis: a proof of concept study.," *J Neuroeng Rehabil,* vol. 6, p. 28, 2009.

[24] *Kinetic Muscles Inc., Hand Mentor*. Available: http://www.kineticmuscles.com/index.html

[25] *Tyromotion GmbH, Amadeo Hand System*. Available: http://www.tyromotion.com/en/products/amadeo/

[26] D Jack, R Boian, *et al.*, "Virtual reality-enhanced stroke rehabilitation," *IEEE Transactions on Neural Systems and Rehabilitation Engineering,* vol. 9, pp. 308-318, 2001.

[27] CD Takahashi, L Der-Yeghiaian, *et al.*, "Robot-based hand motor therapy after stroke.," *Brain,* vol. 131, pp. 425-37, Feb 2008.

[28] L Dovat, O Lambercy, *et al.*, "HandCARE: a cable-actuated rehabilitation system to train hand function after stroke.," *IEEE Trans Neural Syst Rehabil Eng,* vol. 16, pp. 582-91, Dec 2008.

[29] A. Wege and G. Hommel, "Development and control of a hand exoskeleton for rehabilitation of hand injuries," in *Intelligent Robots and Systems, 2005. (IROS 2005). 2005 IEEE/RSJ International Conference on*, 2005, pp. 3046-3051.

[30] M. DiCicco, L. Lucas, *et al.*, "Comparison of control strategies for an EMG controlled orthotic exoskeleton for the hand," in *Robotics and Automation, 2004. Proceedings. ICRA '04. 2004 IEEE International Conference on*, 2004, pp. 1622-1627 Vol.2.

[31] H. Kawasaki, S. Ito, *et al.*, "Development of a Hand Motion Assist Robot for Rehabilitation Therapy by Patient Self-Motion Control," in *Rehabilitation Robotics, 2007. ICORR 2007. IEEE 10th International Conference on*, 2007, pp. 234-240.

[32] BT Volpe, HI Krebs, *et al.*, "A novel approach to stroke rehabilitation: robot-aided sensorimotor stimulation.," *Neurology,* vol. 54, pp. 1938-44, May 2000.

[33] PS Lum, CG Burgar, *et al.*, "Robot-assisted movement training compared with conventional therapy techniques for the rehabilitation of upper-limb motor function after stroke.," *Arch Phys Med Rehabil,* vol. 83, pp. 952-9, Jul 2002.

[34] L. E. Kahn, M. L. Zygman, *et al.*, "Effect of robot-assisted and unassisted exercise on functional reaching in chronic hemiparesis," in *Engineering in Medicine and Biology Society, 2001. Proceedings of the 23rd Annual International Conference of the IEEE*, 2001, pp. 1344-1347 vol.2.

[35] SE Fasoli, HI Krebs, *et al.*, "Effects of robotic therapy on motor impairment and recovery in chronic stroke.," *Arch Phys Med Rehabil,* vol. 84, pp. 477-82, Apr 2003.

[36] J. L. Patton, F. A. Mussa-Ivaldi, *et al.*, "Altering movement patterns in healthy and brain-injured subjects via custom designed robotic forces," in *Engineering in*

Medicine and Biology Society, 2001. Proceedings of the 23rd Annual International Conference of the IEEE, 2001, pp. 1356-1359 vol.2.

[37] B. R. Brewer, R. Klatzky, *et al.*, "Effects of visual feedback distortion for the elderly and the motor-impaired in a robotic rehabilitation environment," in *Robotics and Automation, 2004. Proceedings. ICRA '04. 2004 IEEE International Conference on*, 2004, pp. 2080-2085 Vol.2.

[38] Yejun Wei, P. Bajaj, *et al.*, "Visual error augmentation for enhancing motor learning and rehabilitative relearning," in *Rehabilitation Robotics, 2005. ICORR 2005. 9th International Conference on*, 2005, pp. 505-510.

[39] BR Brewer, R Klatzky, *et al.*, "Visual feedback distortion in a robotic environment for hand rehabilitation.," *Brain Res Bull,* vol. 75, pp. 804-13, Apr 2008.

[40] S. P. Lum, S. L. Lehman, *et al.*, "The bimanual lifting rehabilitator: an adaptive machine for therapy of stroke patients," *Rehabilitation Engineering, IEEE Transactions on,* vol. 3, pp. 166-174, 1995.

[41] P. S. Lum, D. J. Reinkensmeyer, *et al.*, "Robotic assist devices for bimanual physical therapy: preliminary experiments," *Rehabilitation Engineering, IEEE Transactions on,* vol. 1, pp. 185-191, 1993.

[42] DJ Reinkensmeyer, JL Emken, *et al.*, "Robotics, motor learning, and neurologic recovery.," *Annu Rev Biomed Eng,* vol. 6, pp. 497-525, 2004.

[43] D. J. Reinkensmeyer, "How to retrain movement after neurologic injury: a computational rationale for incorporating robot (or therapist) assistance," in *Engineering in Medicine and Biology Society, 2003. Proceedings of the 25th Annual International Conference of the IEEE*, 2003, pp. 1479-1482 Vol.2.

[44] M Kawato, "The feedback-error-learning neural network for supervised motor learning," in *Advanced neural computers*, R. Eckmiller, Ed., ed: North Holland, 1990, pp. 365-372.

[45] JR Carey, E Bhatt, *et al.*, "Neuroplasticity promoted by task complexity.," *Exerc Sport Sci Rev,* vol. 33, pp. 24-31, Jan 2005.

[46] David E. Rumelhart, Geoffrey E. Hinton, *et al.*, "Learning representations by back-propagating errors," *Nature,* vol. 323, pp. 533-536, 1986.

[47] DM Wolpert, Z Ghahramani, *et al.*, "An internal model for sensorimotor integration.," *Science,* vol. 269, pp. 1880-2, Sep 1995.

[48] D. Erol and N. Sarkar, "Intelligent control for robotic rehabilitation after stroke," *Journal of Intelligent & Robotic Systems,* vol. 50, pp. 341-360, Dec 2007.

[49] D. Erol and N. Sarkar, "Coordinated control of assistive robotic devices for activities of daily living tasks," *IEEE Transactions on Neural Systems and Rehabilitation Engineering,* vol. 16, pp. 278-285, Jun 2008.

[50] S. L. Wolf, S. Blanton, *et al.*, "Repetitive task practice: A critical review of constraint-induced movement therapy in stroke," *Neurologist,* vol. 8, pp. 325-338, Nov 2002.

[51] C. J. Winstein, D. K. Rose, *et al.*, "A randomized controlled comparison of upper-extremity rehabilitation strategies in acute stroke: A pilot study of immediate and long-term outcomes," *Archives of Physical Medicine and Rehabilitation,* vol. 85, pp. 620-628, Apr 2004.

CHAPTER II

MANUSCRIPT I: INCORPORATING VERBAL FEEDBACK INTO A ROBOT-ASSISTED REHABILITATION SYSTEM

Duygun Erol Barkana, Furui Wang, Jadav Das, Nilanjan Sarkar and Thomas Groomes

(This work has been published in Robotica, vol.29, no.3, pp.433-443, 2011, and partially published in the IEEE International Conference on Biomedical Robotics and Biomechatronics, BioRob 2008.)

Abstract

This paper presents a control architecture, which has the potential to monitor the task, safety issues, to provide assessment of the progress and alter the task parameters, and to incorporate patient's feedback in order to make the necessary modifications to impart effective therapy during the execution of the task in an automated manner. Experimental results are presented to demonstrate the efficacy of the proposed control architecture.

Keywords – rehabilitation system, human intention recognition system, hybrid systems

Introduction

Stroke is a highly prevalent condition especially among the elderly that results in high costs to the individual and society [1]. In the last few years, robot-assisted rehabilitation for physical rehabilitation of the stroke patients has been an active research area to assist, monitor, and quantify rehabilitation therapies [4]-[11]. Robot-assisted rehabilitation has shown to provide repetitive movement exercise and standardized delivery of therapy with the potential of enhancing quantification of the therapeutic process for stroke patients [4]-[11]. Studies in this field suggest that robot-assisted rehabilitation results in improved performance of functional tasks.

There are two important issues that a robotic rehabilitation system needs to address. First, robotic rehabilitation systems need to comprehensively monitor the task and safety issues, provide assessment of the progress, and alter the task parameters to impart effective therapy. Generally, a therapist administers the therapy where he/she monitors the progress of the tasks as well as patient's safety, and assesses whether the task needs to be updated based on the need of individual patient. As a result, a robotic system will

likely reduce the amount of time of the therapist as well as decrease his/her workload, and consequently, decrease the cost of treatment. MIT-MANUS [4], MIME [5] and GENTLE/s [6] were among the first rehabilitation robotic systems to implement safety. Second, robotic rehabilitation systems need to alter the presentation of the rehabilitation therapy task based on patients' feedback. Altering the presentation of the rehabilitation therapy is an important issue since patients or therapists should be able to express how they feel about the task, and necessary modifications need to be performed about the therapy. Recently developed rehabilitation devices like ARMin [7], ADLER [8], T-WREX [9], HenRiE [10] and HARMiS [11] provide assistance to the patients as needed based on the patients' position, velocity and force feedback. However, this feedback only provides information about patient's motion capabilities, and it does not directly represent the feelings of the patient or the therapist about the task execution. For example, if the patient does not feel comfortable in moving his/her arm at a specified speed, then the therapist or the robot-assisted system may need to change the task execution to slow down. Note that, when a therapist manually administers rehabilitation therapy, he/she keeps the patient in the loop and adjusts the therapy. Therefore, it is important for a robot-assisted rehabilitation system to alter the presentation of the rehabilitation therapy task automatically considering patients and therapists feedback. To our knowledge none of the existing robot-assisted rehabilitation systems use feedback of both patient's and therapist's to modify the presentation of the task. Spoken words of stroke patients or therapists can be one of the available options to incorporate their verbal feedback into the robot-assisted rehabilitation system so that the necessary modifications on the robot-assisted rehabilitation can be made immediately.

In this work, we attempt to address how to augment the capabilities of a robotic rehabilitation system by enabling it to: 1) comprehensively monitor the task and safety issues, provide assessment of the progress, and alter the task parameters to impart effective therapy during the execution of the task in an automated manner; and 2) recognize patient's verbal feedback such that it can address his/her concerns. This work is built upon our preliminary work on an intelligent control framework for robotic rehabilitation [12]-[16] to incorporate patient's feedback within the overall control architecture. The paper is organized into the following sections. It first presents the intelligent control architecture in Section II. A rehabilitation robotic system, a human intention recognition system, and one of the rehabilitation tasks that are used to demonstrate the versatility of the presented control architecture are presented in Section III. Results of the experiments are presented in Section IV to demonstrate the efficacy of the control architecture. Section V discusses potential contributions of this work and possible directions for future work.

Control Architecture

Let us first present the proposed framework in the context of one of the rehabilitation tasks, called the reaching task. The reaching task designed in this work requires a combination of shoulder and elbow movements, which could increase the active range of motion (AROM) in the shoulder and the elbow in preparation for later functional reaching activities in rehabilitation. In this task, the participants are asked to move their arms in the forward direction to reach a desired point in space and then bring it back to the starting position repeatedly within a specified time.

Stroke survivors, in general, may not be able to track the desired motion trajectory in this reaching task because of their motor impairment. A low-level assistive controller will be used to provide robotic assistance to a patient's arm movement as and when needed to help him/her to complete the reaching task. In this architecture, an intention recognition system recognizes the patient's spoken words (e.g., fast, slow, continue and stop) using a microphone and a voice-recognition technique and then converts the spoken words into control commands (Figure II-1). The control commands, which represent his/her intention during the task execution, are sent to the high-level supervisory controller. Once the high-level supervisory controller receives the commands, the decision-making module of the high-level supervisory controller generates sequences of control actions using its decision rules. Additionally, the high-level supervisory controller monitors the safety events during the execution of the reaching task to decide the necessary modifications of the task. The high-level supervisory controller presented in this work ideally plays the role of a human supervisor (therapist) who would otherwise monitor the patient's verbal feedback and safety and then assess whether the task needs to be updated. The high-level supervisory controller is designed considering the requirements of the therapy, and it can be easily modified and extended for new task requirements. The decision of the high-level supervisory controller is sent to the low-level assistive controller to update the task. The updated task is then executed by the low-level assistive controller. This cycle continues to complete the therapy.

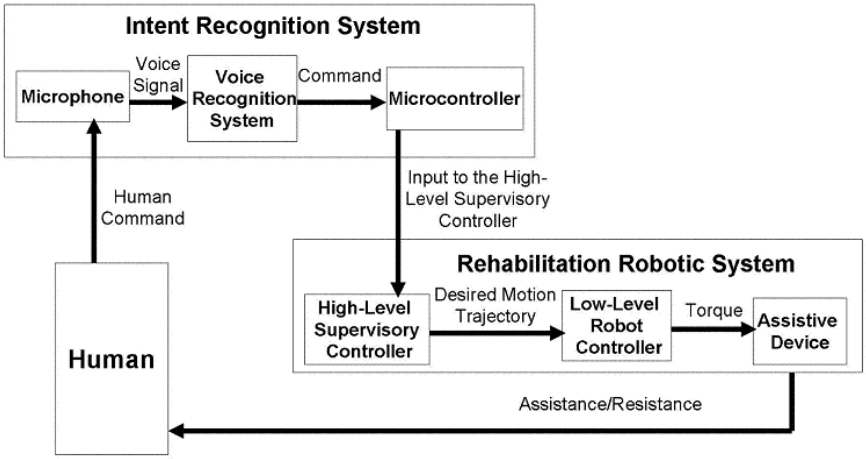

Figure II-1 Control Architecture of a Voice Activated Robotic Rehabilitation System

Methodology

Rehabilitation Robotic System ---- A Test-bed

In order to present the efficacy of the proposed control architecture, we have used a PUMA 560 robotic manipulator as the robotic assistive device. The manipulator is augmented with a hand attachment device (Figure II-2). The microcontroller board of the PUMA is replaced to develop an open architecture system to allow implementation of the advanced controllers (e.g., low-level assistive and high-level controllers). The technical specifications of the robotic manipulator can be found in [17]. We interface the robot with MATLAB/Realtime Workshop to allow fast and easy system development. A computer monitor is placed in front of the subject to provide visual feedback about his/her motion trajectory during the execution of the task. The detailed discussion about the rehabilitation robotic system can be found in our previous work [12]- [16], [18].

Since in this work we are primarily interested in effecting assistance to the upper arm, we design a hand attachment device where the subject's arm is strapped into a splint. The PUMA 560 is attached to that splint to provide assistance to the upper arm movement using the assistive controller (Figure II-2). We further design a steel plate with proper grooves that hold two small flat-faced electromagnets (from Magnetool Inc.) that are screwed on it (Figure II-2). We attach a light-weight steel plate under the splint, which is then attached to the electromagnets of the plate. An automatic release (AU) rectifier controller (Magnetool Inc.) is used to provide a quick release of these electromagnets. A push button, which is connected to the AU Rectifier Controller, is used to magnetize and demagnetize the electromagnets when the subject wants to remove the hand attachment device from the robotic manipulator in a safe and quick manner. Ensuring safety of the subject is a very important issue when designing a rehabilitation robotic system. Thus, in case of emergency situations, therapists can press an emergency button. The patient and/or the therapist can quickly release the subject's arm from the PUMA 560 by using the quick-release hand attachment device (as described above) to deal with any physical safety related events. This quick-release mechanism is identical to the mechanism used in GENTLE/s [6] and ADLER [8]. When the push button is pressed, electromagnets are demagnetized instantaneously and the subject is free to remove the splint from the robot. The safety mechanism in MIME is similar although the implementation is different in some cases (e.g., we introduce joint limits as a hyper-surface in our high-level controller whereas in MIME it is implemented as a limit check since the control architecture is different from ours).

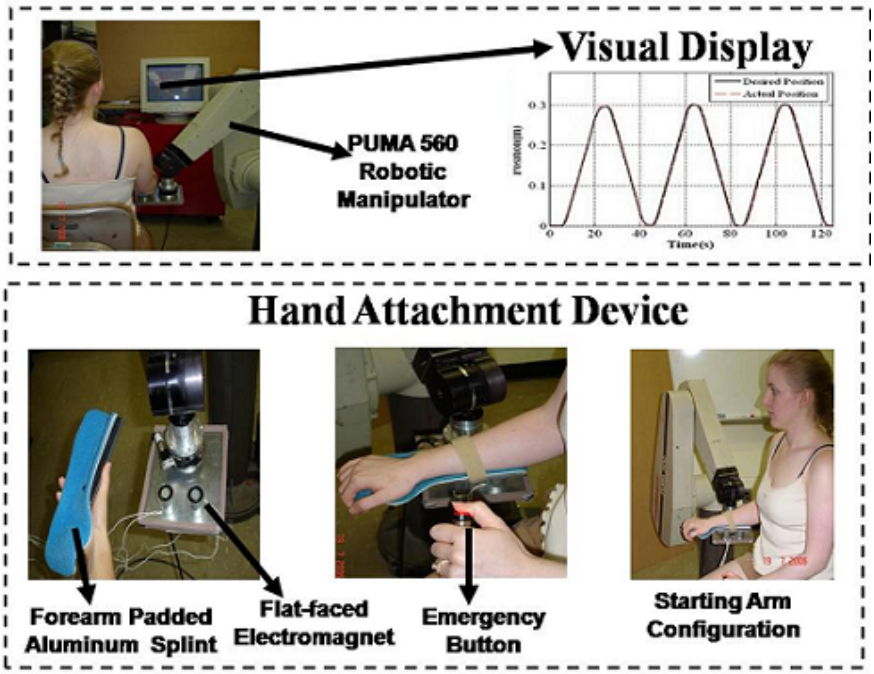

Figure II-2 Subject Arm attached to Robot

In this work, a proportional-integral-derivative (PID) position control is used as a low-level arm assistive controller for providing robotic assistance to a subject to complete the movement task. The subject receives visual feedback of both their actual position and the desired position trajectories on a computer screen, which is placed in front of them. Then the subject is asked to pay attention to tracking the desired position trajectory as accurately as possible, which keeps them focused on the task. If the subject deviates from the desired motion, then low-level assistive controller provides robotic assistance to complement the subject's effort to complete the task as required.

Human Intention Recognition System

Stroke patients may have difficulties to complete the rehabilitation tasks because of their limited upper extremity movements. It is important to include patient's feedback

into the robot-assisted rehabilitation system so that it can immediately make the necessary modifications without therapist's intervention. Recognizing stroke patients' spoken words may be one of the available options to incorporate their feedback into the robot-assisted system.

Various speech recognition techniques have been developed over the years such as a grammar builder from the Microsoft Speech SDK 5.1 [19], fuzzy command interpreter [20], Adaptive Input Neural Network (AINN) [21], [22]. MICROEAR (voice activated hardware) is developed in [23] to recognize a word and then it returns a string which is then converted to a numerical code. Later, the code is compared with the listed words and sets the respective flags. Then the relevant functions form the character strings to be passed on to the robot controller to activate the robot motors using ASCII string. Hidden Markov Model (HMM) based automatic speech recognizers are developed to recognize the human voice in [24]. The spoken word from the human is translated in the form of a quantified desired action for a robot system. New concepts of fuzzy coach-player system and sub-coach to control robots with natural language commands are presented in [25]. A probabilistic neural network based learning method is used to acquire the knowledge from such commands and then implemented in a Mitsubishi PA-10 redundant manipulator.

In our target application domain, we want to incorporate feedback from stroke patients. It is likely that many of the stroke patients may not have sufficient control over their articulatory muscles to communicate long and clear sentences. Moreover, the range of distortion of spoken words could be an issue in stroke patients. Considering these issues, we choose to develop a speech recognition system that is capable of robustly identifying

a few short phrases or words that have relevance with respect to the rehabilitation therapy. We use a well-known voice recognition method, called Mel-frequency cepstral coefficients (MFCCs) in this work [26], [27].

In this work, however, we have used a deterministic approach to speech recognition. Since in this application we have restricted the number of spoken words and since we have employed an individual-specific approach, such a deterministic approach is preferred to a more versatile learning approach. The subject informs his/her intention using simple words such as "fast", "slow", "stop" and "continue" during the rehabilitation task. However, these words can not be used directly as commands for the high-level controller in the control architecture. Initially, each subject is asked to speak each of the selected words three times. The signal is acquired using the Data acquisition toolbox of MATLAB R2007a [28] with 8 KHz sampling frequency. An arithmetic average is computed from these three samples of the same word to account for within person variation of spoken words. The resultant sample is normalized and broken down into a series of frames each of which contains 256 data points. We compute 12 mel-frequency cepstral coefficients (MFCCs) for each frame. The frames and their MFCCs for each word for each person are stored in a set of 2-dimensional arrays as reference. During the execution of the rehabilitation task, as the subject speaks any of the selected words, the start and end points of the sampled speech signal are detected and only the speech portion of the signal is sent to the feature extraction module. The end point determination concept used here is originally proposed in [29] based on two features: short-term root-mean-square-energy and zero crossing rate measures of the signal. The feature extraction module receives the speech portion of the signal and computes the same 12 MFCCs of

the speech by splitting it into frames of 256 samples. The MFCCs are then sent to the pattern matching module to compare the MFCCs of the spoken word with those of the reference MFCCs of all the stored words and finds the best match using the least Euclidean distance measure among the MFCCs between the spoken word and the reference words. Then the pattern matching module generates a command signal for the high-level controller. In order for the high-level controller to receive the generated command, the command is initially sent to the microcontroller (Adapt 9S12D - Technological Arts Company). The microcontroller transmits the command signal to the computer of the robotic rehabilitation system through a RS232 serial port. The command is used by the high-level controller to decide the next plan of action during the execution of the rehabilitation task.

Modeling of a Rehabilitation Task using Hybrid System Modeling Technique

The proposed control architecture, as described in a previous section, consists of a low-level arm assistive controller that is used to provide assistance to the subject's arm movement and a high-level supervisory controller to monitor the task and the patient's safety and to detect the patient's verbal feedback (intention) in order to make the necessary modifications to the task. In this work, we use hybrid system modeling technique to design the proposed control architecture. A hybrid system model has three parts, a "Plant", a "Controller" (supervisor) and an Interface [19], [30], [31] (Figure II-3). A similar hybrid system model has previously designed for same rehabilitation system and the details can be found in [12]-[16]. First we present the theory of the hybrid control

systems. Then the design details of the hybrid control system used for one of the rehabilitation tasks, a reaching task, is given.

The hybrid control systems consist of a plant which is generally a continuous system to be controlled by a discrete event controller (DES) connected to the plant via an interface in a feedback configuration [30], [31]. If the plant is taken together with the interface, then it is called a DES plant model. The DES controller, which is called the high-level supervisory controller in this work, controls the DES plant. Let us first present the DES plant and then describe the DES controller (high-level supervisory controller).

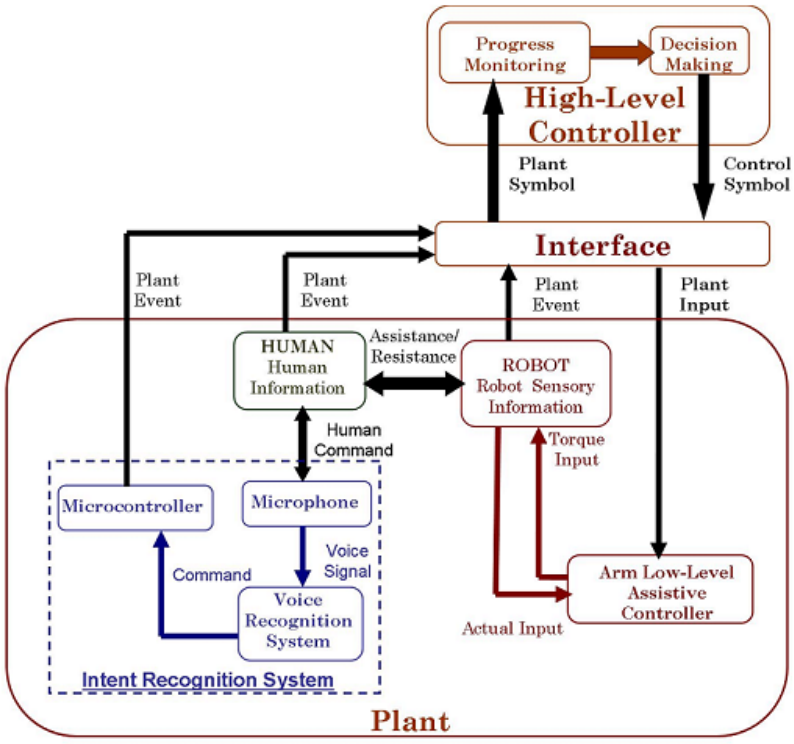

Figure II-3 Control Architecture

DES Plant Model

The DES plant model is a nondeterministic finite automaton, which is represented mathematically by $G=(\tilde{P},\tilde{X},\tilde{R},\psi,\lambda)$. Here, $\tilde{P}$ is the set of discrete states; $\tilde{X}$ is the set of

plant symbols generated based on the events; and $\tilde{R}$ is the set of control symbols generated by the high-level supervisory controller. $\psi : \tilde{P} \times \tilde{R} \to 2^{\tilde{P}}$ is the state transition function. The output function, $\lambda : \tilde{P} \times \tilde{P} \to 2^{\tilde{x}}$, maps the previous and current plant states to a set of plant symbols. The set of DES plant model states $\tilde{P}$ is based upon the set of hypersurfaces that separates different discrete states.

The hypersurfaces defined in this work can be classified into two classes: i) the hypersurfaces describing subject's capability to complete the task; ii) the hypersurfaces describing the capability of the rehabilitation robotic system in order to ensure the execution of the rehabilitation task in a safe manner. The hypersurfaces are defined as follows: $h_1 = v - v_{high}, h_2 = v_{low} - v, h_3 = e, h_4 = \delta - \delta_{limit}$, here, v is the actual speed of the robotic device, v_{low} and v_{high} are the lower and upper limits of the subject's desired speed range. e is binary variable representing the subject's intention to stop or continue the task. δ is the actual robotic device configuration vector and δ_{limit} is the limit vector of the configurations. h_1 detects if the current task is too fast for the subject and he/she may want to decrease the speed; h_2 detects if the current task is too slow for the subject and he/she may want to increase the speed; h_3 detects whether the subject wants to continue or to stop the task; h_4 detects whether the robotic system configurations, joint angles, torque etc. are working in safe range.

The DES plant model is demonstrated in Figure II-4. Here, $\tilde{x}_i$ is the plant symbol, $\tilde{r}_i$ is the control symbol and $\tilde{P}_i$ is the plant state. Note that a temporary state P'_{0000} is introduced to distinguish the current state from the initial state. A plant event occurs when a hypersurface is crossed, which means the plant enters a new state. These plant events

need not be distinct for each distinct hypersurface. A plant event generates a plant symbol to be used by the high-level supervisory controller. The plant symbol, $\tilde{x}$, is generated as an output function of the current and the previous plant state. We define the following plant symbols considering the hypersurfaces discussed before: i) $\tilde{x}_1$, the subject wants to continue the task execution with the current speed; ii) $\tilde{x}_2$, the subject wants to slow down and says the word "slow"; iii) $\tilde{x}_3$, the subject wants to speed up and says the word "fast"; iv) $\tilde{x}_4$, the subject wants to stop and says the word "stop" v) $\tilde{x}_5$, the subject wants to continue the task and says the word "continue"; and vi) $\tilde{x}_6$, safety related issues happened such as the robot configurations are out of limits. Thus $\tilde{X} = \{\tilde{x}_1, \tilde{x}_2, \tilde{x}_3, \tilde{x}_4, \tilde{x}_5, \tilde{x}_6\}$ is the set of plant symbols. However, the plant symbol $\tilde{x}_5$ needs to be further subdivided to uniquely identify the exact plant state where the task execution is paused. If the subject says "continue" while performing the task with the initial conditions in the last state, then $\tilde{x}_{51}$ is generated. If the subject says "stop" while performing the task with slow speed, then $\tilde{x}_{52}$ is generated. Similarly, if the subject says "stop" while performing the task with fast speed, then the plant symbol $\tilde{x}_{53}$ is generated.

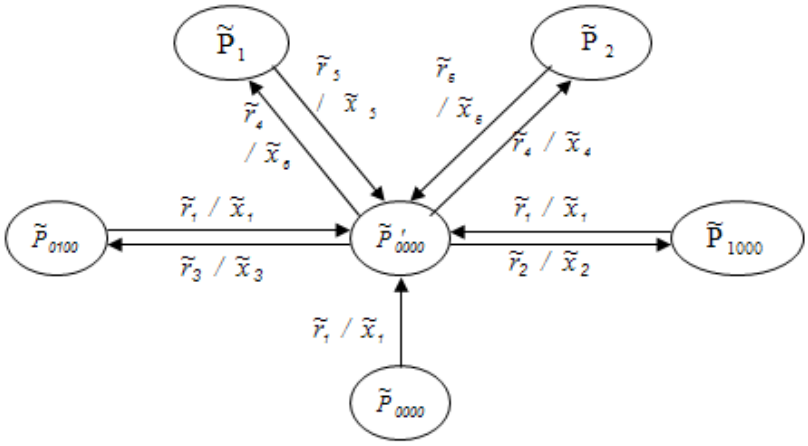

Figure II-4 DES plant for Control Architecture

High-level Supervisory Control

The high-level supervisory controller is a discrete event system that is modeled as a deterministic finite automaton specified by $D=(\tilde{S},\tilde{X},\tilde{R},\delta,\phi)$. Here, $\tilde{S}$ is the set of controller states, $\tilde{X}$ is the set of plant symbols generated by the event in plant, $\tilde{R}$ is the set of controller symbols generated by the high-level supervisory controller, $\delta:\tilde{S}\times\tilde{X}\rightarrow\tilde{S}$ is the state transition function, and $\phi:\tilde{S}\rightarrow\tilde{R}$ is the output function. The high-level supervisory controller for the reaching task is shown in Figure II-5.

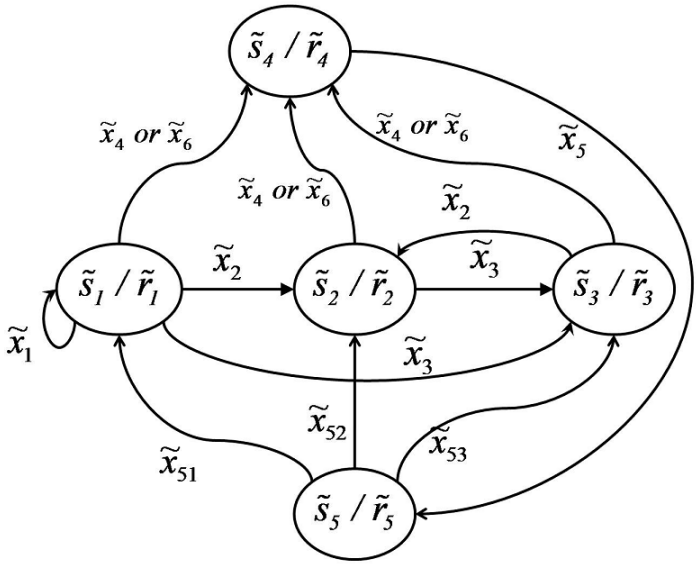

Figure II-5 High-level Supervisory Controller for Reaching Task

In Figure II-5, the convention of labeling the arcs is to list the plant symbols, which enable the transition; the convention in the ellipse is to list the control states, followed by "/", and then the control symbols, which can be generated once the system enters the corresponding states. The control states and control symbols are defined in Table II-1.

Table II-1 Control States and Control Symbols

i	$\tilde{s}_i$	$\tilde{r}_i$
1	active with initial speed	device on
2	active with decreased speed	device speed down
3	active with increased speed	device speed up
4	idle	device off
5	active with previous speed	device on

Interface in this application is designed to recognize the above-mentioned plant symbols and control symbols. It is clear from the above discussion that the design of the various elements of the DES plant and the DES controller is not unique and is dependent on the task, the sensory information available from the robot-assisted rehabilitation system, and the subject's verbal feedback.

Results

The main focus of this paper is to present the control architecture and the high-level supervisory controller design which was shown in Figure II-5. However, the human intention recognition system is an important part of this new control framework that is responsible for generating the commands to the high-level controller based on patient's verbal feedback to modify the task requirements. Hence we first summarize the validation of the evaluation of human intention recognition system.

Validation of Human Intention Recognition System

Recognition accuracy of human intention recognition system has been checked with both healthy subjects and stroke patients. First, 10 healthy subjects were invited to our

laboratory to record the voice signals of the four words which were “slow”, “fast”, “stop” and “continue”. 4 females and 6 males, 20-32 years old, right-handed, unimpaired subjects participated in this study. Voice from each subject was captured by a microphone and then it was sampled by the data acquisition module in Matlab R2007a at a sampling rate of 8 kHz using a sound card installed in the PC. Each single word was recorded three times and was then normalized for every sample to an equivalent level to find the arithmetic average. Then the MFCCs of average signals of each word for each subject were computed to be used as the reference set for pattern matching.

Subsequently, each subject was asked to speak any of these four words 10 times in a random order and the output speech signal was recorded. We then analyzed how many times the voice recognition system correctly identified the spoken words for the healthy subjects (Table II-2). In general, it can be seen that the human intention recognition system successfully recognized the spoken words for all 10 subjects with high accuracies.

Additionally, we evaluated the recognition accuracy of the proposed human intention recognition system with stroke patients. 1 female and 3 male subjects within the age range of 65-78 years took part in the study. Each patient was asked to speak any of these four words 5 times in a random order. The experiments were conducted at the Vanderbilt Stallworth Rehabilitation Hospital under the supervision of an occupational therapist. The stroke patients who participated in this study had no aphasia or language deficits interfering output of the speech. However, the quality and clarity of spoken words could be an issue. We then analyzed how many times the voice recognition system correctly identified the spoken words for the stroke patients (Table II-3). As can be seen from

Table II-3, the proposed human intention recognition system successfully recognized the spoken words of stroke patients with recognition accuracy between 90% and 100%.

Table II-2 Human Intention Recognition System Accuracy (%) for Healthy Subjects

Subject	Accuracy (%)			
	Slow	Fast	Stop	Continue
1	90	100	100	100
2	80	100	100	100
3	100	100	90	100
4	90	100	80	100
5	90	100	90	100
6	90	100	100	100
7	100	100	100	100
8	100	90	100	100
9	100	100	100	100
10	90	100	100	100

Table II-3 Human Intention Recognition System Accuracy (%) for Stroke Subjects

Subject	Accuracy (%)			
	Slow	Fast	Stop	Continue
1	100	100	90	100
2	90	100	100	100
3	100	100	90	100
4	100	100	100	100

Evaluation of the Proposed Control Architecture

Experiment Procedure

Subject is seated in a height adjusted chair as shown in Figure II-2. The height of the PUMA 560 robotic manipulator has been adjusted for the subject to start the rehabilitation task in the same arm configuration. The starting arm configuration is selected as shoulder at neutral 0° position and elbow at 90° flexion position. The task requires moving the arm in forward flexion to approximately 60° in conjunction with elbow extension to approximately 0°. Subject is asked to place his/her forearm on the hand attachment device as shown in Figure II-2 when the starting arm configuration is fixed. The push button has been given to the subject that can be used during the task execution in case of emergency situations. The subject receives visual feedback of their position on a computer monitor on top of the desired position trajectory which is placed in front of him/her. Subject is asked to practice the tracking rehabilitation task (described in previous section) 10 times to familiarize him/herself with the task.

Results

Since we experiment with unimpaired subjects who could ideally do the reaching task by themselves (unlike a real stroke patient), we instructed the subjects to be passive so that we can demonstrate that the proposed control architecture was solely responsible for the modification of the task based on subject's verbal feedback. Such an experimental condition is not only helpful to unambiguously demonstrate the efficacy of our proposed control architecture but also could occur when a low functioning stroke survivor

participates in a rehabilitation therapy who will initially need continuous robotic assistance to perform the required rehabilitation task.

We had conducted two experiments to demonstrate the feasibility and usefulness of the proposed control architecture in enabling robotic assistance to a subject to complete the tracking task based on subject's verbal feedback (intention). The subjects were asked to express their intention using one of the following words: "fast", "slow", "stop" and "continue" during the execution of the task. We only presented one set of the subjects' data to demonstrate the efficacy of the proposed control architecture. Initial desired velocity was selected as 0.02m/s, which was chosen in consultation with an occupational therapist who works with stroke patients at the Vanderbilt Stallworth Rehabilitation Hospital.

In the first experiment (E1), the subject was instructed to modify the tracking task only once. When the tracking task started, $\tilde{s}_1$ became active and the initially defined task requirements were used to define the desired trajectory for the subject to be followed (Figure II-6 I-middle). If the subject is comfortable with the initial task requirements then the task execution will be completed with the initially defined parameters (Figure II-6 I-right). However if at point A, the subject said "slow" (he might feel the required motion is too fast for him) (Figure II-6 II-left) and then the human intention recognition system compared the spoken word with the reference ones using the pattern matching module (as described in previous Section) and detected hypersurface h_2 was crossed then $\tilde{x}_2$ was generated. This event was recognized by the high-level controller through the microcontroller. When $\tilde{x}_2$ was generated while $\tilde{s}_1$ was active, then $\tilde{s}_2$ state became active and $\tilde{r}_2$ was generated and sent to low-level controller to change the speed of the task

(Figure II-6 II-middle). Then the subject was required to continue the tracking task with a slower movement (Figure II-6 II-right solid line). If the subject's intention to slow down the movement was not considered then the desired motion trajectory that the subject was required to follow would be the dashed line in Figure II-6 II-right. This could create an unsafe operating condition because the subject could not continue the task execution with a high speed. Later, the subject said "fast" (he thinks the movement was too slow for him) (Figure II-6 III-left) and then human intention recognition system detected h_3 was crossed then $\tilde{x}_3$ was generated. When $\tilde{x}_3$ was generated while $\tilde{s}_1$ was active, then $\tilde{s}_3$ state became active and $\tilde{r}_3$ was sent to low-level controller (Figure II-6 III-middle). Now the subject was required to move faster to complete the tracking task (Figure II-6 III-right solid line). If the subject's intention to move faster was not considered then the desired motion trajectory that the subject was required to follow would be the dashed line in Figure II-6 III-right. This could limit the subject's movement and affect the efficiency of the therapy because he/she was able to move faster than initial speed. The increment and decrement level of the desired motion trajectory was selected as 25% more and less, respectively. The range could be increased or decreased based on the subject's movement ability.

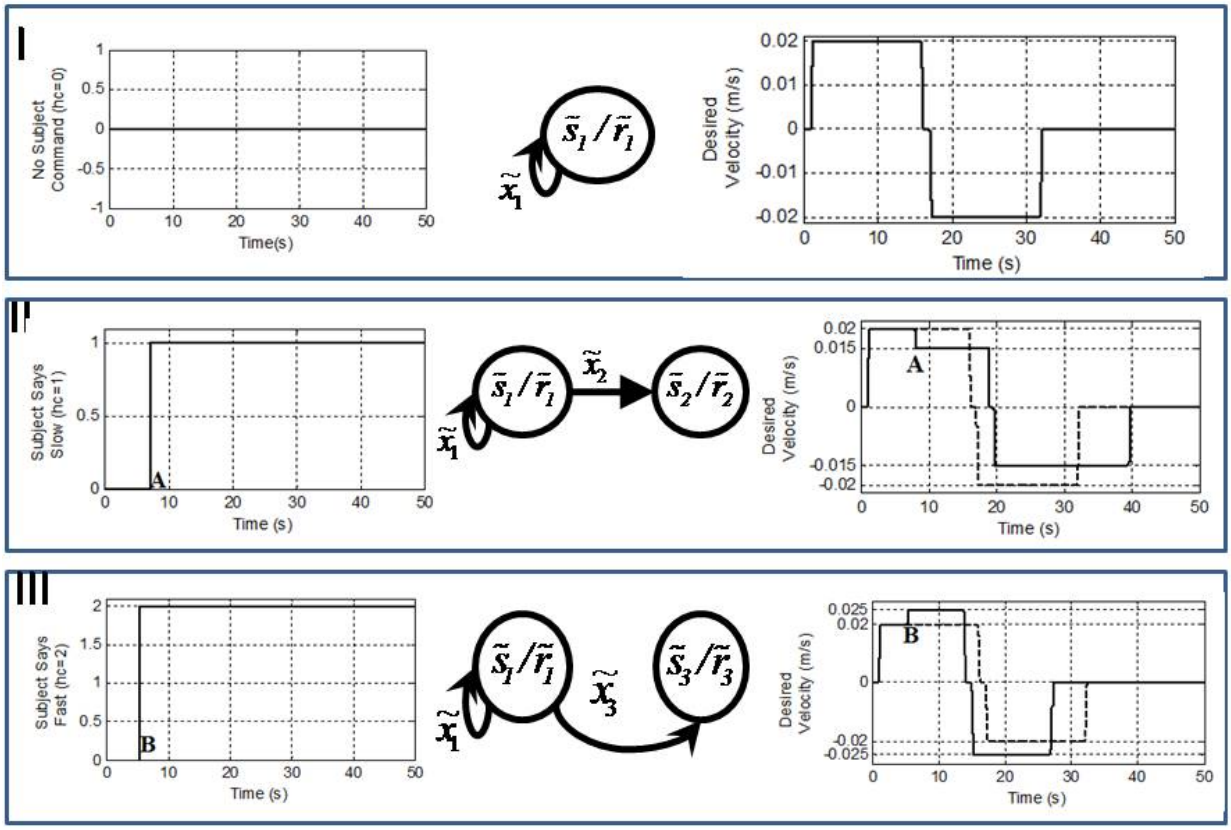

Figure II-6 Experiment 1 Results

The corresponding actual motion trajectories of the subject were shown in Figure II-7. It could be seen from Figure II-7 that the subject was able to track the modified desired motion trajectories. Thus, the actual motion trajectory was same as the desired motion trajectory because the subject was passive and the arm low-level assistive controller provided necessary robotic assistance to follow the desired motion trajectory to complete the task as required.

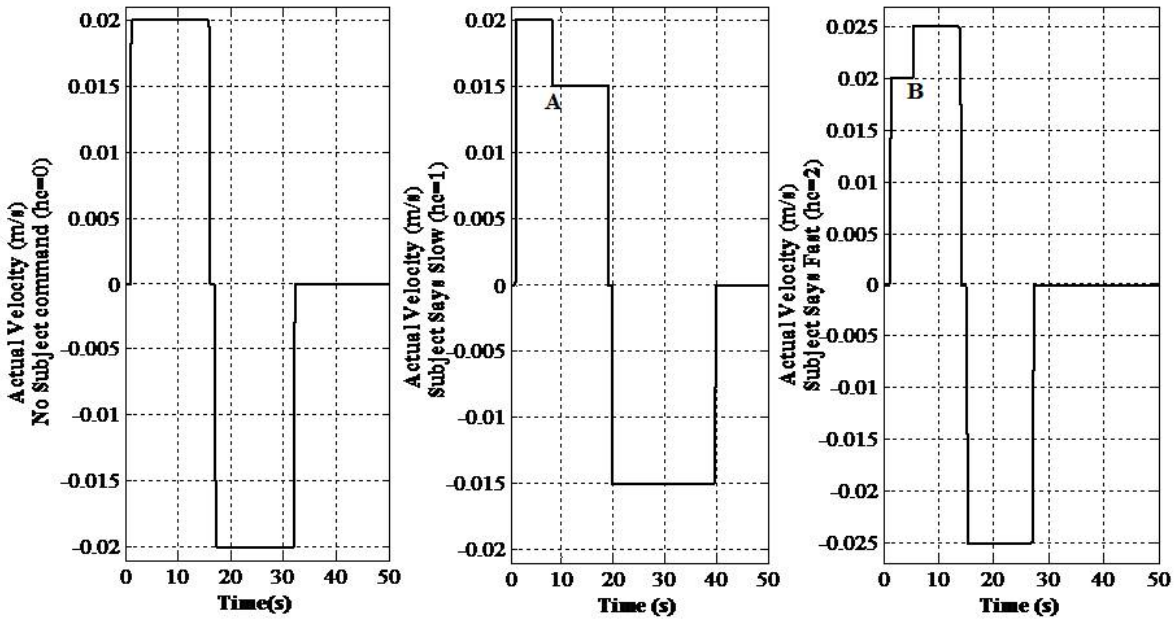

Figure II-7 Actual Velocity Trajectories for Experiment 1

In the second experiment (E2), we asked the subjects to perform the same task as in Experiment 1; however, in this case, the subjects were asked to modify the task more than once. This was done to simulate the movement of a stroke patient who may experience difficulty in performing the task with initially defined requirements. In this experiment, the subject started performing the execution of the task. Then at point A, the subject said "fast" (Figure II-8 I) then $\tilde{x}_3$ was generated, $\tilde{s}_3$ state became active and $\tilde{r}_3$ was sent to low-level controller (Figure II-8 II). Then the subject did not feel comfortable and he said "slow" at point B (Figure II-8 I). When the subject said "slow" then $\tilde{x}_2$ was generated, $\tilde{s}_2$ state became active and $\tilde{r}_2$ was sent to low-level controller (Figure II-8 II). Additionally, we had assumed a safety event had occurred when the subject was performing the task. In this experiment, at some point of time during the task the subject wanted to pause for a while by saying "stop" word and then said "continue" word to restart the task execution where he resumed for completion of the rest of the task (Figure

II-8 I). When the subject said "stop" at point C, then $\tilde{x}_4$ was generated and $\tilde{s}_4$ state became active and $\tilde{r}_4$ is generated (Figure II-8 II). Later when the subject said "continue" at point D, then $\tilde{x}_5$ was generated and $\tilde{s}_5$ state became active and instantaneously $\tilde{x}_{52}$ was generated to go back to state $\tilde{s}_2$ so that subject could continue the task execution where he resumed (Figure II-8 II). This scenario might represent when a stroke patient wanted to pause for a while due to some discomfort. The corresponding desired motion trajectories had been generated dynamically as shown in Figure II-8 III. On the other hand, if we did not use the proposed high-level controller, the desired motion trajectory would not have been automatically modified to register the intention of the subject to pause task execution, to move faster or slower. As a result, the motion trajectory would have followed the dashed line in Figure II-8 III. In such a case, when subject wanted to move faster he would still move with initially defined speed at point A' (Figure II-8 III-dashed line). Furthermore, the desired motion trajectory would start at point C' with non-zero velocity (Figure II-8 III, dashed line), which could create an unsafe operating condition. In addition, since the desired motion trajectory computation would not have included the pause action, restarting the task at point C' would not allow the completion of the task as desired.

High-level controller monitored the progress of the task and the subject's verbal feedback to make decisions on the modification of the task parameters. The corresponding actual motion trajectories of the subject were shown in Figure II-8 IV. It could be seen from Figure II-8 IV that the subject was able to track the modified desired motion trajectory to complete the task in a desired manner. The actual motion trajectory given was same as the desired motion trajectory because the subject was passive and the

arm low-level assistive controller provided necessary robotic assistance to follow the desired motion trajectory to complete the task as required.

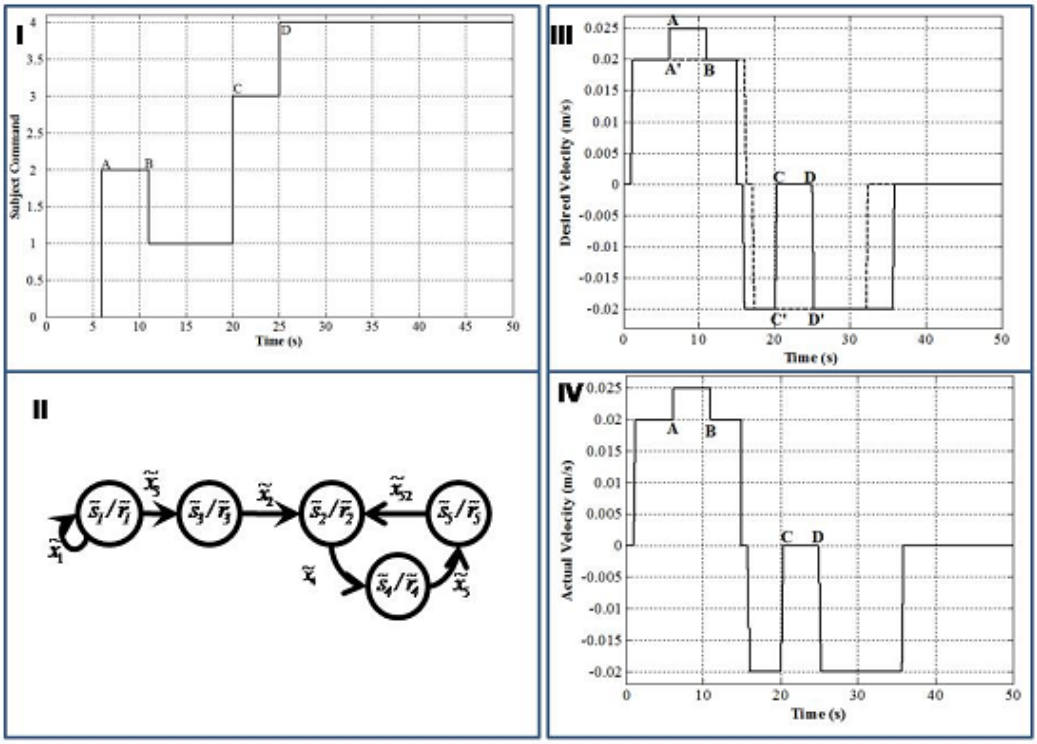

Figure II-8 Experiment 2 Results

Discussion and Conclusion

In this paper we have designed an intelligent control architecture, 1) to monitor the task, safety issues, provide assessment of the progress and alter the task parameters, and 2) to incorporate patient's feedback in order to make the necessary modifications to impart effective therapy during the execution of the task in an automated manner. The control architecture is based on hybrid control that provides theoretical solidity to the existing rehabilitation approach. This architecture provides flexibility so that new safety features as well as new task requirements can be incrementally added to the system by designing new events either by adding new sensors or by further analyzing the current sensory information and by adding new decision rules in the high-level controller.

It is also important to include patient's feedback inside the control architecture because patients should be able to express how they feel about the task, which will then be used to make the necessary modifications about the presentation of the task to accommodate any problem patients perceive during the execution of the task. However, it is not possible to integrate spoken words into the system directly. Thus, we include patient's feedback as words in terms of events like other sensor events inside the control architecture.

As could be seen from the above discussion, hybrid system based control architecture could be useful in robot-assisted system in terms of monitoring safety, assisting patient, and incorporating patient's feelings, which are actually actions of the therapists during the therapy. Thus, the presented control architecture will be helpful to automate some of the actions of the therapists. During the therapy, if a task requirement changes or if the patient does not feel comfortable to move his/her arm at a specified speed, then he/she may speak out and, then a therapist/technician would need to adjust the computer code to reflect these changes. It is conceivable that one cannot anticipate all possible events that might occur during a rehabilitation task. The proposed hybrid system based control architecture provides a systematic procedure to effect changes such that the task execution could be automated. Instead of preprogramming numerous static trees based on if-then-else rules, it provides a dynamic mechanism of generating events that leads to necessary high-level decisions.

We have conducted experiments with unimpaired subjects to demonstrate the efficacy of the proposed control architecture. The results have shown that the task parameters can be determined dynamically based on subject's spoken words and safety-related events to

generate the necessary motion trajectories at the required time using the proposed control architecture. The speed of motion is used as the task parameter in this paper. However, note that sometimes patients cannot move to the initially defined target positions because of their limited movement ability. Thus, in the case the proposed control architecture can be used to determine other task parameters such as a desired reaching position. Subjects can express their intention to move further away from the initially defined target position or closer to themselves using spoken words. In such a case, for example, the high-level controller in the control architecture can determine the target position based on the subject's verbal feedback while monitoring the safety-related events. Thus, new spoken words such as "further", "closer" etc can be included inside the human intention recognition system and then related events and their decision-rules can be defined inside the control architecture as new events.

The proposed control architecture, although implemented on a PUMA 560 robot, is independent of any particular robot and thus can be easily integrated into other existing robot-assisted rehabilitation systems.

As a future work, it is planned to investigate the efficacy of human intention recognition included methodology with severely impaired stroke patients and how it will influence patients' participation in the therapy regime.

Acknowledgment

We gratefully acknowledge the help of occupational therapist Sheila Davy of Vanderbilt University's Stallworth Rehabilitation Hospital for her feedback about our

experimental setup, the task design and giving permission to test the human intention recognition techniques with stroke patients during this work.

References

[1] D.B. Matchar, P.W. Duncan: Cost of stroke, Stroke Clin Updates, 5, 9-12 (1994).

[2] American Heart Association: Heart and Stroke Statistical Update, http://www.Americanheart.org/statistics/stroke.htm (2006).

[3] E. Taub: Harnessing Brain Plasticity through Behavioral Techniques to Produce New Treatments in Neurorehabilitation. American Psychologist, 59(8), 692-704 (2004).

[4] H. I. Krebs, M. Ferraro, S. P. Buerger, M. J. Newbery, A. Makiyama, M. Sandmann, D. Lynch, B. T. Volpe, and N. Hogan, "Rehabilitation robotics: pilot trial of a spatial extension for MIT-Manus," J Neuroengineering Rehabil, vol. 1, p. 5, (2004).

[5] P. S. Lum, C. G. Burgar, H. F. M. Van der Loos, P. C. Shor, M. Majmundar, and R. Yap, " MIME robotic device for upper-limb neurorehabilitation in subacute stroke subjects: A follow-up study," J. of Rehab. Research & Development, vol. 43, pp. 631-642, (2006).

[6] R. Loureiro, F. Amirabdollahian, M. Topping, B. Driessen, and W. Harwin, "Upper limb mediated stroke therapy - GENTLE/s approach," Autonomous Robots, vol. 15, pp. 35-51, (2003).

[7] T. Nef, M. Guidali and R. Riener, "ARMin III – arm therapy exoskeleton with an ergonomic shoulder actuation", Applied Bionics and Biomechanics, Vol. 6, No. 2, pp. 127–142, (2009).

[8] M. J Johnson, "Recent trends in robot-assisted therapy environments to improve real-life functional performance after stroke", Journal of NeuroEngineering and Rehabilitation, vol. 3, No. 29, pp.1-6, (2006).

[9] D.J. Reinkensmeyer, C.T. Pang, J.A. Nessler, C.C. Painter, "Web-based telerehabilitation for the upper extremity after stroke", IEEE Trans Neural Syst Rehabil Eng., vol. 10, No. 2, pp. 102-108, (2002).

[10] M. Mihelj, J. Podobnik, and M. Munih, "HEnRiE – Haptic Environment for Reaching and Grasping Exercise," in Proceedings of the 2nd Biennial IEEE/RAS-EMBS International Conference on Biomedical Robotics and Biomechatronics Scottsdale, AZ, USA, October 19-22, 2008, pp. 907-912.

[11] J. Podobnik, M. Munih, and J. Cinkelj, "HARMiS – Hand and arm rehabilitation system," in Proc. 7th ICDVRAT with ArtAbilitation, Maia, Portugal, 2008, pp. 237-244.

[12] D. Erol & N. Sarkar, "Coordinated Control of Assistive Robotic Devices for Activities of Daily Living Tasks", IEEE Transactions on Neural Systems and Rehabilitation Engineering, vol. 16, pp. 278-285, 2008.

[13] D. Erol & N. Sarkar, "Intelligent Control for Robotic Rehabilitation after Stroke", Journal of Intelligent and Robotic Systems, vol. 50, No.3, pp. 341-360, (2007).

[14] D. Erol & N. Sarkar, "Coordinated Control of Assistive Robotic Devices for Activities of Daily Living Tasks", IEEE Transactions on Neural Systems and Rehabilitation Engineering, vol.16, No.3, pp. 278-285, (2008).

[15] D. Erol Barkana & N. Sarkar, "Towards a Smooth Human-Robot Interaction for Rehabilitation Robotic Systems", Advanced Robotics, vol. 23, no. 12-13, pp. 1641-1662, (2009).

[16] D. Erol Barkana, "Towards Intelligent Robot-Assisted Rehabilitation Systems", International Journal of Systems Science, DOI: 10.1080/00207720903230039, (2010).

[17] PUMA 560 Related Sites on the Internet, http://www.ee.ualberta.ca/~jasmith/puma/pumasites.html.

[18] D. Erol & N. Sarkar, "Design and Implementation of an Assistive Controller for Rehabilitation Robotic Systems", International Journal of Advanced Robotic Systems, vol. 4, No.3, pp. 271-278, (2007).

[19] J. N. Pires. "Robot-by-voice: experiments on commanding on industrial robot using the human voice", Industrial Robot: An International Journal, Volume 32, Number 6, pp. 505-511(7), (2005).

[20] K. Kawamura, M. Bishay, S. Bagchi, A. Saad, M. Iskarous and M. Fumoto, "Intelligent user interface for a rehabilitation robot", Fourth International Conference on Rehabilitation Robotics, Wilmington, DE, pp. 31-35, (1994).

[21] R. Zhou, K. P. Ng and Y S Ng, "A voice controlled robot using neural network", Proceedings of the 1994 Second Australian and New Zealand Conference on Intelligent Information System, vol. 29, issue 2, pp. 130-134, (1994).

[22] R. P. Neco, O. Reinoso, J. M. Sabater, C. Perez, L. M. Jimenez, "Advances in natural language interaction in mobile robots used for practice education", Proceedings in World Automation Congress, vol. 15, pp. 247-252, (2004).

[23] G. W. Leng and D. P. Mittal, "A robotic system with AI", Fourth IEEE Region 10 International Conference, TENCON, Bombay, India, pp. 999-1002, (1989).

[24] A. Chatterjee, K. Pulasinghe, K. Watanabe and K. Izumi, “A particle-swarm-optimized fuzzy-neural network for voice controlled robot systems”, IEEE Transactions on Industrial Electronics, vol. 52, issue 6, pp. 1478-1489, (2005).

[25] C. Jayawardena, K. Watanabe and K. Izumi, “Controlling a robot manipulator with fuzzy voice commands using a probabilistic neural network”, Neural computing and Application, issue 2, vol. 16, pp. 155-166, (2007).

[26] S. Sigurdsson, K. B. Petersen and T. Lehn-Schioler, “Mel frequency cepstral coefficients: an evaluation of robustness of MP3 encoded music”, Proceedings of the Seventh International Conference on Music Information Retieval (ISMIR), Vicoria, Canada, pp. 286-289, (2006).

[27] E. H. C. Choi, “On compensating the mel-frequency cepstral coefficients for noisy speech recognition”, Proceedings of 29th Australasian Computer Science Conference, Hobart, Australia, vol. 48, pp. 49-54, (2006).

[28] Data Acquisition Toolbox User's Guide, Matlab R2007a, Mathworks.

[29] L. R. Rabiner and M. R. Sambur, “An algorithm for determining the endpoints of isolated utterences”, The Bell System Technical Journal, vol. 54, no. 2, pp. 297-315, (1975).

[30] X. D. Koutsoukos, P. J. Antsaklis, J. A. Stiver, and M. D. Lemmon, "Supervisory control of hybrid systems," in IEEE on Special Issue on Hybrid Systems: Theory and Applications, vol. 88, pp. 1026-1049, (2000).

[31] P. J. Antsaklis and X. D. Koutsoukos, "Hybrid Systems: Review and Recent Progress," in Software-Enabled Control: Information Technologies for Dynamical Systems, T. S. a. G. Balas, Ed.: IEEE Press, pp. 1-29, (2003).

CHAPTER III

MANUSCRIPT II: IMPACT OF VISUAL ERROR AUGMENTATION WHEN INTEGRATED WITH ASSIST-AS-NEEDED TRAINING METHOD IN ROBOT-ASSISTED REHABILITATION

Furui Wang, Duygun Erol Barkana and Nilanjan Sarkar

(This work has been published in the IEEE Transactions on Neural Systems and Rehabilitation Engineering, vol.18, no.5, pp.571-579, Oct. 2010, and partially published in the IEEE International Conference on Rehabilitation Robotics, ICORR 2009 and the IEEE/RSJ International Conference on Intelligent Robots and Systems, IROS 2009.)

Abstract

This paper investigates the impact of the integration of the visual error augmentation training method with the assist-as-needed training method in robot-assisted rehabilitation training of upper extremity. A robot-assisted rehabilitation system is developed that integrates an assistive controller, which can provide robotic assistance to the participant as and when needed, with a visual error augmentation mechanism, which amplifies the tracking error to heighten the participant's motivation to improve tracking accuracy. A crossover study is performed to evaluate the impact of the integration of the visual error augmentation method with the assist-as-needed training method. The experimental results on unimpaired participants demonstrate that improved performance has been achieved in the integrated training method.

Keywords: assistive controller, movement tracking training, robot-assisted rehabilitation, assist-as-needed training method, visual error augmentation training method

Introduction

Stroke is a highly prevalent condition [1], especially among the elderly, that results in high costs to the individual and society [2]. According to the American Heart Association (2009), in the U.S., approximately 795,000 people suffer a first or recurrent stroke each year [1]. It is a leading cause of disability, commonly involving deficits of motor function. Recent clinical results have indicated that movement assisted therapy can have a significant beneficial impact on a large segment of the population affected by stroke or

other motor deficit disorders. Experimental evidence suggests that intensive movement training of new motor tasks is required to induce long-term brain plasticity [3]. In recent years, robot-assisted rehabilitation of stroke patients has been an active research area, providing repetitive movement exercise and standardized delivery of therapy with the potential of enhancing quantification of the therapeutic process [4]-[14].

Various robot-assisted rehabilitation systems are developed for the upper-limb rehabilitation such as MIT-MANUS [4]-[6], Mirror Image Movement Enabler (MIME) [7], [8], Assisted Rehabilitation and Measurement (ARM) Guide [9], [10] and GENTLE/s [11]. Similarly robotic systems for wrist rehabilitation have also been reported in recent years [12]-[14]. Studies with these robotic devices verified that robot-assisted rehabilitation results in improved performance of functional tasks. The promising results of robot-assisted rehabilitation systems indicate that robots could be used as effective rehabilitation tools.

Recent research in [15] has suggested that in robot-assisted rehabilitation, assisting every movement of a patient is not as beneficial compared to no assistance or assistance as needed, although it is equivalent in some situations. It has also been proposed in [10], [16] that performance-based therapy showed better results in improving patients' impairment scores than conventional therapies. Thus, a robot-assisted rehabilitation system could be more efficient if the robotic assistance provided to the patient is given as and when needed based on the performance of the patient, which is called assist-as-needed training method. It has also been demonstrated that movement tracking training that requires cognitive processing achieved greater gains in performance than that of movement training that did not require cognitive processing [17]. Meanwhile, latest

research in many models and artificial learning systems such as neural networks suggest that error drives sensory-motor learning of a person, so that one can learn adaptation more quickly if the error is larger [18]. Such error-driven learning processes are believed to be central to adaptation and the acquisition of skill in human movement [19], [20]. It has been shown that visual error augmentation can improve the rate and extent of motor learning in healthy participants and may facilitate neuro-rehabilitation strategies that restore function in brain injuries such as stroke [21]. Feedback distortion has also been utilized to augment the controllability of human limb motion [22] and shown to elicit functional improvements in patients with chronic stroke and traumatic brain injury [23].

As can be seen from the above discussion, both assist-as-needed and visual error augmentation training methods separately have shown promising results in robot-assisted rehabilitation of upper extremity. However, none of the existing robot-assisted rehabilitation system, to our knowledge, is designed to integrate these two training methods together. The objective of this work is to investigate the impact of the integration of these two training methods in robot-assisted rehabilitation of upper extremity. A robot-assisted rehabilitation system that was developed previously by the authors [24] is further enhanced to integrate an assistive controller, which can provide robotic assistance to the participant as and when needed, with a visual error augmentation mechanism, which amplifies the tracking error to heighten the participant's motivation to improve tracking accuracy for this work. Twenty unimpaired participants performed a reaching task in two sessions with only assist-as-needed training method and the integration of the assist-as-needed with the visual error augmentation training methods in different sequences. Nineteen out of twenty participants showed significantly improved

performance in the integrated training session. Thus, it is reasonable to believe that the integration of the visual error augmentation with the assist-as-needed training methods has improved the outcome of the training performance on healthy participants.

This paper is organized as follows. It first presents the robot-assisted rehabilitation system in Section II. The task description, training paradigms, experimental protocol and task parameters are presented in Section III. Experimental results and analysis are given in Section IV. Section V is the discussion of the experimental results and the potential contribution of this work. Section VI concludes the paper and gives the possible future research directions.

The Robot-Assisted Rehabilitation System

A PUMA 560 robotic manipulator is used as the main hardware platform in this work. The manipulator is augmented with a force-torque sensor and a hand attachment device (Figure III-1). An assistive controller is developed to provide robotic assistance to the participants.

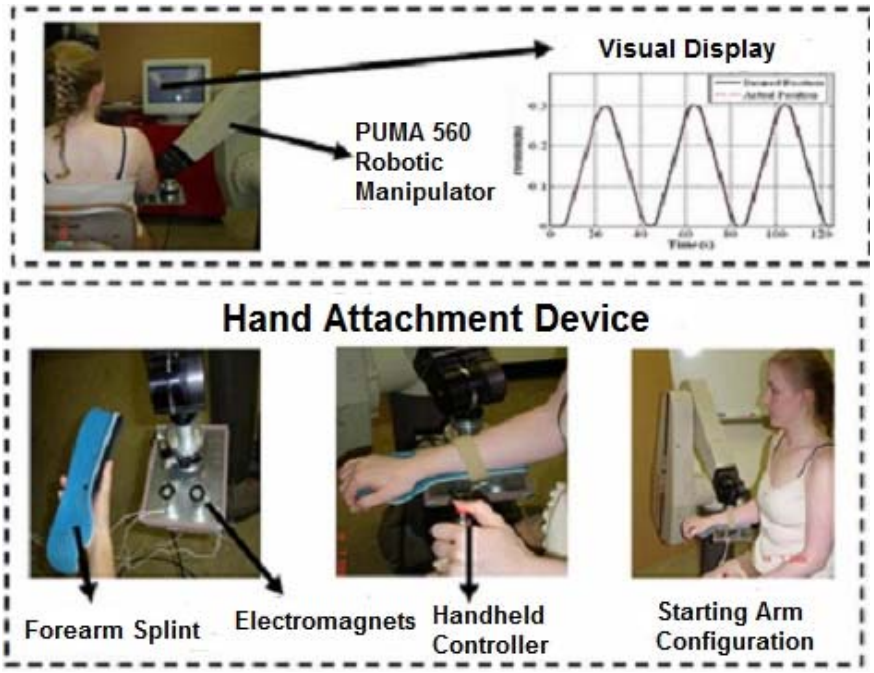

Figure III-1 The Robotic System

Robot Platform

The PUMA 560 manipulator is a 6 degrees-of-freedom (DOF) device consisting of six revolute axes. Each major axis (joints 1, 2 and 3) is equipped with electromagnetic brake, which is activated when power is removed from the motors, thereby locking the robot arm in a fixed position. The technical specifications of this robotic device can be found in [25]. In order to record the force and torque, an ATI Gamma force/torque sensor is used. The robot has been interfaced with Matlab Simulink/Realtime Workshop to allow fast and easy system development. The force values recorded from the force/torque sensor are obtained using a National Instruments PCI-6031E data acquisition card with a sampling rate of 1000Hz. The joint angles of the robot are measured by encoders and received by the computer through a Measurement Computing PCIQUAD04 card with a 1000Hz sampling rate. The torque output calculated by the Simulink model is sent to the robot through a Measurement Computing PCIM-DDA06/16 card with the same sample rate. A

computer monitor is placed in front of the participant to provide visual feedback about his/her motion trajectory during the execution of the task. Design details of the system can be found in [24].

Hand attachment device

In order to provide robotic assistance to the participant's upper arm, a hand attachment device (Figure III-1 bottom) is designed where the participant's arm is strapped into a splint that restricts wrist and hand movement. The PUMA 560 manipulator is coupled with the hand attachment device to provide assistance to the upper arm movement. An ATI gamma force/torque sensor is placed between the manipulator and the aluminum plate to provide a rigid connection and force measurement. The hand attachment device consists of an aluminum plate with two small flat-faced electromagnets (from Magnetool Inc.) fixed on it, and a forearm padded splint (from MooreMedical) attached to the aluminum plate by the magnetic power. These electromagnets are rated for continuous duty cycle (100% duty cycle) at normal room temperature. Pull rating of each magnet is 40lbs. Two electromagnets are installed to generate sufficient pulling force to keep the splint attached to the hand attachment device. An automatic release (AU) rectifier controller (Magnetool Inc.) has been used to provide a quick, clean release of these electromagnets. A handheld controller, which has been connected to the AU Rectifier Controller, is used to magnetize and demagnetize the electromagnets when the participant wants to remove the hand attachment device from the robotic manipulator in a safe and quick manner.

Assistive Controller Design

The assist-as-needed controller designed in this work is responsible for providing robotic assistance to the participant to complete the movement tracking task in the task-space in an accurate manner. In this controller, an outer force feedback loop is designed around an inner position loop (Figure III-2). The tracking of the reference trajectory is guaranteed by the inner motion control [29]. The desired force, which is given as a force reference to the controller, is computed by a planner. The proposed controller is similar to an impedance controller; however it allows specifying the reference time-varying force directly. The details of the assistive controller can be found in [30], [31]. However, since this controller is integrated with the visual error augmentation module in this work, a brief discussion on the controller is presented below.

The equations of the motion for the robot are given by:

$$\Gamma = u - J^T(q) \cdot F = M(q)\ddot{q} + V(q,\dot{q}) + G(q) \tag{1}$$

where $M(q)$ represents the inertia matrix, $V(q,\dot{q})$ is the summation of the Coriolis torques and centrifugal torques, and $G(q)$ is the vector of gravity torques. Γ is the generalized joint force which is calculated using $u - J^T(q)F$, where u is the input to the manipulator, $J(q)$ is the Jacobian matrix and F is the contact force exerted by the manipulator.

Using inverse dynamics control, the manipulator dynamics are linearized and decoupled via feedback. Control input u to the manipulator is designed as follows:

$$u = M(q)y + V(q,\dot{q}) + G(q) + J^T F \tag{2}$$

Here, $y = \ddot{q}$ represents a new input. The new control input y is designed so as to allow tracking of the desired force F_d. For this purpose, the control law is selected as follows:

$$y = J(q)^{-1} M_d^{-1}(-K_d \dot{x} + K_p(x_f - x) - M_d \dot{J}(q,\dot{q})\dot{q}) \tag{3}$$

where x_f is a suitable reference to be related to force error; M_d (mass), K_d (damping) and K_p (stiffness) matrices specify the target impedance of the robot; x and $\dot{x}$ are the position and velocity of the end-effector in the Cartesian coordinates, respectively. The relationship between the joint space and the task space acceleration is used to determine position control equation:

$$\ddot{x} = J(q)\ddot{q} + \dot{J}(q,\dot{q})\dot{q} = J(q)y + \dot{J}(q,\dot{q})\dot{q} \tag{4}$$

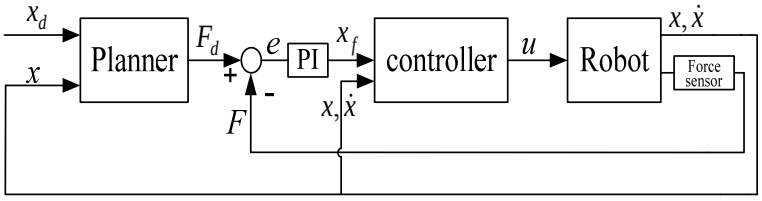

Figure III-2 The Assistive controller

By substituting Equation (3) into Equation (4),

$$\begin{aligned} \ddot{x} &= J(q)\{J(q)^{-1} M_d^{-1}[-K_d \dot{x} + K_p(x_f - x) - M_d \dot{J}(q,\dot{q})\dot{q}]\} + \dot{J}(q,\dot{q})\dot{q} \\ \ddot{x} &= -M_d^{-1} K_d \dot{x} + M_d^{-1} K_p(x_f - x) \end{aligned} \tag{5}$$

$$M_d \ddot{x} + K_d \dot{x} + K_p x = K_p x_f \tag{6}$$

Equation (6) shows the position control tracking of x with dynamics specified by the choices of K_d, K_p and M_d matrices. Impedance is attributed to a mechanical system characterized by these matrices that allows specifying the dynamic behavior. Let F_d be the desired force reference, which is computed using a PID loop:

$$F_d = P_d(x_d - x) + I_d \int (x_d - x)dt + D_d \frac{d(x_d - x)}{dt} \quad (7)$$

where x_d , x , P_d , I_d and D_d are the desired position, actual position, the proportional, integral and derivative gains of the PID position loop, respectively. The relationship between x_f and the force error is expressed in Equation (8) as:

$$x_f = P(F_d - F_i) + I \int (F_d - F_i)dt \quad (8)$$

where P and I are the proportional and integral gains, respectively. The P, I, gains are tested in our previous work to guarantee a smooth and sufficient assistance to the participant [31]. F_i is the force applied by the human. Equations (6) and (8) are combined to obtain below equation:

$$M_d\ddot{x} + K_d\dot{x} + K_p x = K_p(P(F_d - F_i) + I\int (F_d - F_i)dt) \quad (9)$$

From Equation (9), the desired force response is achieved by controlling the position of the manipulator.

Smooth Switching

Note that in the proposed rehabilitation task, the assistive controller switches on and off to provide robotic assistance to the participant only when needed. In order to avoid rough pushing and ensure smooth switching, a switching mechanism is introduced to guarantee smooth switching for satisfactory force response [30]. This mechanism defines the position reference at the time right after the switching occurs, which is also the input for the inner loop of the assistive controller, to be equal to the position reference at the

time right before the switching occurs, so that no sudden change in position will happen during the switching.

The control action in Equation (8) can be modified as below:

$$x_{fp}(t) = x(t), x_{ff}(t) = P * e_f(t) + I * (x_i(t) + x_{io}) \tag{10}$$

where $x_{fp}(t)$ is the position reference when the assistive controller is not active, which is equal to the current position of the human/robot $x(t)$. $x_{ff}(t)$ is the position reference determined using the P and I gains when the controller is active. $x_i(t)$ represents the error integral action $\int (F_d - F_i)dt$, and x_{io} is the initial condition of the error integrator. $e_f(t)$ is the force error defined as $F_d - F_i$. If t_s is the time of switching, the position reference just before and after the time of switching can be found using (11), respectively:

$$\begin{aligned} &x_{fp}(t_s^-) = x(t_s^-), \\ &x_{ff}(t_s^+) = P * e_f(t_s^+) + I * (x_i(t_s^+) + x_{io}) \end{aligned} \tag{11}$$

where t_s^- is moment just before the switching occurs, t_s^+ is the moment just after the switching occurs. The integral action associated with the assistive controller is reset during the switching so $x_i(t_s^+) = 0$. The initial condition of the integrator is set as $x_{io} = x(t_s^-)/I$. The force error $e_f(t_s^+)$ is set to zero just after the time of the switching so $P * e_f(t_s^+) = 0$. When these conditions are substituted in Equation (11), we get Equation (12). Equation (12) ensures that the position reference is indeed continuous during switching, which guarantees smooth activation and deactivation of the controller.

$$x_{ff}(t_s^+) = x_{fp}(t_s^-) \tag{12}$$

Safety Consideration of the Robotic System

Ensuring safety of the participant is a very important issue when designing a robot-assisted rehabilitation system. Thus, in case of emergency situations, the therapist can press a power button to stop the PUMA robot. With the quick-release hand attachment device, the patient and/or the therapist can also quickly release the patient's arm from the PUMA 560 by pressing the handheld controller, which comes with the hand attachment device, to deal with any physical safety related events. When the controller is pressed, the electromagnets are demagnetized instantaneously and the participant is free to remove the splint from the robot. The controller can also be operated by the therapist. Moreover, rotation angle and torque limits of each joint of the robot are monitored inside the software to disable the robot motion to satisfy both joint and torque limits. The switching mechanism described above guarantees smooth switching between activation and deactivation of the robotic assistance.

Methods

Task Design

We choose a reaching task that is commonly used for rehabilitation of upper extremity after stroke. In this task, the participant is asked to move his/her arm in the forward direction to reach a desired point in space and then bring it back to the starting position repeatedly within a specified time, i.e., to follow a desired position trajectory. The reaching task designed here requires a combination of shoulder and elbow motion which could increase the active range of motion (AROM) in the shoulder and the elbow in preparation for later functional reaching activities in rehabilitation. The allowable motion

is restricted only to the direction of the task. For example, if the task requires the participant to move his/her arm in the Y-direction, then he/she will not be able to move the arm in X or Z directions. The idea here is to improve the ability of the participant's arm movement in one direction at a time by helping him/her improve his/her ability to complete a desired reaching task, which is an important everyday activity.

It has been shown in the literature that a movement tracking task that required cognitive processing achieved greater gains in performance than that of movement training that did not require cognitive processing [26]-[28]. In order to include cognitive processing within this reaching task, the participant is asked to follow a visually presented desired motion trajectory that is intended to command his/her concentration. The participant receives visual feedback of both the actual and the desired position trajectories on a computer screen, which is placed in front of him/her. The participant is asked to pay attention to tracking the desired position trajectory as accurately as possible, which keeps him/her focused on the task. The visual feedback is used not only to inform the participant of how closely he/she is tracking the desired motion but also as a motivational factor to keep him/her focused on the task. During the execution of the reaching task, the number of times the participant needed robotic assistance to track the desired motion is recorded.

Assist-As-Needed: Decision of Robotic Assistance Activation during Task Execution

It is intuitive that a robotic system that provides continuous assistance without considering the patient's actual performance will not be as effective as the one that does. Assisting every movement of a patient has been shown to be not beneficial compared to

no assistance or assistance as needed, although it is equivalent in some situations [15]. It has also been suggested in [16] that performance-based therapy showed better results in improving patients' impairment scores than conventional therapies. In the active-assistance therapy with the ARM Guide system reported in [10], the stroke patients who received robotic assistance when the tracking performance of their upper limbs fell outside a predefined deadband showed significant improvement in the time to complete functional tasks and in supported reaching range and velocity [10]. Thus, a robot-assisted rehabilitation system could be more efficient if the assistance provided to the patient is given only as and when needed. In our robot-assisted rehabilitation system, the assistive controller is designed to provide robotic assistance based on the participant's actual performance of the tracking task. The idea of the assistive controller in our robotic system is to assist the participant when his/her arm position goes out of the predefined acceptable position band. A similar therapy algorithm was implemented with the ARM Guide system in [10].

Initially, a desired trajectory x_d is defined and then the acceptable position band (Figure III-3) with the upper bound x_{upper} and the lower bound x_{lower} are calculated using Equation (13).

$$\begin{aligned} x_{upper} &= x_d + (x_d * percentage\ ), \\ x_{lower} &= x_d - (x_d * percentage\ ) \end{aligned} \tag{13}$$

where *percentage* is the value chosen to set the upper and lower bounds for the defined position trajectory. In order to define the task position trajectories x_d, a generator block using Matlab/Simulink Blockset is developed. This block generates the minimum-jerk position and velocity trajectories with a specified distance, maximum velocity and

acceleration using user defined function. If the actual position *x(t)* lies within the acceptable band, then the participant is considered to be able to track the trajectory without robotic assistance. If the actual position x is not between the upper bound x_{upper} and the lower bound x_{lower} , then the assistive controller is activated to provide assistance to bring the participant's position back into the desired range.

However, note that each participant requires a certain amount of time (settling time) to generate the desired motion, thus the controller should not be activated until it is determined that the participant is not able to generate the required motion by his/her own effort. Thus, the averages of the participant's actual position x_{ave} (which is different from the instantaneous position in [10]), the upper bound x_{upper}, and the lower bound x_{lower} are calculated in a given time interval. These averages are used to decide whether the robotic assistance is needed. x_{ave}, x_{upper_ave} and x_{lower_ave} are calculated using the equations:

$$x_{ave} = \frac{t_s}{(t_f - t_i)} \bullet \sum_{t_i}^{t_f} x(t), \quad x_{lower\_ave} = \frac{t_s}{(t_f - t_i)} \bullet \sum_{t_i}^{t_f} x_{lower}(t), \quad x_{upper\_ave} = \frac{t_s}{(t_f - t_i)} \bullet \sum_{t_i}^{t_f} x_{upper}(t) \qquad (14)$$

where t_f , t_i and t_s are the final time, starting time and sampling time, respectively. The participant's actual position at time t is *x(t)*.

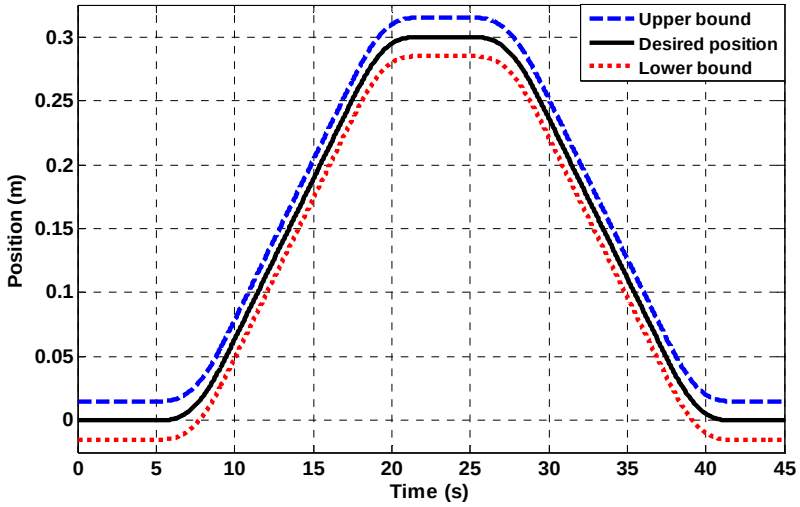

Figure III-3 The Acceptable Position Band

If condition: $x_{lower\_ave} < x_{ave} < x_{upper\_ave}$ is satisfied, then the assistive controller is not activated and the participant continues the tracking task without robotic assistance. If condition is not satisfied, then the assistive controller is activated to provide robotic assistance.

Visual Error Augmentation

It has been shown that visual error augmentation training makes small errors more noticeable to the participant and motivates the participant to make faster responses to correct the error [21]. Faster responses may lead to larger changes in performance of the participant. Additionally, amplified error can also increase signal-to-noise ratios which may improve cognitive processing and self-evaluation [21]. It has been previously verified that training performance of the patients had been improved only when the original errors had been magnified, but not when the errors were reduced or absent [32]. Hence visual error amplification training may be an effective way to promote functional

motor recovery for people after stroke. However, it is important to select a proper gain *K* in the visual error amplification. If the gain is too small, the effect of error augmentation will be quite limited; if the gain is too large, it is possible that the sensory-motor learning will become unstable, which may cause sensor inaccuracy, over-correction, and even frustration and anxiety in the participants.

In this work, the gain is selected as *2*, which is shown to elicit the best experimental result in [21]. A gain of *2* means any deviation from the desired trajectory will be displayed as twice the real distance from the desired trajectory (Figure III-4). The error *e* is calculated by equation (15). Here, x(t) is the actual arm position.

$$e(t) = x_d(t) - x(t) \tag{15}$$

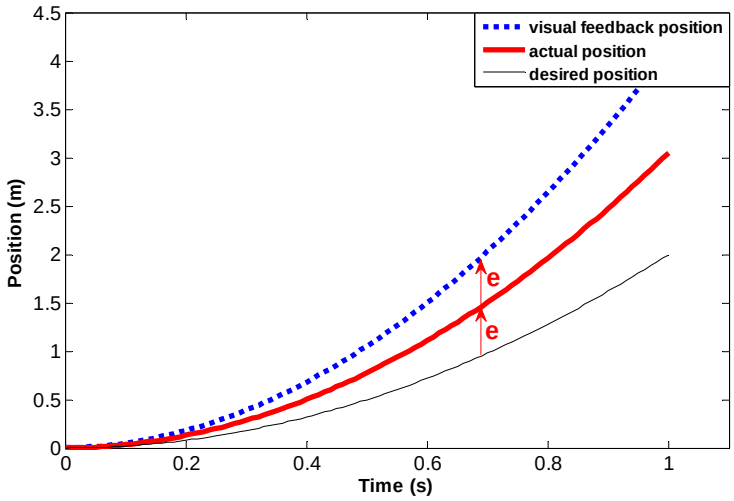

Figure III-4 Illustration of the Visual Error Augmentation.
Figure Notes: The thick line is the actual position trajectory, which is not shown on the monitor. The thin solid line is the desired position trajectory and the dotted line is the augmented position trajectory. Those two lines are shown on the monitor.

The participant's performance is expected to be better when visual error augmentation training is applied. However, for stroke patients, it may still happen that the patient is not capable of completing the task by himself/herself. In this case, the assistive controller

described in the previous section will be activated so that the robot will help the patient come back into the acceptable band to continue the task execution. Note that the errors fed back to the assistive controller are not amplified, which guarantees the robotic system works in an accurate manner.

Participants

Two groups of 10 right-handed participants between the ages of 25-35 took part in the experiment. Both groups consisted of 7 males and 3 females. None of the participants had any motor impairment in their arms.

Protocol

Participants were seated in a height adjustable chair as shown in Figure III-1 (top left) and were required to place their forearm on the hand attachment device as shown in Figure III-1 (bottom left) when the starting arm configuration was fixed. The height of the PUMA 560 robotic manipulator was adjusted for each participant to start the tracking task in the same arm configuration. The starting arm configuration was selected as shoulder at neutral 0^o position and elbow at 90^o flexion position. The task required moving the arm in forward flexion to approximately 60^o in conjunction with elbow extension to approximately 0^o and then coming back to the starting position. The release button of the hand attachment device was given to the participants in case of emergency situations during the task execution (Figure III-1 bottom middle). The participants received visual feedback of the task trajectories and their own position trajectories on a computer monitor in front of them (Figure III-1 top right).

We conducted two sessions of the experiment to evaluate the proposed robot-assisted rehabilitation system with only assist-as-needed training method (AAN Session) and the integration of the assist-as-needed with the visual error augmentation training methods (INT Session). In both sessions, the participants used their non-dominant arms to perform the task. This was done in order to create imperfect tracking condition so that the robotic training had some room to elicit improvement. In the AAN Session, the aim was to evaluate the outcome of the system with the assist-as-needed training method. Participants were required to perform the tracking task with the robotic assistance but without the visual error augmentation training. In INT Session, the aim was to evaluate the outcome of the enhanced system when the visual error augmentation training was integrated. Since the eventual aim is to apply the robot-assisted rehabilitation system to stroke patients who are not likely to complete the task by their own efforts and may need robotic assistance, we make robotic assistance available in both sessions in these experiments.

In order to make a comparison of the two presented training methods, a crossover study was performed to evaluate the difference of the training effects between the two sessions. Group A were asked to participate in the AAN Session first and then followed by the INT Session, while Group B were asked to participate in the INT Session first and then followed by the AAN Session. The two sessions of both groups were conducted with at least two weeks of interval as a washout period. The crossover design is able to increase the precision of comparison because each participant serves his/her own control, so the comparisons of treatment effect are based on within-participant variability (which is usually less than the between-participant variability). Meanwhile, the carryover effect

between the two sessions is also investigated by the between group comparison [33]. This study was approved by the Institutional Review Board of Vanderbilt University (IRB #90736).

Before each session, the participant took part in a trial practice first, during which the participant executed the same tracking task several times to get a basic understanding of the task execution. Typically, a participant practiced 3 forward and backward motions requiring no more than 3 minutes. Once the session started, the participants were asked to execute the forward and backward tracking task 25 times, which was distributed into 5 training groups. Thus the participant performed the required task 5 times in each training group without a break. The participant took a 3 to 5 minute break between two training groups. Additionally, after finishing the INT Session, the participant took part in additional practice without visual error augmentation to wash out the possible sensor-motor distortion.

Task Parameters

The maximum velocity of the task was defined as *0.02*m/s and the maximum acceleration was *0.008*m/s^2. These two parameters were chosen in consultation with an occupational therapist who works with stroke patients at the Vanderbilt Stallworth Rehabilitation Hospital. The task distance was selected from 0.2m, 0.25m or 0.3m based on the length of participants' arms. All three parameters were necessary in creating a desirable tracking task for each participant. Once these task parameters were decided, x_d, $\dot{x}_d$, x_{upper} and x_{lower} trajectories were generated by reference blocks in Simulink. Since the participants were healthy subjects, the percentage of position error band was chosen as

5%; x_{ave} , x_{upper_ave} , and x_{lower_ave} were calculated every *4* seconds ($t_f - t_i = 4$) using Equation (14); then the criterion $x_{lower\_ave} < x_{ave} < x_{upper\_ave}$ was checked to decide the activation of the assistive controller. Once activated, the robotic assistance would continue for 4 seconds. The *P* and *I* gains in Equation (8) of the assistive controller were properly selected, which guaranteed that sufficient robotic assistance was provided to move the arm position back within the acceptable position band in 4 seconds.

These parameters were chosen to challenge the participants and train them to make fast responses to errors and make the tracking more accurate. It is quite possible that the time interval to determine the activation of robotic assistance and the acceptable position band need to be adjusted in clinical application with stroke patients to encourage the patients without frustrating them to complete the training.

Experimental Results

During the experiments, the numbers of times of robotic assistance needed by participants and the actual position trajectories were recorded. For better representation of the experimental results, the participants were sorted in descending order based on their average position errors in the AAN session, i.e., Participant 1 had the largest average position error while Participant 10 had the smallest average position error in the AAN Session of Group 1; Similarly, Participant 11 had the largest average position error while Participant 20 had the smallest average position error in the AAN Session of Group 2. The participant labels were consistent for all the results presented in this work.

Activation of Robotic Assistance

The assistive controller of the robot-assisted rehabilitation system monitored the actual arm position and provided robotic assistance to keep the actual arm position within the acceptable position band when needed in both sessions. The activation of the assistive controller to provide robotic assistance for each participant was recorded.

A segment of the activation of the assistive controller for Participant 4 (as an example) is shown in Figure III-5. When the average actual position calculated over a period of *4* seconds using Equation (14) was out of the position band, the controller initiated robotic assistance, which brought the arm position back into the acceptable range within one period (*4s*). The position error during this period is shown in Figure III-6.

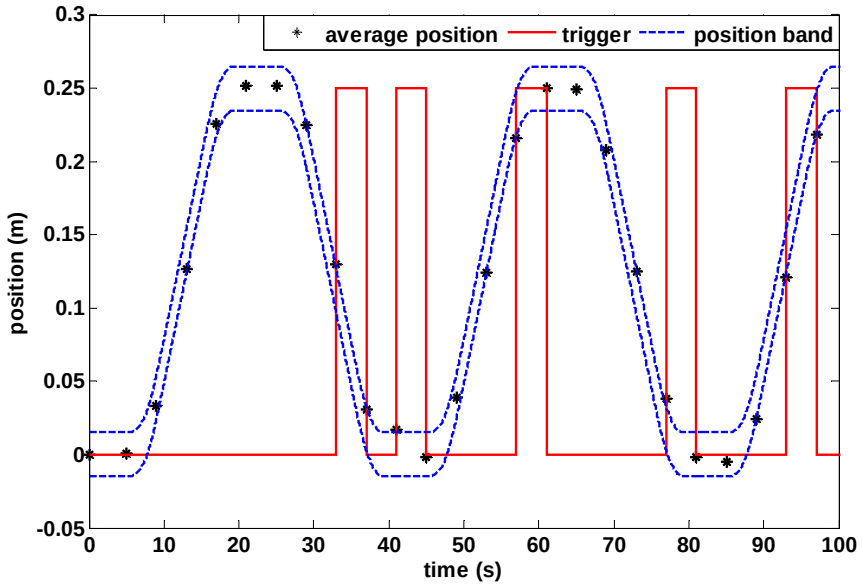

Figure III-5 Calculated Average Position Points for Participant 4 in Experiment 1.
Figure Notes: The robotic assistance was provided when the average position was out of the acceptable position band. The average positions were calculated at t=1s, 5s, 9s, 13s… in this plot.

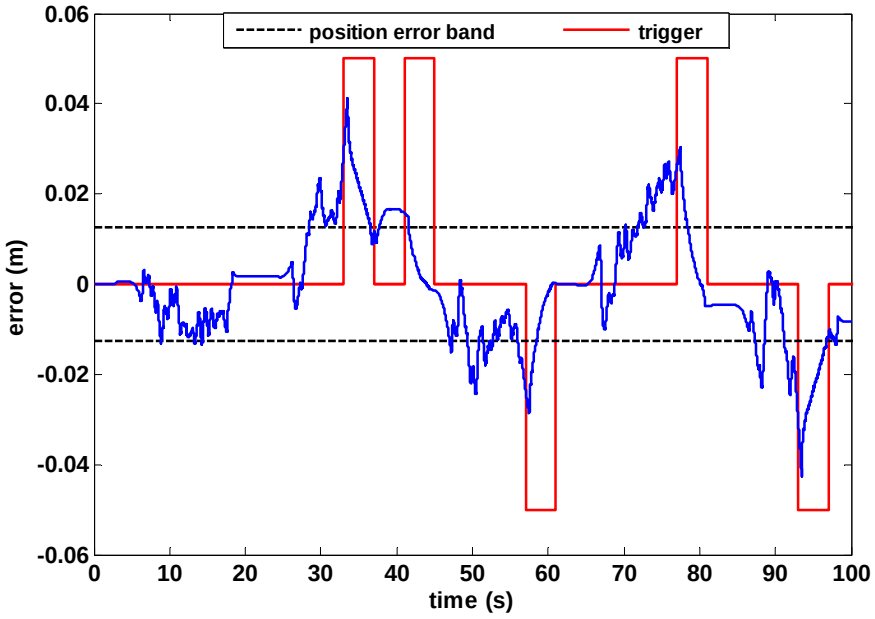

Figure III-6 The Position Error during Robotic Assistance for Participant 4

Figure Notes: Once activated, robotic assistance continued for 4 seconds and was sufficient to bring the arm position back into the acceptable error band. Note that, for example, around t=30, the robotic assistance was not activated until t=33s when it was determined that the average position error in 4s interval (t=29~33s) was out of acceptable error band.

Times of Assistance Needed

The total numbers of times of assistance needed by each participant in two training sessions for both Group A and Group B are shown in Figure III-7 and Figure III-8, respectively.

Comparing the numbers of times of assistance needed in two sessions of group A, who participated in the AAN Session followed by the INT Session, participants significantly improved their tracking performance (i.e., the participants needed less numbers of times of robotic assistance) when the assist-as-needed training method was integrated with the visual error augmentation training method in the INT Session (Figure III-7). The total number of times of robotic assistance needed by each participant decreased significantly,

for P1 (33.3%), P2 (56.41%), P3 (39.47%), P4 (76.67%), P5 (75.86%), P6 (23.81%), P7 (16.67%), P8 (36.84%), P9 (60%) and P10 (17.65%), in the INT Session compared to the AAN Session. The paired t-test, which compared the group mean of the numbers of times of robotic assistance needed by the participants in the AAN Session with that in the INT Session, showed that the difference was statistically significant ($p<0.001$).

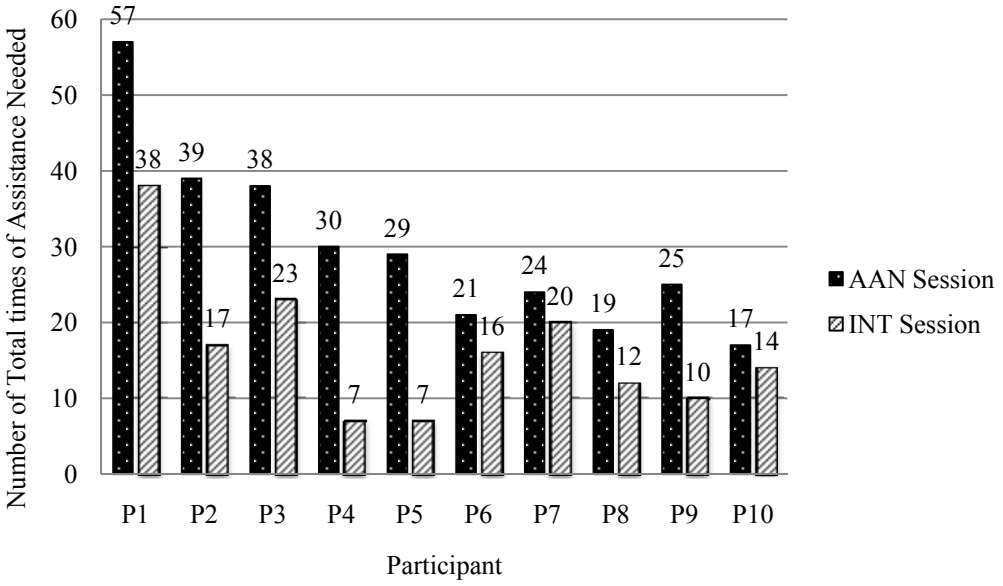

Figure III-7 Comparison of Two Sessions of Group A
Figure Notes: Each participant needed less numbers of times of robotic assistance in the INT Session.

Comparing the total numbers of assistance needed in the two sessions of Group B, who participated in the INT Session followed by the AAN Session, 9 out of 10 participants' achieved better tracking performance (i.e., the participants needed less numbers of times of robotic assistance) when the assist-as-needed training method was integrated with the visual error augmentation training method in the INT Session (Figure III-8), except for Participant 15, who showed a slight decrease in times of robotic assistance needed (9.52%). The total number of times of robotic assistance needed by

each participant increased, for P11 (17.78%), P12 (25%), P13 (8.33%), P14 (20%), P16 (27.27%), P17 (26.92%), P18 (16%), P19 (31.58%) and P20 (52.17%), from the INT Session to the AAN Session. The paired t-test showed that the difference of times of robotic assistance needed by all participants between the INT Session and the AAN Session was statistically significant ($p<0.001$).

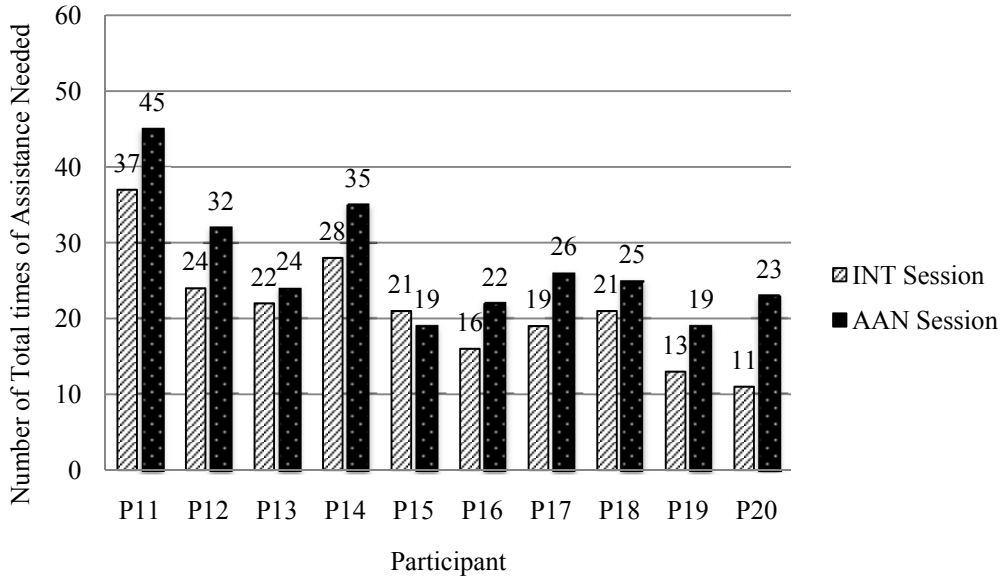

Figure III-8 Comparison of Two Sessions of Group B
Figure Notes: 9 out of 10 participant needed less numbers of times of robotic assistance in the INT Session.

Note that the carryover effects, which are the training residuals from the first training session into the second training session, might have affected the training performance in the second training session. Thus further analysis of the crossover study was performed to make a comparison of the difference of times of robotic assistance needed by the participants between the two sessions with the existence of carryover effects. Table III-1 shows the number of times of robotic assistance needed by each participant in each

session. The steps and analysis of a general two-period crossover study are briefly described in the Appendix.

Table III-1 Number of Times of Robotic Assistance Needed by Each Participant in Each Session

Group A					Group B				
ID	AAN	INT	Sum (T1i)	Difference (D1i)	ID	INT	AAN	Sum (T2j)	Difference (D2j)
P1	57	38	95	19	P11	37	45	82	-8
P2	39	17	56	22	P12	24	32	56	-8
P3	38	23	61	15	P13	22	24	46	-2
P4	30	7	37	23	P14	28	35	63	-7
P5	29	7	36	22	P15	21	19	40	2
P6	21	16	37	5	P16	16	22	38	-6
P7	24	20	44	4	P17	19	26	45	-7
P8	19	12	31	7	P18	21	25	46	-4
P9	25	10	35	15	P19	13	19	32	-6
P10	17	14	31	3	P20	11	23	34	-12

First, an unpaired t-test was carried out between T_{1i} and T_{2j} to test the equality of carryover effect. The result of the unpaired t-test showed that the difference was not significant ($p=0.813$). So the carryover effect between the AAN Session followed by the INT Session in Group A had no significant difference from that between the INT Session followed by the AAN Session in Group B, which indicated that the carryover effect was consistent between the two groups.

To test the difference of the numbers of times of robotic assistance needed by participants in two sessions, knowing that the carryover effect was not significantly different between the two groups, an unpaired t-test was performed between D_{1i} and D_{2j}. The result of one-sided unpaired t-test showed that the difference of training effects was

statistically significant ($p<0.001$), which indicated that better training performance were achieved by participants in the INT Sessions than in the AAN Sessions.

Analysis of Position Error

The average absolute position errors of each participant in both groups in two sessions were calculated using Equation (16).

$$e_{ave} = \frac{1}{5}\sum_{i=1}^{5}\left(\frac{1}{T_{f,i} - T_{s,i}}\sum_{t_{s,i}}^{t_{f,i}}\left(\left|x_{d,i}(t) - x_i(t)\right|\right)\right), \qquad (16)$$

where i is the i-th training group, $T_{s,i}$ and $T_{f,i}$ are the starting and final times of i-th training group. $x_{d,i}(t)$ and $x_i(t)$ are the desired and actual positions in the i-th training group.

In Group A, the average absolute position errors of each participant in the INT Session was much smaller than that in the AAN Session, which meant more accurate tracking performance was achieved by the participants in the INT Session (Figure III-9). The paired t-test, which compared the group mean of average absolute position errors of the participants in the AAN Session with that in the INT Session, showed that the difference of average absolute position errors was statistically significant ($p < 0.001$).

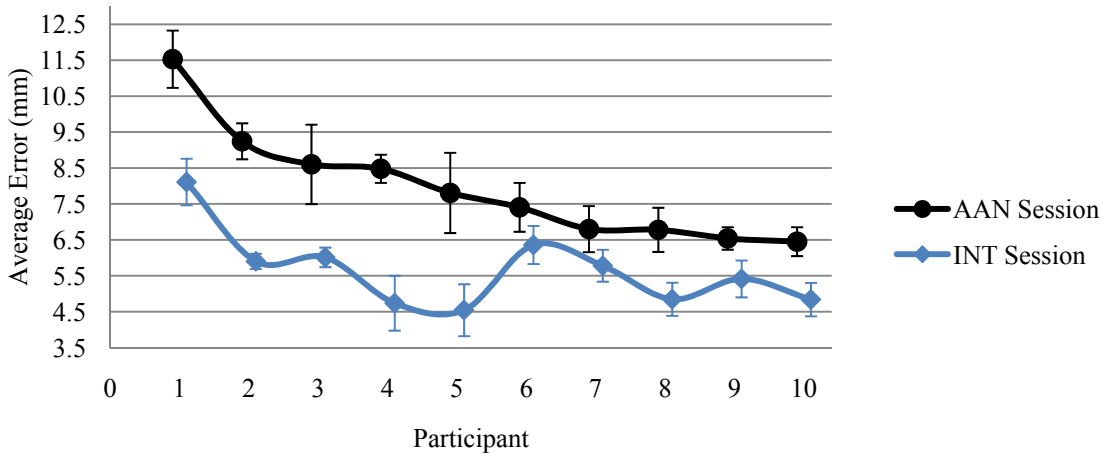

Figure III-9 The Average Absolute Position Errors in Two Sessions of Group A
Figure Notes: The average absolute position errors of all participants are smaller in the INT Session. Error bar is the standard error of the mean.

Meanwhile, in Group B, the average absolute position errors of each participant in the INT Session was still smaller than that in the AAN Session, except for Participant 15, which meant that for 9 out of 10 participants of Group B, more accurate tracking performance was achieved in the INT Session (Figure III-10). The paired t-test showed that the difference of average absolute position errors between the AAN Session and the INT Session was statistically significant ($p = 0.0014$).

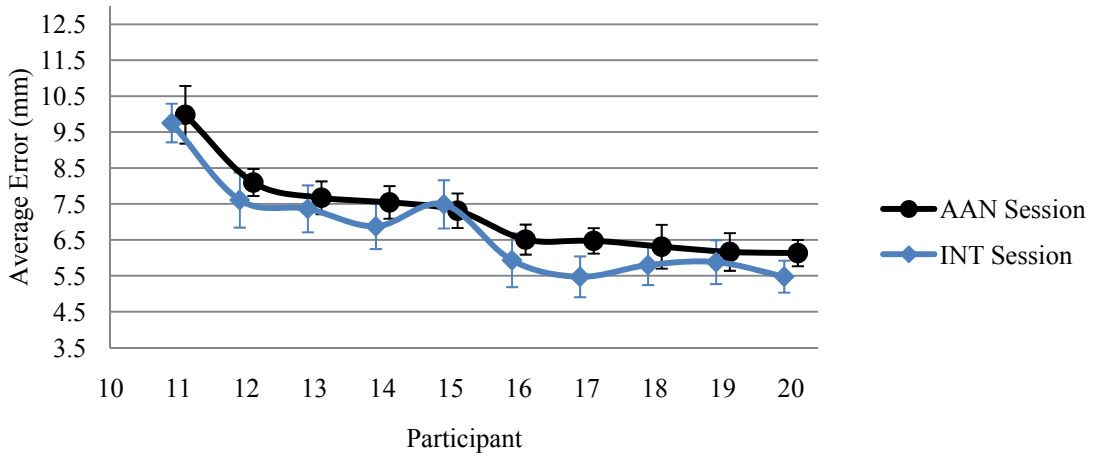

Figure III-10 The Average Absolute Position Errors in Two Sessions of Group B
Figure Notes: The average absolute position errors of 9 out of 10 participants are smaller in the INT Session. Error bar is the standard error of the mean.

The analysis of the crossover design was performed to test the difference of position error between two training sessions. Table III-2 shows the average error of each participant in both sessions. The unpaired t-test between T_{1i} and T_{2j} showed that there was no significant difference of carryover effect between the two groups ($p = 0.747$). The result of one-sided unpaired t-test between D_{1i} and D_{2j} showed that the difference of training effect between the two groups was statistically significant ($P<0.001$), which implied the participants were able to perform the tracking task more accurately in the INT Sessions.

Table III-2 Average Absolute Position Error of Each Participant in Each Sessions

Group A					Group B				
ID	INT	AAN	Sum (T1i)	Difference (D1i)	ID	INT	AAN	Sum (T2j)	Difference (D2j)
P1	11.53±0.80	8.11±0.78	19.64	3.42	P11	9.75±0.54	9.98±0.80	19.73	-0.23
P2	9.24±0.50	5.90±0.21	15.15	3.34	P12	7.61±0.77	8.10±0.38	15.71	-0.49
P3	8.60±1.11	6.01±0.27	14.62	2.59	P13	7.36±0.65	7.67±0.46	15.04	-0.31

P4	8.48±0.39	4.74±0.52	13.22	3.74	P14	6.88±0.63	7.54±0.45	14.42	-0.67
P5	7.81±1.12	4.54±0.72	12.35	3.26	P15	7.49±0.67	7.31±0.48	14.80	0.18
P6	7.41±0.68	6.36±0.53	13.76	1.05	P16	5.93±0.75	6.51±0.42	12.44	-0.57
P7	6.80±0.64	5.78±0.44	12.58	1.02	P17	5.47±0.57	6.47±0.35	11.95	-1.00
P8	6.78±0.61	4.85±0.46	11.63	1.93	P18	5.80±0.56	6.31±0.61	12.11	-0.51
P9	6.54±0.31	5.41±0.51	11.95	1.13	P19	5.88±0.61	6.16±0.52	12.04	-0.28
P10	6.45±0.40	4.84±0.46	11.29	1.61	P20	5.48±0.45	6.13±0.37	11.61	-0.65

Note: Values are mean ± standard error of the mean (SEM). Units: mm.

Discussion

The primary goal of this study was to explore the impact of visual error augmentation training method, when it was integrated with assist-as-needed training method in robot-assisted rehabilitation. Both assist-as-needed [10], [16] and visual error augmentation [21], [23], [32] training methods have been investigated separately on healthy subjects and stroke patients for upper extremity. While the algorithmic details differ in these studies, the overall ideas have been similar. In all these studies, improved performances have been achieved across training sessions. We began our investigation knowing that both these training methods, individually, had the potential to improve the rehabilitation outcome. We wanted to extend the understanding of the impact of these two training methods when they were integrated together in robot-assisted rehabilitation. In this study, significant improvements were observed in both AAN Session and INT Session, which was in agreement with the results of the prior works [10], [16], [21], [23]. The detailed performance in each training session was reported in our previous work [34]. Moreover, regardless of the sequence of the two sessions, 19 out of 20 participants needed fewer times of robotic assistance to complete the task in the INT Session. This result indicated

that the participants became more capable of executing the task when the visual error augmentation training method had been integrated with the assist-as-needed training method in the robot-assisted rehabilitation system. It was also observed that the tracking performances were better in terms of smaller average position errors for 19 out of 20 participants in the INT Session. Only one participant in Group B, who took part in the INT Session followed by the AAN Session, showed a better performance in the assist-as-needed session.

Comparing the participants' overall performances in the INT Session with that in the AAN Session within the same groups, improved training performances were achieved in the INT Session in both groups (i.e., less times of robotic assistance needed and smaller average position errors), and differences in the improvements between two sessions were statistically significant (Figure III-11 and Figure III-12, Comparison 1 and 2). Thus, it is reasonable to believe that the integration of the visual error augmentation training method with the assist-as-needed training method has contributed towards the improved training performance.

On the other hand, the unpaired t-tests for the training performances in the same training sessions of different groups did not show statistically significant differences, which means no matter conducted with or without the influence of carryover effect (Figure III-11 and Figure III-12, Comparison 3 and 4), the training effects in either training session were consistent between groups. Meanwhile, no statistically significant difference in carryover effects was observed between the two groups, which indicated the influence of carryover effects was consistent between groups.

Table III-3 Average Value for Each Group in Each Session

Variable	Group A		Group B	
	AAN Session (AAN1)	INT Session (INT1)	INT Session (INT2)	AAN Session (AAN2)
Robotic Assistance Needed	29.9±3.81	16.4±2.92	21.2±2.37	27±2.57
Average Error (mm)	7.96±0.50	5.65±0.34	6.77±0.43	7.22±0.38

Note: Values are mean ± standard error of the mean (SEM).

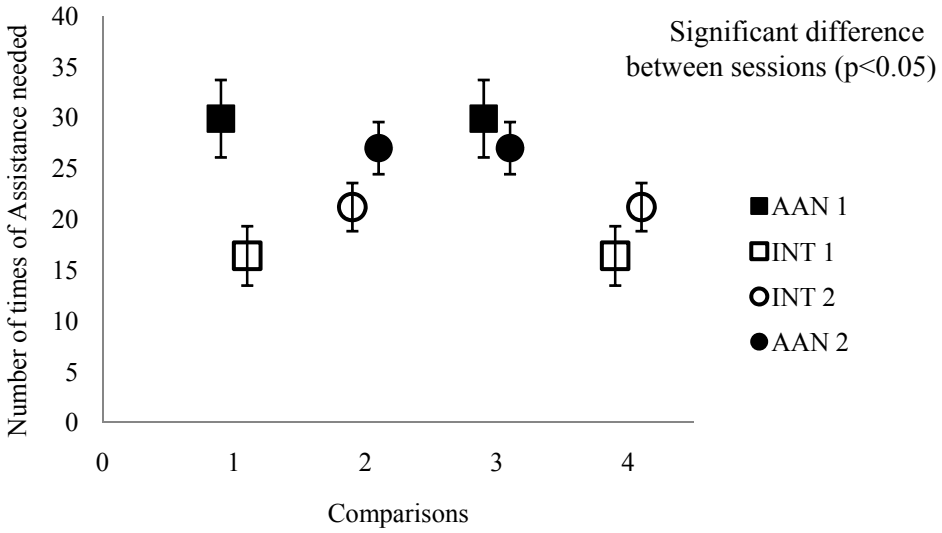

Figure III-11 The Average Number of Times of Robotic Assistance Needed in Each Session

Figure Notes: Error bars are the SEM. Note that Comparison 1 and 2 are the paired t-tests for the different sessions in the same group. Comparison 3 and 4 are the unpaired t-tests for the same sessions in different groups.

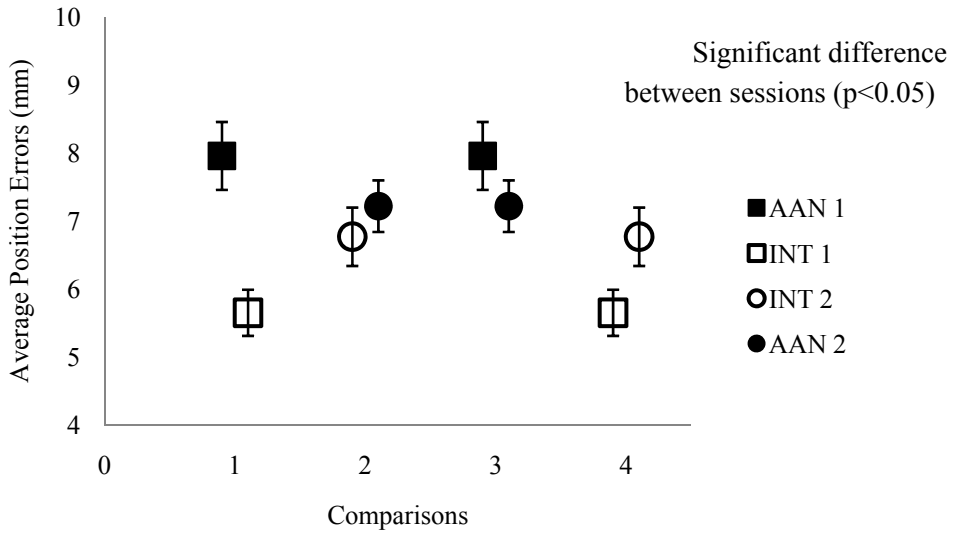

Figure III-12 The Average Position Error in Each Session (Error bars are the SEM)
Figure Notes: Note that Comparison 1 and 2 are the paired t-tests for the different sessions in the same group. Comparison 3 and 4 are the unpaired t-tests for the same sessions in different groups.

Note that this is a preliminary investigation on complex research questions such as -- what is the best training method for stroke rehabilitation? Do these training methods need to be applied separately, or are they more effective when integrated in a specific manner? Although our initial research does not address these issues in relation to stroke patients directly, the findings with unimpaired participants do suggest that an integration of visual error augmentation with assist-as-needed training methods improve the tracking performance significantly. Based on the experimental results presented here, it is reasonable to suggest that integrating visual error augmentation training method with the assist-as-needed training method might have the potential to improve the performance of stroke rehabilitation and should be explored.

Conclusion

An enhanced robot-assisted rehabilitation system, with the assist-as-needed and the visual error augmentation training methods, is evaluated with two groups of unimpaired participants in two experimental sessions. As a crossover design, Group A participants took part in the AAN training session followed by the INT training session, while the Group B participants took part in the INT training session followed by the AAN training session. The experimental results demonstrate that improved performance, in terms of times of robotic assistance needed and average position errors, are achieved in the integrated training session on unimpaired participants. The integration of visual error augmentation training method with the assist-as-needed training method might have the potential to improve the performance of stroke rehabilitation and should be further explored.

As future work, a new assistive controller, which can adaptively choose the proper control gains for participants with different levels of motor abilities, will be developed so that participants can achieve better training performance with appropriate robotic assistance. Our previous work [31] has proposed a technique that predicts proper control gains based on parameter estimation and neural network prediction methods for each participant. It is also possible to test various error amplification gains or error offset values in the visual error augmentation training method to achieve a comprehensive understanding of this training method. Additionally, an important direction for future development involves testing the usability of the enhanced robot-assisted rehabilitation system with stroke patients. Functional magnetic resonance imaging (fMRI) procedure can also be introduced to investigate whether the robot-assisted rehabilitation system that

integrates visual error augmentation with assist-as-needed training methods result in long-term brain reorganization.

Acknowledgements

This work is partially supported by NIH grants R24HD050821 and 5 R21HD055478-02. We acknowledge the help of Dr. Thomas E. Groomes, who is the Medical Director of Spinal Cord and Traumatic Brain Injury Program, and therapist Sheila Davy of Vanderbilt University's Stallworth Rehabilitation Hospital for their feedback about task design. We gratefully acknowledge Statistician Fei Ren from Abbott Laboratories for the assistance in the statistical analysis. We also gratefully acknowledge the associate editor and the anonymous reviewers for their valuable feedback during the reviews of the manuscript.

Appendix: Analysis of the crossover design

Table III-4 lists all the possible effects in a two-period crossover design [33].

Table III-4 possible effects in a general two period crossover design

Sequence	Period 1	Period 2	Sum	Difference
AB	$\mu+\pi_1+\tau_1$	$\mu+\pi_2+\tau_2+\rho_1$	$\overline{T_1}$	$\overline{D_1}$
BA	$\mu+\pi_1+\tau_2$	$\mu+\pi_2+\tau_1+\rho_2$	$\overline{T_2}$	$\overline{D_2}$

Where μ denotes the overall mean, π_i denotes the i-th period effect regardless of treatment, τ_i denotes the i-th treatment effect, ρ_i denotes the first treatment's residual or carryover effect into the second treatment in sequence i.

From the table, expectation of sum $\overline{T_1}$ and $\overline{T_2}$,

$$E(\overline{T_1}) = 2\mu + \pi_1+\tau_1+ \pi_2+\tau_2+\rho_1,\ E(\overline{T_2}) =2\mu + \pi_1+\tau_1+ \pi_2+\tau_2+\rho_2 . \quad (16)$$

Therefore, an unbiased estimator of $\rho_1 - \rho_2$, which measures the difference in carryover effects, is,

$$(\rho_1 - \rho_2)_{est} = \overline{T_1} - \overline{T_2} . \quad (17)$$

If $\rho_1=\rho_2$, the unbiased estimator of $\tau_1 - \tau_2$, which measure the average difference between treatment 1 and treatment 2, is,

$$(\tau_1 - \tau_2)_{est} = (\overline{D_1} - \overline{D_2})/2. \quad (18)$$

If $\rho_1\neq\rho_2$, the expectation of an unbiased estimator of $\tau_1 - \tau_2$ is,

$$E((\tau_1 - \tau_2)_{est}) = (\tau_1 - \tau_2) - (\rho_1 - \rho_2)/2. \quad (19)$$

In this case, an unbiased estimator of $\tau_1 - \tau_2$ is,

$$(\tau_1 - \tau_2)_{\text{corrected est}} = \overline{X_1} - \overline{Y_1} \quad (20)$$

where $\overline{X_1}$, $\overline{Y_1}$ are the measurements in Period 1 of each sequence.

So the analysis is conducted in three steps:

1) Test the equality of carryover effect between two groups with hypothesis $\rho_1=\rho_2$;

2) If the carryover effect is not equal, use only the data from the first session to test the difference of times of assistance needed by participants in two sessions;

3) If the carryover effect is equal, use data from both sessions.

References

[1] American Heart Association: Heart and Stroke Statistical Update, http://www.Americanheart.org/statistics/stroke.htm, (2009). *Updates,* vol. 5, pp. 9-12, 1994.

[2] Matchar D.B., Duncan P.W., “Cost of stroke”, Stroke Clin Updates, 5, 9-12 (1994).

[3] Judith D. Schaechter, “Motor rehabilitation and brain plasticity after hemiparetic stroke”, Progress in Neurobiology 73 (2004) 61–72.

[4] Krebs H. I., Hogan N., Aisen M.L., Volpe B.T., “Robot–aided neurorehabilitation”, IEEE Trans. on Rehab. Eng. 6, 75-87 (1999).

[5] Krebs H.I., Palazzolo J.J., Dipietro L., Ferraro M., Krol J., Rannekleiv K. , Volpe B.T. , Hogan N., “Rehabilitation Robotics: Performance-Based Progressive Robot-Assisted Therapy”, Autonomous Robots, 15(1), 7-20 (2003).

[6] Krebs H. I, Ferraro M., Buerger S.P, Newbery M. J., Makiyama A., Sandmann M., Lynch D., Volpe B. T., Hogan N., “Rehabilitation robotics: pilot trial of a spatial extension for MIT-Manus”, Journal of NeuroEngineering and Rehabilitation. 1(5), 1-15, (2004).

[7] Burgar C.G., Lum P.S., Shor P.C., Van der Loos H.F.M., “Development of robots for rehabilitation therapy: The Palo Alto VA/Stanford experience”, J. of Rehab. Research & Development, 37(6), 663-673 (2000).

[8] Lum, P.S.; Burgar, C.G., Van der Loos, H.F.M., Shor, P.C., Majmundar M., Yap R. “MIME robotic device for upper-limb neurorehabilitation in suacute stroke subjects: A follow-up study”, J. of Rehab. Research & Development, 43(5):631-642 (2006).

[9] Reinkensmeyer D. J., Kahn L. E., Averbuch M., McKennaCole A., Schmit B.D., Rymer W.Z., “Understanding and treating arm movement impairment after chronic brain injury: Progress with the Arm Guide”, J. of Rehab. Research & Development. 37(6), 653-662 (2000).

[10] Kahn L.E., Zygman M.L.Rymer W.Z, Reinkensmeyer D.J, “Robot-assisted reaching exercise promotes arm movement recovery in chronic hemiparetic stroke: a randomized controlled pilot study”, Journal of NeuroEngineering and Rehabilitation, 3(12), 1-13 (2006).

[11] Loureiro R., Amirabdollahian F., Topping M., Driessen B., Harwin W., “Upper limb mediated stroke therapy - GENTLE/s approach”, Autonomous Robots, 15, 35-51 (2003)

[12] Hesse, S., Schulte-Tigges, G., Konrad, M., Bardeleben, A. and Werner, C., “Robot-assisted arm trainer for the passive and active practice of bilateral forearm and wrist movements in hemiparetic subjects” Arch Phys Med Rehabil, 84(6), 915–20, (2003).

[13] Charles, S., Krebs, H., Volpe, B., Lynch, D. and Hogan, N., “Wrist rehabilitation following stroke: initial clinical results,” in Proc. IEEE International Conference on Rehabilitation Robotics (ICORR’2005), Chicago, IL, USA, 13–16, (2005).

[14] Gupta, A., O'Malley, M. K., Patoglu, V. and Burgar, C., "Design, control and performance of RiceWrist: a force feedback wrist exoskeleton for rehabilitation and training" The International Journal of Robotics Research, 27, 233-251, (2008).

[15] Reinkensmeyer D.J., Emken J.L., Cramer S.C. "Robotics, motor learning, and neurological recovery", Ann Rev Biomed Eng., 6, 497–525, (2006).

[16] Kahn L.E., Lum P.S., Rymer W.Z., Reinkensmeyer D.J., "Robot-assisted movement training for the stroke-impaired arm: Does it matter what the robot does?", J Rehabil Res Dev, 43, 619-30 , (2006).

[17] Carey, J.R.; Bhatt, E. and Nagpal, A., "Neuroplasticity Promoted by Task Complexity", Exercise and Sport Science Review, 33, 24-31, (2005).

[18] Rumelhart D. E., Hinton G. E., and Williams R. J., "Learning representations by back-propagating errors", Nature (London), 323, pp. 533-536, (1986).

[19] Kawato M., "Feedback-error-learning neural network for supervised learning, Advanced neural computers", R. Eckmiller, Ed. Amsterdam: North-Holland, 365-372, (1990).

[20] Wolpert D. M., Ghahramani Z., and Jordan M. I., "An internal model for sensorimotor integration, Science, 269, 1880-1882, (1995).

[21] Wei Y., Bajaj P,Scheidt R. and Patton J., "Visual Error Augmentation for Enhancing Motor Learning and Rehabilitative Relearning", IEEE Intl. Conf. on Rehabilitation Robotics, 505-510, Chicago, USA, (2005).

[22] Dellon, B., and Matsuoka, Y. "Feedback Distortion to Augment Controllability of Human Limb Motion," in Proceedings of Virtual Rehabilitation, 2008.

[23] Brewer, B.; Klatzky, R.; Matsuoka, Y., "Visual feedback distortion in a robotic environment for hand rehabilitation", Brain Research Bulletin 75, 804, (2008).

[24] Erol D. and Sarkar N., "Coordinated control of assistive robotic devices for activities of daily living tasks", IEEE Transaction on Neural and Rehabilitation Engineering, 16(3), 278-285, (2008).

[25] PUMA 560 Related Sites on the Internet, Available from: www.ee.ualberta.ca/~jasmith/puma/pumasites.html.

[26] Carey J.R., Kimberley T.J., Lewis S.M., Auerbach E., Dorsey L., Rundquist P., Ugurbil K., "Analysis of fMRI and Finger Tracking Training in Subjects with Chronic Stroke", Brain, 125, 773-788, (2002).

[27] Carey J.R., Anderson K.M., Kimberley T.J., Lewis S.M., Auerbach E.J., Ugurbil K., "fMRI anaysis of ankle movement tracking training in Subjects with Stroke", Exp Brain Res., 154, 281-290, (2004).

[28] Carey J., Durfee W., Bhatt E., Nagpal A., Weinstein S., Anderson K., Lewis S., “Tracking vs. movement Telerehabilitation training to change hand function and brain reorganization in stroke”, Neurorehabilitation and Neural Repair, (2006).

[29] Sciavicco, L. & Siciliano, B. , “Modeling and Control of Robot Manipulators”, McGrawHill, (1996).

[30] Erol D. and Sarkar N., “Intelligent Control for Robotic Rehabilitation after Stroke”, Journal of Intelligent and Robotic Systems, 50(4), 341-360, (2007).

[31] Erol D. and Sarkar N., “Smooth Human-Robot Interaction in Robot-Assisted Rehabilitation”, IEEE 10th Intl. Conf. on Rehabilitation Robotics, 5-12, (2007), Netherlands.

[32] J. L. Patton, M. E. Phillips-Stoykov, M. Stojakovich, and F. A. Mussa-Ivaldi, "Evaluation of robotic training forces that either enhance or reduce error in chronic hemiparetic stroke survivors," Experimental Brain Research, vol. Accepted pending revisions, 2004.

[33] Fleiss J. L., “The Design and Analysis of Clinical Experiments”, John Wiley & Sons Publication, (1986), ISBN-10: 0-471-82047-4.

[34] Furui Wang; Barkana, D.E.; Sarkar, N.; , "Evaluation of a robot-assisted rehabilitation system with assist-as- needed and visual error augmentation training methods," Intelligent Robots and Systems, 2009. IROS 2009. IEEE/RSJ International Conference on , pp.3555-3560, 10-15 Oct. 2009

CHAPTER IV

MANUSCRIPT III: DESIGN AND DEVELOPMENT OF AN ACTUATED FINGER EXOSKELETON FOR HAND REHABILITATION FOLLOWING STROKE

Christopher L. Jones, Furui Wang, Robert Morrison, Nilanjan Sarkar and Derek Kamper

(This work has been partially published in the IEEE International Conference on Biomedical Robotics and Biomechatronics, BioRob 2010, and submitted to the IEEE Transactions on Mechatronics.)

Abstract

Finger impairment following stroke results in significant deficits in hand manipulation and the performance of everyday tasks. While recent advances in rehabilitation robotics have shown promise for facilitating functional improvement, it remains unclear how best to employ these devices to maximize benefits. Current devices for the hand lack the capacity to fully explore the space of possible training paradigms. Particularly, they cannot provide the independent joint control and levels of velocity and torque required. To fill this need, we have developed a prototype for one digit, the Actuated Finger Exoskeleton (AFX), a three degree-of-freedom robotic exoskeleton for the index finger. This paper presents the design and development of the AFX, with performance testing results.

Keywords: Actuated Finger Exoskeleton, Hand rehabilitation, Robot-assisted Rehabilitation System

Introduction

Precise finger and thumb interactions are fundamental to human motor control. These movements are used constantly in everyday tasks. Neurological disorders such as stroke greatly impair this core function [1], directly impacting quality of life [3].

Stroke is the leading cause of serious, long-term disability in the United States [4]. Out of an estimated 7 million stroke survivors in the U.S. [5], 30-50% will require ongoing care or experience chronic impairment [4]. The economic costs of stroke, including direct and indirect expenses, exceeded $73 billion for 2010 in the U.S. alone [5].

Thus, current research focuses on improving the efficacy of rehabilitation. Recent studies have shown that repetitive practice of desired movement leads to promising recovery. For example, promotion of use of the paretic upper limb through constraint-induced therapy has led to improved motor control [6]-[8]. Practice has been shown to improve plasticity and incite cortical functional reorganization leading to improved motor control following stroke [9], [10].

Because of the complexity of the hand, with 21 mechanical degrees-of-freedom (DOF) and even more muscles, and the need for lengthy and consistent repetition of movement, researchers have begun to implement robotics for rehabilitation. Robot-assisted rehabilitation has been demonstrated to enable longer training sessions while reducing the workload on therapists [11].

In recent years, a number of devices have been developed expressly for, or applied to, hand rehabilitation. These include both commercial products, such as CyberGrasp (Immersion Corporation, San Jose, CA) [12], the Hand Mentor (Kinetic Muscles Inc., Tempe, AZ), and the Amadeo System (Tyromotion GmbH, Graz, Austria) and experimental devices, including the Rutgers Master II-ND [13], HWARD [14], and HandCARE [15], among others [16]-[19].

A fundamental question, however, is how to best use these devices for rehabilitation. The extent to which rehabilitation robots should assist, resist, or otherwise alter movement of the user is unclear and requires further study. Unfortunately, existing devices do not provide the complete range of speed, force, and independence of joint control to thoroughly explore the space of different training algorithms and environments. For example, stroke survivors may generate substantial coactivation, especially during

intended finger extension [20], such that significant joint torques may need to be provided by the exoskeleton to overcome the misapplied joint torques of the user. Abnormalities in impedance and motor control may vary from joint to joint such that independent control of each joint through the exoskeleton may be beneficial for training. Additionally, to examine and mitigate power deficits [21] and peak tracking limitations, high joint rotational velocity may be needed.

A device possessing these capabilities would greatly facilitate the scientific investigation of hand function and therapy following stroke. In accordance with these goals, we have developed a prototype for a single finger. The Actuated Finger Exoskeleton (AFX), presented here, will improve on current rehabilitation robotics solutions by providing a versatile framework with high performance, real-time control, individual actuation of each of the finger joints, and forces and speeds comparable to normal human function. The AFX will allow for normal task execution enabling direct comparisons between distinct rehabilitation strategies and motor control studies within a single platform. This paper describes the AFX and analyzes preliminary kinematic and torque control performance.

Finger Exoskeleton Design

Design Requirements

To enable the exploration of rehabilitation and motor control strategies of the finger, the AFX must satisfy several design criteria. A device meeting these criteria would enable detailed analysis of index finger control through interaction with its joints across the range of normal, dynamic movements.

First, the exoskeleton must be biomechanically compatible with an individual's natural joint rotation and provide independent actuation of each of the joints of the finger. In order to implement the rehabilitation training algorithms and create natural joint rotation for the affected finger, it is necessary to provide individual actuation for each of the finger joints, as alterations in impedance and motor control may vary from joint to joint following stroke.

Next, to reduce impedance of normal movement, the exoskeleton must be lightweight, have low inertia and have a relatively small physical profile with respect to the index finger.

Third, for application to practical finger manipulation tasks, the device must support peak angular velocities on the order of 1000°/s [23], representative of the speeds we have observed in normal movements. This speed requirement is also necessary for the study of sensory perception as the finger movement ranges from low to high speed. Similarly, requirements for maximum sustained torques were set to 2.0, 0.75 and 0.25 N-m at the MCP, PIP and DIP joints, respectively. These values, equaling roughly half of the average maximal torque found in normal individuals (unpublished data), are sufficient to overcome the unwanted flexion torques which can be unintentionally generated by stroke survivors due to excessive coactivation of finger flexor muscles during task performance (Kamper et al., Muscle Nerve, 2003).

Finally, to control finger manipulation tasks, the AFX must support both position and torque control at each joint. Thus, both joint angle and torque measurements are required for feedback control and for data collection.

From these requirements, the exoskeleton was designed, fabricated, actuated and instrumented as described in the following sections.

Mechanical structure

To achieve biomechanical compatibility with an individual's natural joint rotation, the rotational movement of the device must match that of the digit. While this can be achieved with a remote center of rotation [24], the most direct means is to align the joints of the device with the rotational axes of the user's finger, avoiding off axis forces and moments that would otherwise be present. In the AFX, this is achieved with a serially-segmented exoskeleton that runs along the radial side of the index finger (Figure IV-1). The three rotational joints of the exoskeleton are aligned with the flexion/extension axes of the metacarpophalangeal (MCP), proximal interphalangeal (PIP), and distal interphalangeal (DIP) joints. Pairs of parallel bars connect the structure to the proximal, middle, and distal segments of the finger. Rotation of the exoskeleton produces equivalent rotation of the finger joint across large ranges of motion: -15 to 75°, 0 to 90° and 0 to 90° for the MCP, PIP and DIP joints, respectively.

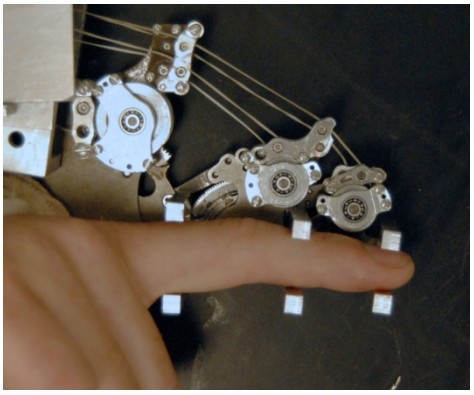

Figure IV-1 AFX located on radial side of the index finger with parallel bars interfacing with each finger segment. Transmission pulleys above the corresponding joint transmit force from the appropriate cable to the target joint. Guide pulleys direct cables over each joint toward distal targets.

For application across users, the AFX must be able to accommodate finger segments of different lengths and thicknesses while maintaining proper alignment. This is achieved through interchangeable linkages connecting each joint of the exoskeleton. A set of linkages have been fabricated for each joint so that the appropriate linkage can be matched to the finger. The contact rod brackets are sized to accommodate a wide range of the population, with shims for adjustment between users.

To reduce impedance and inertia, the mass of the exoskeleton was minimized. All components were fabricated from aluminum or steel as necessary to withstand the relatively high torques required of the device. The portion of the exoskeleton that actually moves with the finger has a mass of 138 g. Physical dimensions were minimized wherever possible while maintaining mechanical rigidity and safety for the wearer. The maximum width of the structure running along the finger is only 8mm.

Thrust bearings at the MCP and PIP joints serve to accommodate potentially significant off-axis moments. Mechanical stops limit the range of motion of each joint to prevent accidental injury. These stops can be adjusted to match the passive range of motion of the user.

The complete exoskeleton is attached to a plate on a fiberglass cast which encases the wrist and thus maintains its posture (Figure IV-2). The device is externally supported to remove weight from the user [26].

Actuation

To achieve independent movement/torque production at each joint, separate actuators are employed at each joint of the AFX. DC servomotors were chosen due to their

performance in all four quadrants of the torque-velocity space. To maximize backdrivability, motors were selected which could meet the requirements of joint angular velocities on the order of 1000°/s and sustained joint torques of 2.0, 0.75 and 0.25 N-m at the MCP, PIP and DIP joints, respectively, without any gearing. Specifically, AKM motors (Kollmorgen, Munkekullen, Sweden) are being used, with AKM13C, AKM12C and AKM11C for the MCP, PIP and DIP joints, respectively.

In order to reduce the added mass on the hand, the DC motors are located on the forearm. Cables (Spectra kite line) transmit motor torque to the exoskeleton joints. The cable drive design reduces friction and backlash in comparison with standard transmissions, thereby allowing the motors to be located a significant distance from the joints. Cable transmissions have been successfully implemented in commercial robots such as the Phantom (SensAble Technologies, Woburn, MA) and WAM (Barrett Technologies, Cambridge, MA). As these cables can only pull, similar to muscles, two cables and thus two motors are used for each joint for a total of 6 cables and motors (Figure IV-2).

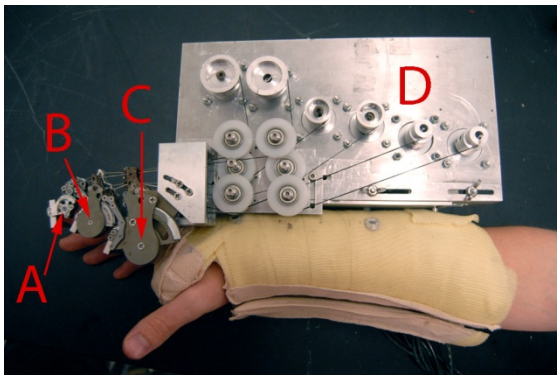

Figure IV-2 AFX attached to mounting plate on forearm cast. AFX joints (A-C) and motor pulleys (D) are indicated. The vertical plate is adjustable with slots which allow accurate translational placement of the MCP joint.

Primary gear reduction from motor cable to exoskeleton joint occurs directly at the joint. Namely, the cables are connected to pulleys which subsequently drive a section of a gear fixed to a rotating segment of the exoskeleton. This gear reduction directly at the joint reduces the tension in the cables from the motors, thereby providing as much bandwidth for control as possible [25]. Total reduction is 11.8, 3.7, and 1.4 at the MCP, PIP, and DIP joints, respectively. A set of bearing and pulley cable guides leads each cable across more proximal joints to its proper transmission pulley, as necessary.

Sensing

Joint angles are computed from the motor shaft rotations, as measured from optical encoders (2000 counts per revolution, Kollmorgen, Munkekullen, Sweden) integrated into each motor. Motor shaft rotation is converted to joint rotation through consideration of the pulley and gear reduction between the motor and the joint.

Joint torque is computed from the contact forces measured at each finger segment. The custom contact rods consist of two horizontal beams, one above and one below the user's digit (Figure IV-3). Each aluminum beam is configured with four strain gauges (SGT-1/350-TY13, Omega, Stamford, CT) oriented at 45° from the principle bending axis of the beam and connected in a full Wheatstone bridge. This strain gauge configuration rejects the bending moment and measures only the perpendicular shear force in the beam [27], allowing for accurate contact force measurement regardless of finger size, contact location, shear forces or off axis moments. The signal from the Wheatstone bridge is amplified by a gain of 1000, and subsequently filtered by a low-pass filter at 400Hz, before input to the controller.

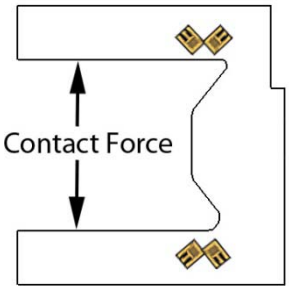

Figure IV-3 Schematic of the finger contact rods with strain gauges. In this configuration, 45° from the neutral axis, the gauges reject the bending moment and transduce the precise contact force.

Control System

Control of either position or torque can be implemented at each joint.

Joint Position Control

The joint position controller is responsible for executing the target joint trajectory in an accurate manner.

At each joint, two cables act on the joint pulley in opposite directions, one for flexion and one for extension. These agonist-antagonist cables must be adjusted simultaneously to achieve the desired torque differential to actuate the joint. One motor actively winds its cable and the antagonist motor passively unwinds its cable while a baseline tension torque is provided to both motors. Critically, tension must be maintained in both cables to keep either from going slack.

In this configuration, one motor is selected as the driving motor and the other is selected as the following motor by a planner in the controller. For example, if net flexion is desired, the motor providing counter-clockwise joint rotation is designated as the driving motor and the motor providing clockwise rotation is designated as the following motor.

Both feed-forward and PI feedback control is instituted at each joint (Figure IV-4). PI parameters were tuned heuristically to produce a stable motion when no external resistance is applied. Joint angle is computed from the signals from the quadrature encoders at the motor shafts. Each motor in the pair for a given joint independently tracks joint angle, wherein for a given movement of the joint, one encoder will increase and the opposing encoder will decrease. The differential between two encoder values is then divided by two and taken as the actual angle of the joint.

With cables driving three joints in series, the cables for the distal joints PIP and DIP, must first cross the more proximal joints. The cable lengths to these distal joints will be affected by the motion of the joints they cross. As the routing of each cable varies slightly, the impact of the rotation of the more proximal joint(s) on cable length will differ for each cable. Thus, a linear mapping is generated to actively compensate for the discrepancies in cable routing and applied through feed-forward control.

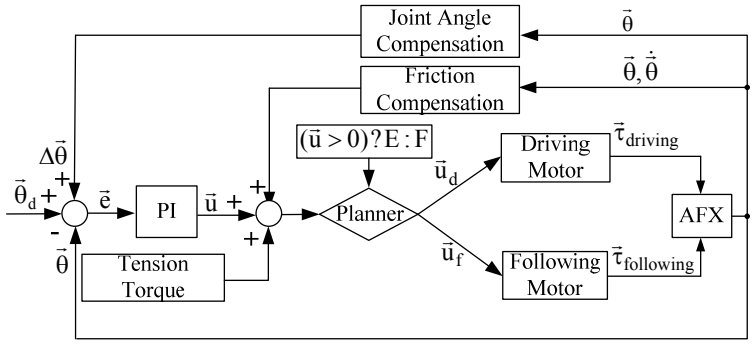

Figure IV-4 PI angular position controller for the AFX. The driving and following motors are selected by the planner according to the control command $\vec{u}$.

Friction is unavoidable in cable transmission. To improve the performance of the controller, friction compensation is integrated into the controller. The friction compensation block (as shown in Figure IV-4) is a 2D look-up table with velocity and

position indices. The friction factors corresponding to the velocity and position indices were calibrated in our experiments.

Joint Torque Control

A torque controller with PI loops and feed-forward compensation was developed for all three joints (Figure IV-5). The feedback signal for each PI loop is the joint torque calculated from the contact force measured by the strain gage oh the parallel bar brackets. As the contact bars reside at a fixed distance from the preceding joint, net torque may be computed from the measured force. As with position control, a planner again selects the driving and following motors based on intended torque direction. One motor provides flexion torque while the other creates extension torque. Similarly, one beam from each bracket measures the flexion contact force while the other beam provides the extension contact force relative to the desired output.

Of course, for the open-link chain configuration of the exoskeleton, torque production at more distal joints requires compensation at more proximal joints, in accordance with the system Jacobian. Feed-forward compensation was instituted to deliver these torques to more proximal joints.

The controller also includes a predictive feed-forward term that is adjusted to reduce delay and achieve rapid-onset torques as might be required for perturbation experiments.

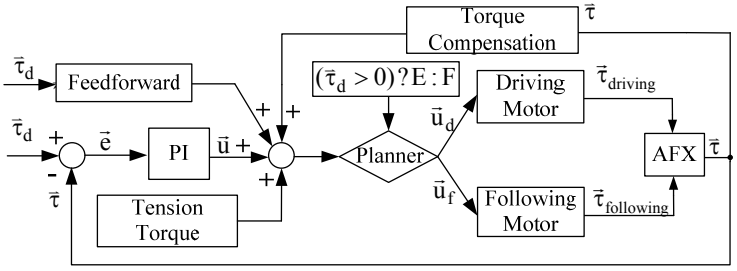

Figure IV-5 PI torque controller for the AFX. The driving and following motors are selected by the planner according to the target torque. The appropriate feedback signal from the AFX contact rods is also selected to match the driving motor.

Real-time Control Implementation

The control system of the finger exoskeleton is implemented using the MATLAB xPC Target. The xPC Target is a real time kernel that runs on an independent computer allowing for real-time control. Executable code is loaded onto this target PC from the host PC running MATLAB Simulink software [29]. The data signals are acquired in real-time by the target PC and uploaded to the host PC over a direct crossover Ethernet cable. The experimenter can monitor the signal data and tune the model parameters on the host computer (Figure IV-6).

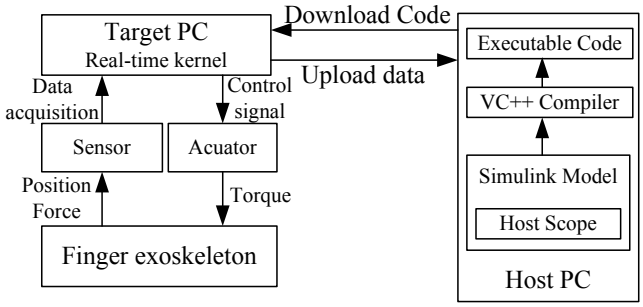

Figure IV-6 Real-time control system using xPC Target. The host PC manages the control program, visual feedback and data storage; the target PC runs the real-time control and acquires sensor data.

A PCI-6220 ADC board (National Instruments, Austin, TX) is installed on the target PC to perform analog-digital conversion of the signals from the tension sensors. The CNT32-8M encoder board (CONTEC, Sunnyvale, CA) records the digital encoder signals and the PCI-6703 DAC board (National Instruments) converts digital command signals into the analog signals which drive the S200 motor amplifiers (Kollmorgen). All signals are sampled at 10 kHz.

Safety Consideration

For safety, an over-damped or critically damped behavior in the joint angle control is preferred to an under-damped system. The joint angles and torques are continuously monitored by the control program to ensure that pre-defined limits are not exceeded.

Mechanically, guide slots restrict the range of motion of each joint and can be adjusted to limit joint range as needed. In our design, differently sized motors are used for the different joints. In this manner, peak motor torque can be better matched to peak voluntary subject torque and the potential for excessive torque is minimized. An emergency switch immediately terminates all power to the motors.

Performance Testing

Experiments were designed to test the performance of the AFX, including kinematic control performance and force control performance.

Testing of Kinematic control performance

A two-camera setup employing high-resolution, monochrome CCD cameras (IPX-1M48, Imperx, Inc., Boca Raton, FL) was employed to examine kinematic performance

of the AFX. Namely, the cameras were used to measure exoskeleton joint angles to compare with the desired angles. Markers were attached to the exoskeleton to record movement. The markers were covered with ultraviolet- sensitive fluorescent paint (Wildfire, Modern Masters, Inc., N. Hollywood, CA) and illuminated with a UV light source.

Motion capture and analysis were performed using a digital motion analysis suite (DMAS7, Spica Technology, Co., Maui, HI). The cameras were calibrated using the software provided in DMAS7 and a custom calibration form. An average calibration error of < 0.6 mm between cameras was achieved. During motion capture, the 3-dimensional position of each marker was recorded and these positions were used to compute joint angles.

To test the exoskeleton's ability to appropriately track a desired position trajectory, both ramp and sinusoidal inputs were employed. Separate ramp inputs were specified for the MCP, PIP and DIP joints, respectively. The exoskeleton began each trial at either the extension or flexion limit of the joint.

To examine the ability of the AFX to achieve high rotational speed, a desired sinusoidal trajectory was generated for the MCP joint with an amplitude of 30º and an angular frequency of 10π. This results in a theoretical maximum instantaneous velocity of 942°/s. The AFX began in a central posture to allow room for the tracking task.

Finally, to examine the ability of the AFX to simultaneously control each joint independently, target sinusoidal trajectories were generated with 20° amplitude for 4 seconds, at distinct angular frequencies for each joint: π/4 (MCP), π/2 (PIP), and π (DIP). The AFX began in a central posture to allow room for oscillations.

Testing of torque control performance

Calibration of the custom force beams was first performed by comparing the voltage output of the strain gage bridge with known loads. Isometric joint torque generation was then examined for a desired step input in torque. For this study, a rigid link was used to represent a finger, with the rotational joint of the link aligned with the AFX MCP joint. An external load cell (20E12A, JR3, Inc., Woodland, CA) was employed to further verify the torque control performance of the AFX. The load cell was attached at the tip of the rigid link in order to measure the end-point force. The reflected torque at MCP joint was then calculated from the tip force. The torque was also measured from the signals in the force beam.

Maximum joint torque was then examined by increasing the output joint torque in a series of 0.5V motor command steps. MCP joint torque was computed form the force measured at the tip of the link with the load cell.

Analysis

The position data during ramp tracking and simultaneous sinusoids tracking were processed by aligning the camera data with the command signals for the desired trajectories. To quantify the accuracy of the tracking performance, the actual position data were regressed against the target position data for each trial. We calculated the sample correlation and the root mean square error (RMSE) between observed and desired trajectories.

Accuracy of the encoder readings was then confirmed by comparing the encoder outputs to the camera data for movements within the tracking capabilities of the camera

system (with its peak sampling speed of 48 Hz). The sample correlation between the encoder angles in relation to the camera angles was computed for each trial. Once the accuracy of the encoder readings was confirmed, the encoder readings were then used to evaluate device performance at higher speeds.

For torque control experiments, calibration curves were first formulated for the strain gage beams. Then the actual joint torque, derived from both the beam and load cell, was compared with the desired torque step to examine the control performance. The RMS steady-state error between the desired torque and the actual achieved torque was calculated to show the control accuracy. Maximal torque was computed from load cell recordings as the load cell was calibrated beyond the desired capacity of our device.

Results

Both position and force control experiments were conducted to evaluate the capabilities of the device. In the position control experiments, we recorded the desired position generated by the controller and the actual position as measured by motor encoder and observed by the external camera. In the force control experiments, we recorded the desired joint torque generated by the controller and the actual joint torque computed from the contact force at contact rods measured by strain gage. The contact force at the tip of the rigid link measured by the external load cell was also recorded for validation of the joint torque.

Kinematic Tracking

For ramp experiments, we examined encoder and camera observed angles for ramp trajectories with the joint speed of 10°/s, 15°/s, and 15°/s for MCP, PIP and DIP, respectively. For three example trials, R^2 values were greater than 0.99, the slope values were within 3% of the desired value of 1, and the mean squared error for each joint was 0.657°, 0.972°, and 2.043° for the MCP (Figure IV-7), PIP and DIP, respectively.

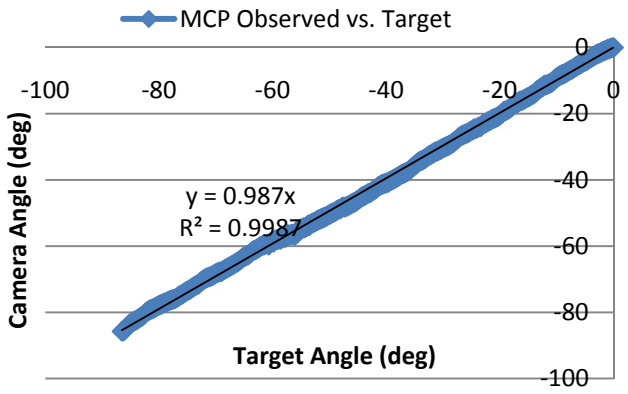

Figure IV-7 Target angle (x-axis) vs. camera observed angle (y-axis) for the MCP joint during constant velocity movement.

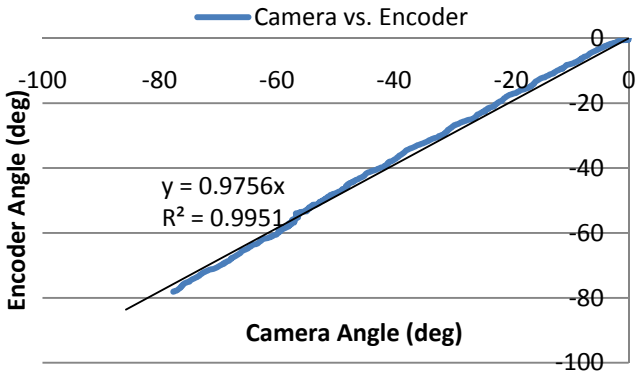

Figure IV-8 Example of camera (x-axis) vs. encoder (y-axis) validation during constant MCP angular movement

Joint angles computed from the motor encoders closely matched the angles measured with the camera system (see Figure IV-8 for an example). The sample correlations between encoder and camera observed position were greater than 0.99 for all three

trajectories and the regression slope values fell within 4.2 % of the desired value of 1 across 5 independent trials (Table IV-1). The encoder data were subsequently used to analyze the kinematic performance at a higher speed.

Table IV-1 Encoder vs. observed joint angle correlations for individual ramp angular trajectories at each joint demonstrating encoder validity

Joint	**MCP**	**PIP**	**DIP**
Slope	0.976	1.010	1.042
r^2	0.995	0.999	0.993

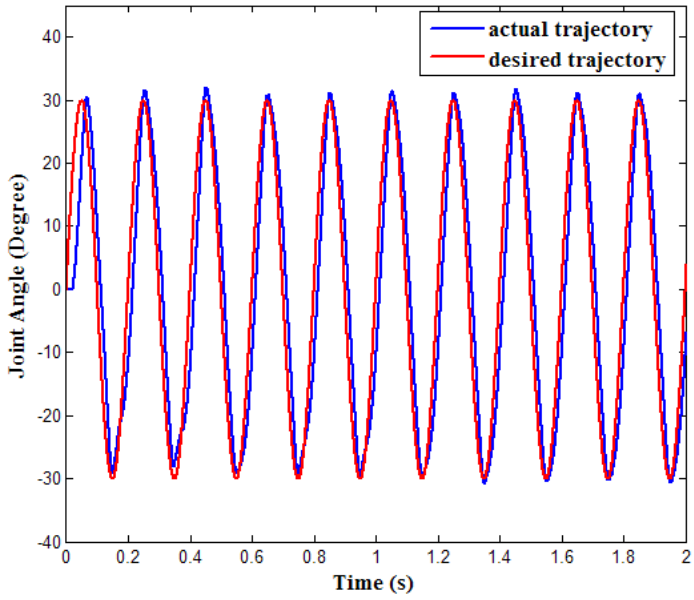

Figure IV-9 MCP sinusoid at angular frequency 10π and amplitude 30° demonstrating a peak velocity of 940°/s for this trial

Namely, a sinusoidal input frequency of 10π was sent to the MCP joint. The AFX was able to track this trajectory even as the rotational speed reached 940°/s (Figure IV-9). For this high-speed sinusoid, the average phase lag is 0.009s with an average overshoot of 1.11°. Considering the high speed and angular frequency, this tracking performance is satisfactory.

The desired and measured (camera system) trajectories for MCP, PIP and DIP in the tracking of three simultaneously applied sinusoids were then compared (Figure IV-10). Sample correlation coefficients between observed and desired angular positions were greater than 0.99 for all joints. Phase lag was less than 0.3s and average overshoot was less than 1.1° for each joint during the simultaneous movement (Table IV-2). These results demonstrated the capability of the AFX to provide individual actuation to all three finger joints.

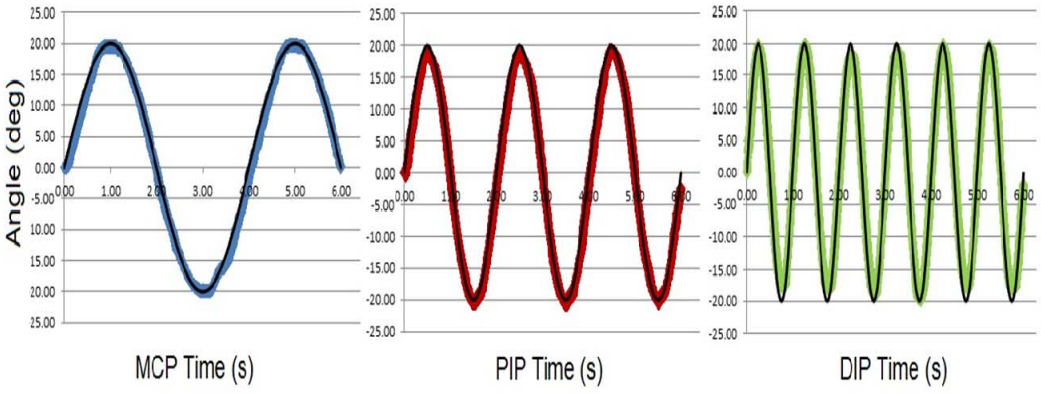

Figure IV-10 Camera observed MCP (blue), PIP (red), and DIP (green) joint angles versus target (black) joint angles during simultaneous tracking of sinusoids with different frequencies at each joint, π/4 (MCP), π/2 (PIP), and π (DIP). All correlation coefficients are greater than 0.99.

Table IV-2 Average phase lag and overshoot for each joint during a 6 second simultaneous sinusoidal movement of all three joints.

Joint	**MCP**	**PIP**	**DIP**
Phase Lag (s)	0.029	0.013	0.013
Overshoot (°)	-0.251	-0.262	-1.094

Kinetic Control

The calibration curve of the strain gage force sensor was highly linear ($R^2 > 0.999$). Importantly, hysteresis was minimal. Force readings were largely invariant to position along the beam.

We conducted step torque experiments to evaluate the torque control of the system. The torque controller was left slightly underdamped to improve rise time. The output torque reached the target torque of 0.57 N-m (corresponding to a 20 N flexion force on the finger) in less than 0.06 seconds for a single trial (Figure IV-11). The RMS error of the contact beams at steady-state is $5.3*10^{-3}$ N-m (0.93% of the target torque) with an average error of $6.0*10^{-3}$ N-m (0.1%) for the same trial. Contact beam differed from the load cell measurement by a RMS steady-state error of 2.3%.

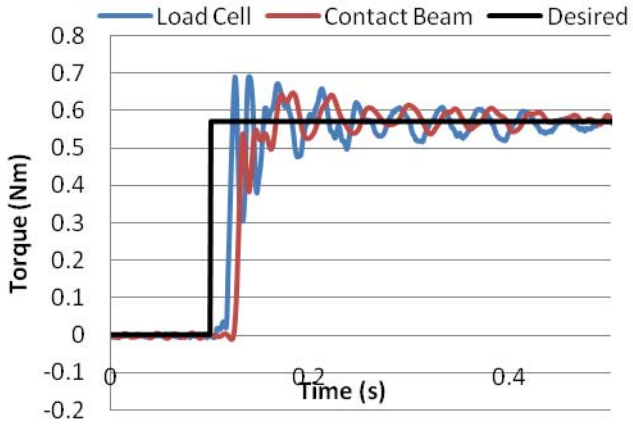

Figure IV-11 Example 0.572 Nm step torque at the MCP joint with desired torque step (black), external load cell (blue) and contact rod (red) measurements.

To test the torque capacity, the motor command voltage was increased until the output torque exceeded the design torque of 2.0 N-m at the MCP joint (Figure IV-12). This isometric output was achieved at stall around a motor excitation of 2V, 20% of the maximum possible excitation. Taken together, these results demonstrated the capability of the AFX to promptly provide the required joint torque.

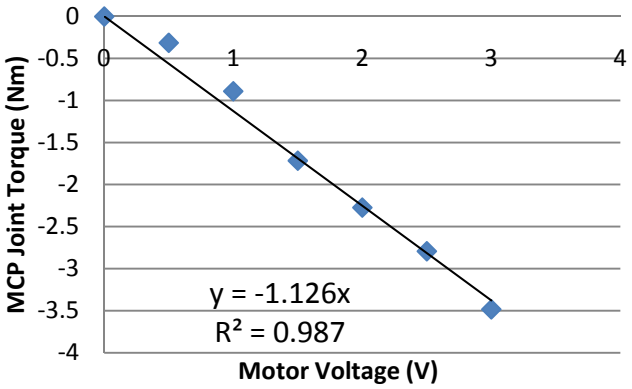

Figure IV-12 Flexion torque at the MCP in response to steps in motor voltage. The torque output surpasses the design requirement at less than 2 V.

Discussion

While adding only 138 g of mass to the finger, the AFX is capable of moving at substantial speeds and providing considerable joint torque while retaining much of its backdrivability. With active control input, further compensation for the device can be provided to lessen its effects on voluntary movement. Thus, the AFX can be employed to examine the impact of a number of different control algorithms, from full assistance (position servo) to no interference (zero impedance). This flexibility is valuable for testing the efficacy of rehabilitation strategies and pursuing the study of motor control.

The high level of backdrivability is made possible by the implemented cable actuation system. The cable transmission, with gearing located directly at the joints, permits the actuators to be placed proximal to the hand while minimizing the frictional losses that are inherent to other transmissions, such as Bowden cables. Of course, a trade-off must be made in terms of control complexity and additional hardware.

Namely, two motors are needed to control each joint, as each cable is only capable of pulling. These motor pairs must act in concert to allow joint movement while maintaining tension in all cables. Additionally, the cables to more distal joints must respond to

movement of more proximal joints; cable length is a function of all preceding joint angles as well as the joint the cable controls. A benefit of this biomimetic actuation is the ability to set the joint stiffness, as can be done in the human finger, as the agonist-antagonist cable co-activation can be adjusted in tandem. Thus, impedance control can be implemented, in addition to position or torque control.

Kinematic testing confirmed the ability of the AFX to track desired angle trajectories over time. Tracking of the desired ramps was quite good, with R^2 values of 0.99 or greater. Tracking of the independent sinusoids simultaneously with each digit was also successful as evidenced by correlation factors exceeding 0.99. Precise control could be maintained even at velocities approaching maximum values in humans.

Examination of kinetic control confirmed the ability of the AFX to precisely provide a desired isometric torque to finger joints. Even with a rapid rise time of 60 ms, RMS steady state error was only 0.93% with an average error of 0.1%. The exoskeleton also proved to be quite strong. Almost 3.5 N-m of torque (well exceeding the 2.0 N-m requirement) could be achieved at the MCP joint without damage to the exoskeleton.

The sensory feedback provided by the AFX was accurate and reliable. Joint angles derived from the encoders were in close agreement with those obtained from an external camera system ($R^2 = 0.999$). This suggests that inconsistencies in cable winding around the pulleys and motor spools have minimal effect on joint angle. The torque measurements obtained with strain gages on the contact beams closely match with the commercial load cell (2.3% RMS steady-state error).

The AFX achieved excellent tracking of kinematic trajectories oscillating at 5 Hz and reaching speeds close to 1000°/s. Additionally, independent trajectories could be tracked

with each joint simultaneously. Joint torques greater than 2 N-m could be attained. The AFX is also contained in a platform allowing for a wide finger workspace, low interference and arm mobility as necessary. These capabilities, which exceed those of other current exoskeletons in power, control and feedback resolution, and impedance to movement, will permit careful evaluation of the motor control of stroke survivors and of different rehabilitation strategies. For example, the high achievable speeds will permit assessment of spasticity [31] and isokinetic strength and power. The large torque capabilities will permit evaluation of peak strength. High backdrivability with the capacity for large perturbation forces permits implementation of force fields, such as viscous curl fields [32], [33], for motor learning paradigms.

Future advancement of the control system will include a high-level supervisory controller to provide different training tasks. Additional training strategies, e.g., assist-as-needed, resist-as-needed, visual error augmentation will be integrated in this high-level supervisory control to enhance the functionality of the AFX. Performance of the device with human subjects will be examined next.

Acknowledgment

We acknowledge the contributions of Tom Worsnopp to the initial design of the AFX, and Drs. Edward Colgate and Michael Peshkin from the Laboratory for Intelligent Mechanical Systems at Northwestern University for their insight and continued support of this project.

References

[1] E. G. Cruz, et al., "Kinetic and kinematic workspaces of the index finger following stroke," Brain, vol. 128, pp. 1112-21, May 2005.

[2] N. J. Seo, et al., "Altered digit force direction during pinch grip following stroke," Exp Brain Res, vol. 202, pp. 891-901, May 2010.

[3] G. S. Seale, et al., "Change in positive emotion and recovery of functional status following stroke," Rehabil Psychol, vol. 55, pp. 33-9, Feb 2010.

[4] CDC, "Outpatient rehabilitation among stroke survivors: 21 states and the District of Columbia," MMWR Morb Mortal Wkly Rep. no. 56, pp. 504-507, 2007.

[5] AHA, "Heart Disease and Stroke Statistics 2010 Update," Circulation no. 121, pp. 46-215, 2009.

[6] S. L. Wolf, et al., "Repetitive task practice: a critical review of constraint-induced movement therapy in stroke," Neurologist, vol. 8, pp. 325-38, Nov 2002.

[7] C. J. Winstein, et al., "A randomized controlled comparison of upper-extremity rehabilitation strategies in acute stroke: A pilot study of immediate and long-term outcomes," Arch Phys Med Rehabil, vol. 85, pp. 620-8, Apr 2004.

[8] S. J. Page, et al., "Efficacy of modified constraint-induced movement therapy in chronic stroke: a single-blinded randomized controlled trial," Arch Phys Med Rehabil, vol. 85, pp. 14-8, Jan 2004.

[9] J. Liepert, et al., "Motor cortex plasticity during constraint-induced movement therapy in stroke patients," Neurosci Lett, vol. 250, pp. 5-8, Jun 26 1998.

[10] J. Liepert, et al., "Treatment-induced cortical reorganization after stroke in humans," Stroke vol. 31, pp. 1210-1216, 2000.

[11] L. Pignolo, "Robotics in neuro-rehabilitation," J Rehabil Med, vol. 41, no. 12, pp. 955-960, 2009.

[12] S. V. Adamovich, et al., "Design of a complex virtual reality simulation to train finger motion for persons with hemiparesis: a proof of concept study," J Neuroeng Rehabil, vol. 6, p. 28, 2009.

[13] D. Jack, et al., "Virtual reality-enhanced stroke rehabilitation," IEEE Trans Neural Syst Rehabil Eng, vol. 9, pp. 308-18, Sep 2001.

[14] C. D. Takahashi, et al., "Robot-based hand motor therapy after stroke," Brain, vol. 131, pp. 425-37, Feb 2008.

[15] L. Dovat, et al., "HandCARE: a cable-actuated rehabilitation system to train hand function after stroke," IEEE Trans Neural Syst Rehabil Eng, vol. 16, pp. 582-91, Dec 2008.

[16] A.Wedge, and G. Hommel, "Development and control of a hand exoskeleton for rehabilitation of hand injuries," IEEE/RSJ International Conference on Intelligent Robots and Systems, pp. 3046 - 3051 2005.

[17] I. Sarakoglou, et al., "Occupational and physical therapy using a hand exoskeleton based exerciser," IEEE/RSJ International Conference on Intelligent Robots and Systems Proceedings, vol. 3, pp. 2973 – 2978, 2004.

[18] M. DiCicco, et al., "Comparison of control strategies for an EMG-controlled orthotic exoskeleton for the hand," IEEE International Conference on Robotics and Automation, vol. 2, pp. 1622-1627 2004.

[19] H. Kawasaki, et al., "Development of a hand motion assist robot for rehabilitation therapy by patient self-motion control," IEEE 10th Intl Conf Rehab Rob, pp. 234-240, 2007.

[20] D. G. Kamper and W. Z. Rymer, "Impairment of voluntary control of finger motion following stroke: role of inappropriate muscle coactivation," Muscle Nerve, vol. 24, pp. 673-81, May 2001.

[21] D. H. Saunders, et al., "Association of activity limitations and lower-limb explosive extensor power in ambulatory people with stroke," Arch Phys Med Rehabil, vol. 89, pp. 677-83, Apr 2008.

[22] D. G. Kamper, et al., "Relative contributions of neural mechanisms versus muscle mechanics in promoting finger extension deficits following stroke," Muscle Nerve, vol. 28, pp. 309-18, Sep 2003.

[23] B. Gutnik, et al., "Power of performance of the thumb adductor muscles: effect of laterality and gender," Medicina (Kaunas), vol. 42, pp. 653-60, 2006.

[24] R. Baumann, et al., "The PantoScope: a spherical remote-center-of- motion parallel manipulator for force reflection," IEEE International Conference on Robotics and Automation,, vol.1, pp. 20-25, Apr 1997.

[25] W. Townsend and J. Salisbury, "Mechanical bandwidth as a guideline to high-performance manipulator design," IEEE International Conference on Robotics and Automation, 1989.

[26] Iwamuro BT, Cruz EG, Connelly LL, Fischer HC, Kamper DG., Effect of a gravity-compensating orthosis on reaching after stroke: evaluation of the Therapy Assistant WREX. Arch Phys Med Rehabil. 2008 Nov; 89(11):2121-8.

[27] Omega WEB Technical Reference, http://www.omega.com/faq/ pressure/pdf/positioning.pdf

[28] J. J. Craig, Introduction to Robotics: Mechanics and Control. Reading, MA: Addison-Wesley, 1989.

[29] T. K. Podder and N. Sarkar, "A unified dynamics-based motion planning algorithm for autonomous underwater vehicle-manipulator systems (UVMS)," Robotica, vol. 22, pp. 117-128, 2004.

[30] xPC Target documents, Mathworks, http://www.mathworks.com/access/helpdesk/help/toolbox/xpc/ref_endref_end.

[31] D. G. Kamper and W. Z. Rymer, "Quantitative features of the stretch response of extrinsic finger muscles in hemiparetic stroke," Muscle Nerve, vol. 23, pp. 954-61, Jun 2000.

[32] R. A. Scheidt, et al., "Persistence of motor adaptation during constrained, multi-joint, arm movements," J Neurophysiol, vol. 84, pp. 853-62, Aug 2000.

[33] J. L. Patton, et al., "Evaluation of robotic training forces that either enhance or reduce error in chronic hemiparetic stroke survivors," Exp Brain Res, vol. 168, pp. 368-83, Jan 2006.

CHAPTER V

MANUSCRIPT IV: DESIGN AND DEVELOPMENT OF AN ACTUATED THUMB EXOSKELETON FOR HAND REHABILITATION FOLLOWING STROKE

Furui Wang, Milind Shastri, Christopher L. Jones, Derek G. Kamper, and Nilanjan Sarkar

(This work has been partially published in the 2011 IEEE/RAS International Conference on Robotics and Automation, ICRA 2011, and is in preparation for submission to the IEEE Transaction ons Mechatronics.)

Abstract

Chronic hand impairment is a common target for rehabilitation following stroke. This paper presents an actuated thumb exoskeleton (ATX) to facilitate research in hand rehabilitation therapy. The ATX presented in this work permits independent bi-directional actuation in each of the 5 degrees-of-freedom (DOF) of the thumb using a mechanism that has 5 active DOF and 3 passive DOF. The ATX is able to provide considerable joint torques for the user while still allowing backdrivability through flexible shaft transmission. A prototype was built and experiments were conducted to evaluate the closed-loop position control. Further improvement and future work are discussed.

Introduction

Hand impairment is a prevalent outcome for a variety of neuromuscular disorders, such as stroke. Up to 795,000 people in the U.S. experience a stroke each year [1]. Of these, 60-75% will live beyond one year after the incidence, resulting in a current stroke population of 7 million [1]-[3]. Arm function is acutely impaired in a large majority of those diagnosed with stroke [4]-[6]. Furthermore, acute hemiparesis presages chronic hemiparesis in over 40% of individuals [4], [5]. Chronic deficits are prevalent in the distal upper extremities, especially with regard to finger extension [7].

This distal limb impairment can be especially disabling, as proper hand function is crucial to manual exploration and manipulation of the environment. Indeed, loss of hand function due to neuromuscular disorders frequently prevents effective self-care and limits employment opportunities. One study reported that more than half of the subjects they

observed were dependent on others for help in the activities of daily living six months post-stroke [8].

An assortment of interventions has been tried in an effort to improve function or to treat the resulting peripheral alterations following stroke. Those with the most success to date tend to focus on repetitive practice. Indeed, numerous studies employing the constraint-induced technique, in which focus is placed on intensive practice with the impaired arm without using the less impaired arm, have shown improvement in hand capabilities [9]-[11]. This supports the observations in animal models of stroke in which practice appears to be the primary factor leading to synaptogenesis and brain plasticity [12]-[14]. Indeed, imaging performed during constraint-induced training studies has shown evidence of cortical plasticity following the training [15], [16].

Unfortunately, many stroke survivors do not possess sufficient sensorimotor control to practice the desired movements. For the upper extremity, robots have been created to assist with therapeutic training of the wrist, arm and shoulder [17]-[21]. It has been reported that robot-delivered sensorimotor training enhanced the motor performance of the exercised shoulder and elbow with improved functional outcomes [22] and that practicing with a robot that assisted reaching movements helped the users learn how to generate smoother unaided reaching trajectories [23].

A fundamental question, in robot-assisted rehabilitation, is how to best use these robotic devices to facilitate rehabilitation. Should the device assist or resist movement? Should movement error actually be augmented, as some have suggested [24]? Should emphasis be placed on practice of movement of individual joints [25] or on the

coordination of multiple joints? In order to answer these questions for rehabilitation of the hand, a device is needed to provide precise control of individual hand joint.

In recent years, a number of devices have been developed expressly for or applied to hand rehabilitation. These include both commercial products, such as CyberGrasp (Immersion Corporation, San Jose, CA) [26], the Hand Mentor (Kinetic Muscles Inc., Tempe, AZ) and the Amadeo System (Tyromotion GmbH, Graz, Austria), and experimental devices, such as Rutgers Master II-ND [27], HWARD [28] and HandCARE [29], among others [30]-[33].

However, the majority of the developed systems do not provide individual control of the thumb. The thumb is a unique digit in the hand typically modeled with five degrees-of-freedom (DOF) [34]-[37]. The role of thumb is crucial in hand function as it is involved in 40-50% of hand function, which is almost equivalents the function of all other fingers. Some devices allow individual control of the thumb [30], [33], however, these devices do not have sufficient speed or torque to thoroughly explore the space of different training algorithms and environments. For example, stroke survivors may generate substantial coactivation, especially during intended thumb extension [38], such that significant joint torques may need to be provided by the exoskeleton to overcome the misapplied joint torques of the user. Abnormalities in impedance and motor control may vary from joint to joint such that independent control of each joint through the exoskeleton may be beneficial for training. Additionally, to examine and mitigate power deficits [39] and peak tracking limitations, high joint rotational velocity may be needed.

Thus, in this work, we present the design and development of an actuated thumb exoskeleton (ATX). The ATX provides individual actuation at each thumb joint with

high joint torque and speed capacities that are necessary for rehabilitation research. The transmission through flexible shafts offers good backdrivability and permits the natural motion of the thumb. The ATX will facilitate direct comparisons between various rehabilitation strategies and motor control studies within a single platform. This paper is organized as follows: Section II presents the mechanical design of the ATX; Section III introduces the kinematic analysis; Section IV shows the analysis of the flexible shaft transmission and instrumentation of torque and position sensors; Section V presents results of the kinematic and kinetic performance testing; Section VI discusses the ATX design and experimental results; Section VII concludes the paper and proposes future work.

The ATX Design

In this section, we present the design considerations and their rationales in the ATX design.

Independent Actuation of Each Thumb DOF

The human thumb is generally modeled as a five DOF manipulator with the virtual links connected by revolute joints, in accordance with anatomical models of the thumb [34]-[37]. The 5 DOF are: flexion/extension (F/E) of the carpometacarpal (CMC) joint followed by abduction/adduction (Ab/Ad) of the CMC joint, then Ab/Ad followed by F/E of the metacarpophalangeal (MCP) joint, and finally by F/E of the interphalangeal (IP) joint. Consecutive rotational axes may be non-orthogonal and non- intersecting. The orientation of the axes of rotation in the thumb model follows the anatomical descriptions (Figure V-1). The anatomy-based kinematic model of the thumb has been converted into

a robotics-based description with the standard Denavit-Hartenberg (D-H) parameters in [37], thus, it is possible to approximate thumb kinematics using an exoskeleton with hinged linkages.

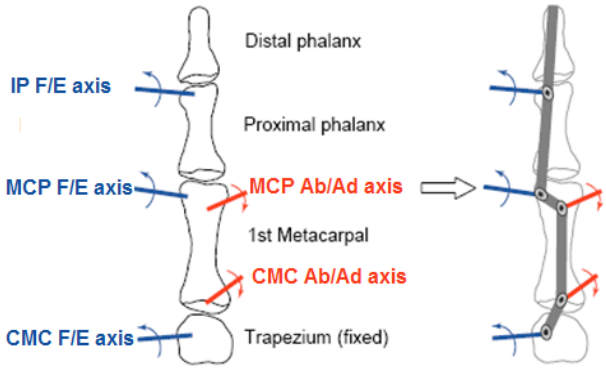

Figure V-1 A Virtual Five-link Model of the Thumb [37]

In order to achieve independent actuation of each thumb joint, the ATX presented in this paper has 5 active DOF and 3 Passive DOF. The five active joints produce F/E of the CMC, MCP and IP joints, and Ab/Ad of the CMC and MCP joints (Figure V-2). The exoskeleton physically attaches to the distal, proximal, and metacarpal segments of the thumb. The attachment points which actuate the MCP and IP joints are connected through two-bar linkages, which accommodate the variation in segment lengths across the population. The F/E and Ab/Ad of the CMC joint are directly actuated; the rotational axes of the ATX can be adjusted to align them with the axes of the user (Figure V-2). Note that because the thumb joints are non-orthogonal and non-intersecting, an axial rotation will be observed between the metacarpal and proximal segments when MCP Ab/Ad occurs. Thus a universal joint, which has 2 passive DOF, is developed for the thumb exoskeleton to allow this axial rotation (Figure V-3). This motion is important for thumb opposition.

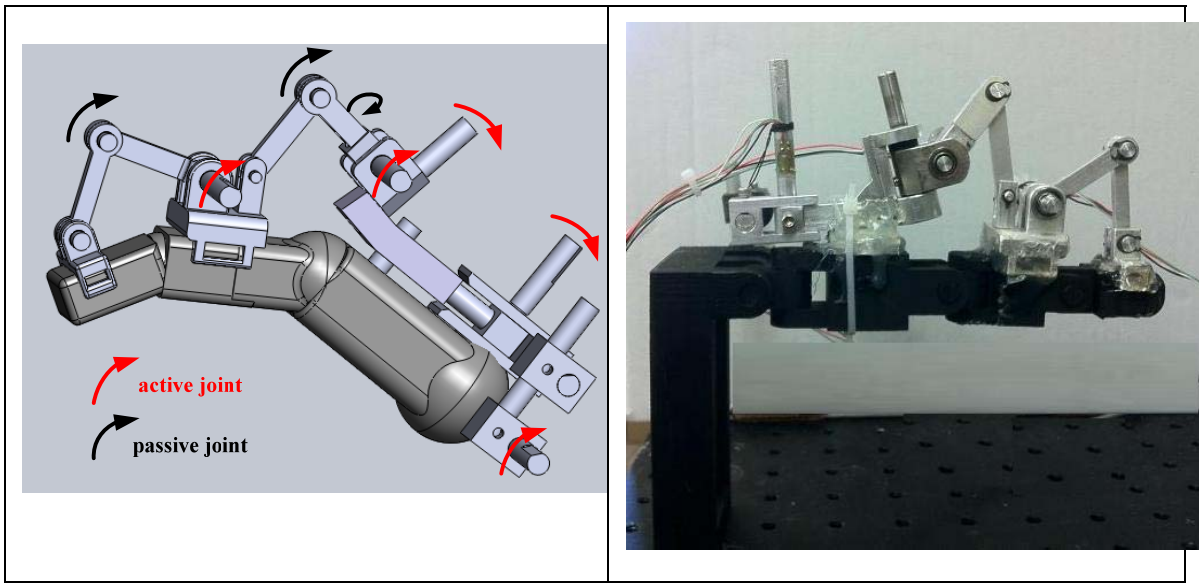

Figure V-2 ATX Solidworks Model (left) and Current Prototype (Right)

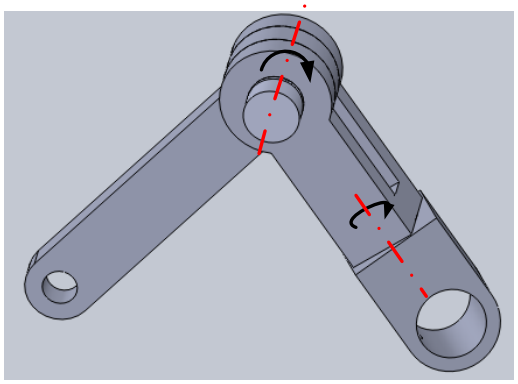

Figure V-3 The Universal Joint connecting CMC and MCP joints

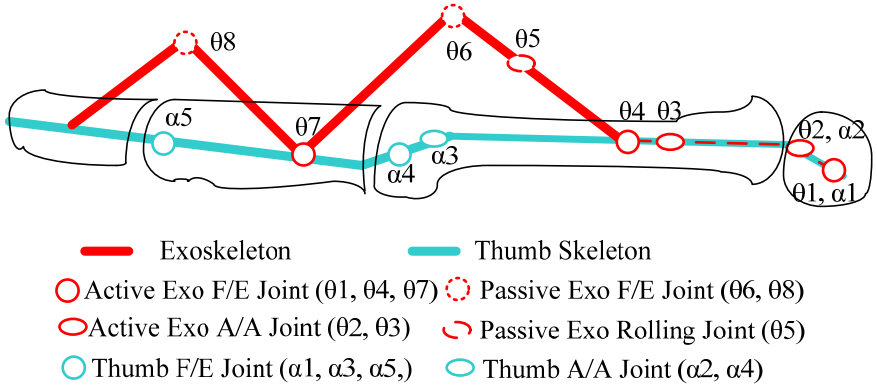

Figure V-4 The simplified thumb and ATX models

Joint Range of Motion

Each joint of the thumb has a wide range of motion. The individual joints themselves do not have a significant amount of mobility on their own but when added together they are able to move in unique ways. The way in which each joint in the thumb can move varies from thumb to thumb. Table V-1 lists comparative data from three different researchers, quantifying the range of motion in the different thumb joints. A few of the values are close to each other but the majority has a significant amount of variance.

Table V-1 Thumb Joint Range of Motion (Unit: Degree)

Thumb Axis	Cooney [40]	Buchholz [41]	Katarincic [42]
IP F/E		85	80
MCP F/E	56±15	50	70
MCP Ab/Ad	19±8.8	30	30
CMC F/E	53±11	50	45
CMC Ab/Ad	42±4	40	40

With properly designed lengths of the linkages for each joint, the current ATX is able to produce equivalent joint motion on the thumb across full ranges of thumb motion: -30 to 60° for CMC F/E, -30 to 30° for CMC Ab/Ad, -10 to 75° for MCP F/E, -20 to 20° for MCP Ab/Ad, and -10 to 90° for IP F/E.

Joint Velocity Capacity

The maximum angular velocity of thumb movement has been recorded at the level of 1000°/s for thumb-tip motion [43]. So in our design, the maximum angular velocity of the equivalent thumb-tip motion produced by the ATX is also targeted at 1000°/s. The capability to produce high speed motion is necessary for the application to practical thumb manipulation task and the implementation of sensory perception study as the thumb movement ranges from low to high speed.

Joint Torque Capacity

In order to implement thumb rehabilitation algorithms for stroke patients, the ATX needs to be able to generate sufficient torque to overcome the excessive coactivation and increased stiffness in the affected thumb. To estimate the output torques of the actuators for the ATX, experiments were carried out to gauge the maximum forces generated at the thumb-tip by stroke survivors and neurologically intact individuals. Nine subjects with severe hand impairment and nine subjects with moderate hand impairment, as rated by the Stage of Hand section of the Chedoke-McMaster Stroke Assessment [45] participated, along with ten control subjects.

In the experiments, subjects were required to generate isometric thumb-tip force in 6 intended directions: distal/proximal, adduction/abduction, flexion/extension (Figure V-5). The configuration of the thumb posture was 50° for CMC extension, 20° for CMC abduction, 20° for MP flexion, 10° for MCP Abduction and 30° for IP flexion. Details of the experimental setup and procedure are in preparation for a separate publication. The experiment was approved by the Institutional Review Board of Northwestern University.

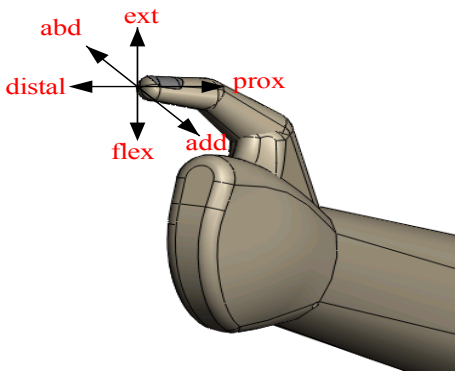

Figure V-5 Directions of Applied Thumb-tip Force

The measured thumb-tip forces were converted into joint torques using

$$\vec{\tau} = J^T \cdot \vec{f} \quad (1)$$

Here, $\vec{\tau} \in \Re^{5\times1}$ is the vector of joint torques; J is the Jacobian matrix of the thumb model; $\vec{f} \in \Re^{3\times1}$ is the vector of the thumb-tip force recorded by the force. The D-H parameters used in the Jacobian matrix were obtained from literature (Table V-2). Table V-3 shows the maximum torque calculated for each joint for all subject groups.

Table V-2 D-H parameters for the thumb model [37]

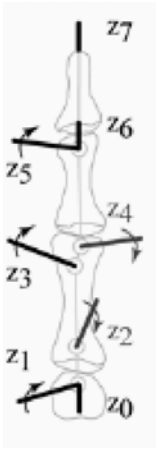

	θ	d (cm)	a (cm)	α (degree)
Z_6 to Z_7	0	3.42	0.03	0
Z_5 to Z_6	θ_5	-0.71	0	94.89
Z_4 to Z_5	θ_4	-1.16	3.99	106.43
Z_3 to Z_4	θ_3	0.85	0.31	-110.37
Z_2 to Z_3	θ_2	0.51	4.45	88.41
Z_1 to Z_2	θ_1	0.21	1.31	-86.86
Z_o to Z_1	0	0.59	-0.12	-93.86

Table V-3 Calculated Maximum Joint Torques of the Thumb (Nm)

Thumb Joint	Subjects		
	Control	Stroke - Moderate	Stroke - Severe

CMC F/E	5.59	2.66	0.99
CMC Ab/Ad	-4.81	-2.40	-0.91
MCP F/E	3.67	1.54	0.94
MCP Ab/Ad	-3.09	-1.78	-0.85
IP F/E	1.85	0.58	0.48

To accommodate the majority of our target population, we chose the peak joint torque outputs of the exoskeleton to be comparable to those of moderate stroke subject, which are 2.5 Nm at CMC F/E, 2 Nm at Ab/Ad joints, 1.5 Nm at MCP F/E and Ab/Ad joints, 0.5 Nm at IP F/E joint.

Actuation System

The ATX is actuated by DC motors (AKM Series Motor, Kollmorgen, Munkekullen, Sweden). DC motors were chosen due to their high torque and velocity performance in all four quadrants of the torque-velocity space. To minimize the weight of the exoskeleton carried by the user, the motors are located remotely from the thumb exoskeleton, and supported by an external platform. This is made possible by the use of flexible shafts to transmit motor torque to the ATX. The flexible shaft, coupled to both the motor shaft and the driving shaft on the ATX joint (Figure V-6), transmits rotary motion between the motors and the exoskeleton while allowing flexibility in its shape between its two ends. The flexible shaft can change shape to accommodate variations in distance between the motor and the exoskeleton as the digit moves. This flexibility makes the system backdrivable. As the flexible shaft provides rigid couplings to the motor shaft and the driving shaft of the ATX at its two ends, it can rotate the joint in either the

clockwise or the counter-clockwise direction, thus, only one motor is needed for each DOF. To maximize backdrivability, the motor for IP joint has no gearing and motors for CMC and MCP joints have only 3:1 gearing ratio.

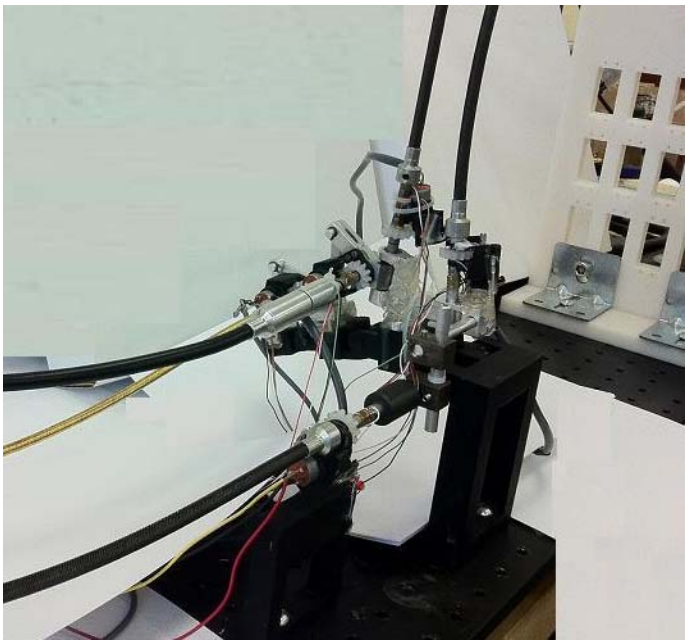

Figure V-6 The ATX with flexible shaft connected

Sensory System

To control thumb manipulation tasks, the ATX must support both position and torque control at each joint. Thus, both joint angle and torque measurements are required for feedback control and for data collection. Joint angles and torques are measured directly at the joints of the ATX. The joint angles are measured by potentiometers (Precision Electronics Corp., Toronto, Canada) affixed to the shafts of the ATX with gear sets (Figure V-7). The motors also have integrated encoders, however, due to the flexible shaft transmission, the values measured at the motor shafts and the ATX shafts may deviate. The deviation between the two measurements can be used to detect mechanical

failure. The joint angles of the thumb can be calculated by the joint angles of the ATX through kinematic equations.

Joint torque is measured through full-bridge strain gages attached on the cylindrical driving shafts of the ATX (Figure V-7). Namely, two rosettes of strain gauges are attached (one in front and on in back) of each cylindrical drive shaft and these gauges are then incorporated into a Wheatstone bridge. The full-bridge strain gage circuit is able to eliminate nonlinearity and hysteresis in the torque measurement.

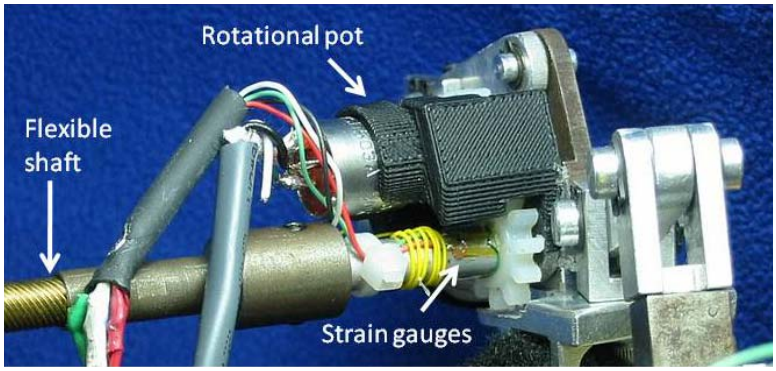

Figure V-7 Potentiometer and strain gages on one ATX joint with flexible shaft connected

The Real-time Control System

The angular position and torque signals are used to implement low level feedback control of each joint. Depending on the application, either position control or force control may be required. Position controller enables the tracking of specific trajectories while force control is needed in order to implement virtual interactions with the user, as well as during periods when we want the user to perform tasks with little or no impedance from the exoskeleton.

All control programs is developed in MATLAB Simulink. The real-time control of the thumb exoskeleton is implemented using MATLAB xPC Target software [46]. The xPC

Target is a real-time environment running on a designated PC for real-time applications. The control system of the ATX consists of two parts (Figure V-8): a host PC with MATLAB Simulink software, to create the controller model using Simulink blocks and then compile the model to the executable code; and a target PC running the xPC Target real-time kernel, which downloads the executable code from the host PC and runs it in real-time. The data signals are acquired in real-time by the target PC and uploaded to the host PC through Ethernet. The experimenter can monitor the data signal in the host scope and tune the parameters in the Simulink model created in the host PC.

A PCI-6229 ADC board (National Instruments, Austin, TX) is installed on the target PC to perform analog-digital conversion of torque sensor signals and potentiometer signals. A CNT32-8M encoder board (CONTEC, Sunnyvale, CA) records quadrature encoder signals and a PCIM-DDA06/16 DAC board (Measurement Computing, Norton, MA) converts digital command signals into the analog signals which drive the S200 motor amplifiers (Kollmorgen, Munkekullen, Sweden). All signals are sampled at 1 kHz.

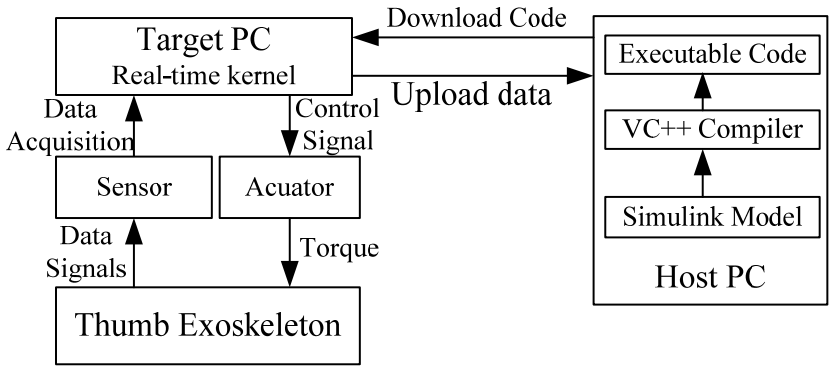

Figure V-8 The Real-time Control System using xPC Target. The host PC manages the control program, provides visual feedback and stores experimental data; the target PC runs the real-time control program and acquires sensor data.

Safety and Limitations

A number of safety mechanisms are implemented to ensure safe interaction with the individual's hand. The lever linkages restrict the angular position of each joint of the ATX in the acceptable range. An emergency kill switch is provided to immediately disable all motors. Software monitoring of both joint position and motor torque, will continuously check to see if specified limits are exceeded and will immediately disable the system should this occur.

In our design, individually sized motors and flexible shafts are used for the different joints. In this manner, peak motor torque can be better matched to peak voluntary subject torque and thus the potential for excessive torque is minimized.

Kinematic Analysis

In this section, we analyze the kinematics of the coupled system of the ATX model and the thumb model.

The thumb and the ATX can be modeled as chains of rigid links as shown in Figure V-4. Both the thumb and the ATX models have individual kinematic redundancy for the 3 DOF of their tip locations, as the thumb model has 5 DOF and the ATX has 5 active DOF and 3 passive DOF in the joint-space (orientation of the end-effectors is not considered for the current application). Thus, for a given task-space trajectory, there will be an infinite number of possible joint-space trajectories for either the thumb or the ATX model. One concern of this redundant system is whether a unique mapping can be established between the joint-space trajectories of the thumb and the ATX models.

The task-space trajectories of the thumb model and the ATX model are represented by the joint-space trajectories using forward kinematics:

$$\vec{X}_{thumb} = \vec{f}_{thumb}(\vec{\alpha}), \quad \vec{X}_{exo} = \vec{f}_{exo}(\vec{\theta}) = \vec{f}_{exo}(\vec{\theta}_a, \vec{\theta}_p) \tag{2}$$

where $\vec{X}_{thumb}, \vec{X}_{exo} \in \Re^{3X1}$ are the thumb-tip position and the end-effector position of the ATX model in the Cartesian space, respectively. $\vec{\alpha} \in \Re^{5X1}$ is the vector of the joint angles of the thumb model; $\vec{\theta}_a \in \Re^{5X1}$, *a*=1, 2, 3, 4 and 5, and $\vec{\theta}_p \in \Re^{3X1}$, *p*=6, 7 and 8, are the vectors of the active and the passive joint angles of the ATX model, respectively.

The position of the attachment points can be written as,

$$\begin{aligned} \vec{X}_{C1} &= \vec{F}_1(\theta_1, \theta_2) \\ \vec{X}_{C2} &= \vec{F}_2(\theta_1, \theta_2, \theta_3, \theta_4, \theta_5, \theta_6) \\ \vec{X}_{C3} &= \vec{F}_3(\theta_1, \theta_2, \theta_3, \theta_4, \theta_5, \theta_6, \theta_7, \theta_8) \end{aligned} \tag{3}$$

and,

$$\begin{aligned} \vec{X}_{C1} &= \vec{G}_1(\alpha_1, \alpha_2) \\ \vec{X}_{C2} &= \vec{G}_2(\alpha_1, \alpha_2, \alpha_3, \alpha_4) \\ \vec{X}_{C3} &= \vec{G}_3(\alpha_1, \alpha_2, \alpha_3, \alpha_4, \alpha_5) \end{aligned} \tag{4}$$

where $\vec{F}_1$, $\vec{G}_1 \in \Re^{2X1}$, $\vec{F}_2, \vec{F}_3$, $\vec{G}_2, \vec{G}_3 \in \Re^{3X1}$ are the functions of the positions at constraint points.

Since the functions $\vec{F}(\vec{\theta}_a, \vec{\theta}_p) = \left[\vec{F}_1; \vec{F}_2; \vec{F}_3\right]$ and $\vec{G}(\vec{\alpha}) = \left[\vec{G}_1; \vec{G}_2; \vec{G}_3\right]$ represent the positions of the same set of constraint points,

$$\vec{H}(\vec{\theta}_a, \vec{\theta}_p, \vec{\alpha}) = \vec{F} - \vec{G} = 0 \ , \ \vec{H} \in \Re^{8X1}. \tag{5}$$

It is unrealistic to solve Equation (6) to obtain the joint angle of the thumb from the measured joint angle of the ATX directly as those equations are highly nonlinear. Thus, Equation (6) is differentiated once to obtain the mapping at the velocity level,

$$\frac{\partial \vec{H}}{\partial \vec{\theta}_a}\dot{\vec{\theta}}_a + \frac{\partial \vec{H}}{\partial \vec{\theta}_p}\dot{\vec{\theta}}_p + \frac{\partial \vec{H}}{\partial \vec{\alpha}}\dot{\vec{\alpha}} = 0 \tag{6}$$

$$\begin{bmatrix} \frac{\partial \vec{H}}{\partial \vec{\theta}_a} & \frac{\partial \vec{H}}{\partial \vec{\theta}_p} \end{bmatrix} \begin{bmatrix} \dot{\vec{\theta}}_a \\ \dot{\vec{\theta}}_a \end{bmatrix} = -\frac{\partial \vec{H}}{\partial \vec{\alpha}}\dot{\vec{\alpha}} \tag{7}$$

Let $\begin{bmatrix} \frac{\partial \vec{H}}{\partial \vec{\theta}_a} & \frac{\partial \vec{H}}{\partial \vec{\theta}_p} \end{bmatrix} = J_{H_\theta}$, $\frac{\partial \vec{H}}{\partial \vec{\alpha}} = \mathrm{J}_{\mathrm{H}_\alpha}$, then Equation (7) can be written as,

$$\dot{\vec{\alpha}} = -(\mathrm{J}_{\mathrm{H}_\alpha})^{-1} \cdot \mathrm{J}_{\mathrm{H}_\theta} \cdot \dot{\vec{\theta}}_a = \mathrm{J}_1 \cdot \dot{\vec{\theta}}_a \tag{8}$$

where $\mathrm{J}_1 = -\left(\mathrm{J}_{\mathrm{H}\alpha}\right)^{-1} \mathrm{J}_{\mathrm{H}_\theta}$.

Equation (8) gives the constraints between the angular velocities of the ATX joints and the thumb joints. Note that the coupled system of the thumb model and the ATX model has a total of 13 DOF in the joint-space while Equation (8) introduces 8 constraint equations, which means once the joint-space trajectories of the ATX model are defined, the corresponding joint-space trajectories for the thumb model will be determined by the constraint equations, and vice versa. Thus, there is a unique mapping between the joint-space trajectories of the thumb and the ATX models. Details of the kinematic analysis can be found at [44].

Instrumentation

Flexible Shaft Transmission Testing

In our design, the transmission through the flexible shafts allows the actuators to be placed remotely from the ATX. Our major concerns regarding the flexible shaft transmission are the transmission loss of both motion and torque; the off-axis forces/torques in unintended directions and the helixing of the flexible shaft under high

load. Preliminary tests were performed to investigate the transmission performance of the flexible shafts (Figure V-9). The flexible shaft was bent with a 90° curvature in the tests. Bending with this curvature had been tested to render good flexibility at its two ends. The flexible shafts in the ATX use the same curvature.

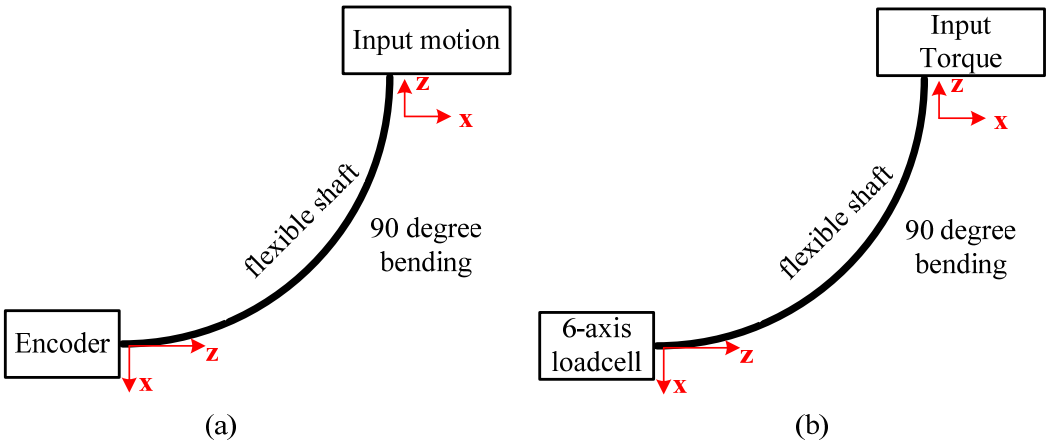

Figure V-9 (a) Schematics of motion transmission test; (b) Schematics of torque transmission test

First, we analyzed the mapping between rotation at one end of the shaft and the corresponding rotation produced at the other end of the shaft (Figure V-9 (a)). With no external resistance imposed on the flexible shaft, the rotation produced by the shaft was equivalent to that imposed on it (within the precision limit of the encoder we were using to measure rotation at one end: 0.25°). Thus, there were no losses within the shaft under voluntary motion (Figure V-10 (a)). When external resistance was imposed, however, output rotation produced by the flexible shaft was less than the angular displacement put into the shaft in the open-loop tests (Figure V-10 (b)). Some of the input produced twisting, or "helixing", of the shaft rather than rotation of the other end. The tendency to helix can be mitigated by placing an outer casing around the shaft. Thus, in closed-loop

control under high torque, the angular position measurements have to be measure directly at the exoskeleton end rather than the motor end.

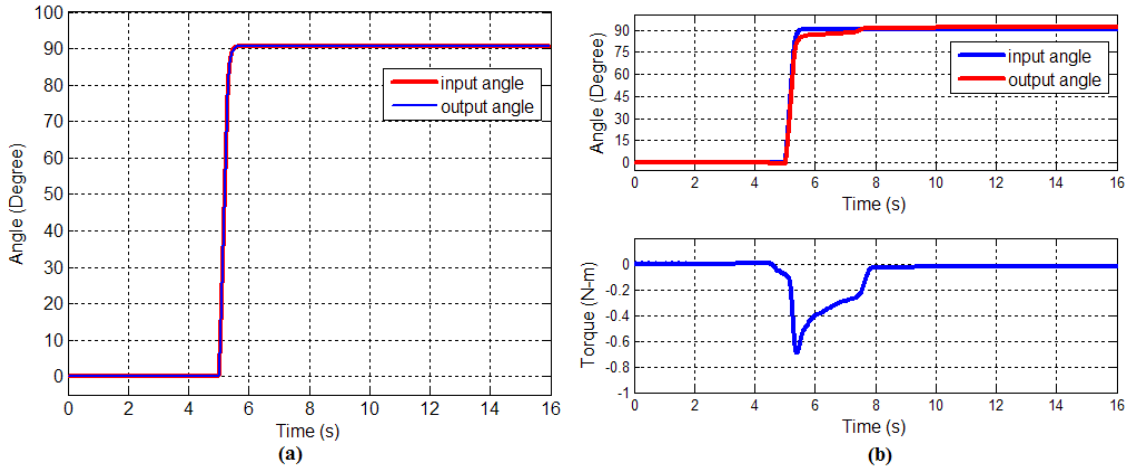

Figure V-10 Kinematic transmission through the flexible shaft: (a) motion transmission under no torque load; (b) motion transmission under torque.

Torque transmission performance through the flexible shaft was examined as well (Figure V-9 (b)). Figure V-11 shows the torque transmission performance of the flexible shaft. Output torque at the distal end of the shaft stayed within 10% error of the input torque imposed at the proximal end of the shaft for input torques up to 1 Nm. Shaft efficiency is dependent upon the shape of the shaft. With a straighter shaft, as opposed to the curved posture we used in our tests, correspondence between input and output torque improves. Thus, in closed-loop control, torque needs to be measured directly at the driving shaft for the actuated joint of the ATX.

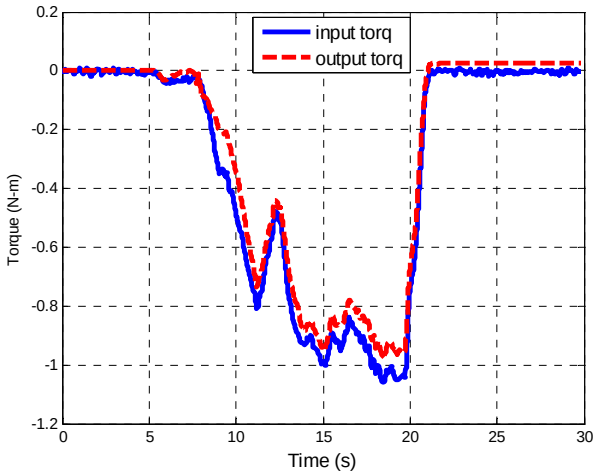

Figure V-11 Torque transmission through flexible shaft

We also tested off-axis forces and torques produced by the flexible shaft at its distal attachment point (Figure V-9 (b)). In addition to the desired torque that was transmitted about the z-axis, small residual moments could be present about other axes and small forces could be produced as well, depending on the shaft configuration. Figure V-12 and Figure V-13 show the experimental results of the tests. When the input torque manually applied along the shaft axis (z-axis) was low (up to 0.5 Nm), which was more than sufficient for free motion, the off-axis forces and torques in other directions were minimal (<1.5N, Figure V-12). When the input torque was increased to around 1.5 Nm (the maximum torque required for the MCP and IP joints of the ATX), the maximum off-axis force was about 6N, directed along the z-axis, and the maximum off-axis torque was less than 0.3 Nm, about the x-axis. No significant helixing of the flexible shafts was observed during the experiments. Note that this high torque is only needed when the user applies force on an object or has exceptionally high stiffness in the thumb joint. In such cases, the effect of off-axis forces and moments will be minimized due to the structural rigidity of the ATX. Moreover, the structure of the exoskeleton is designed to reject some

of these unwanted moments/forces. The pin joints only allow rotation about the desired axis and strong coupling between the ATX and the hand resists the small off-axis forces.

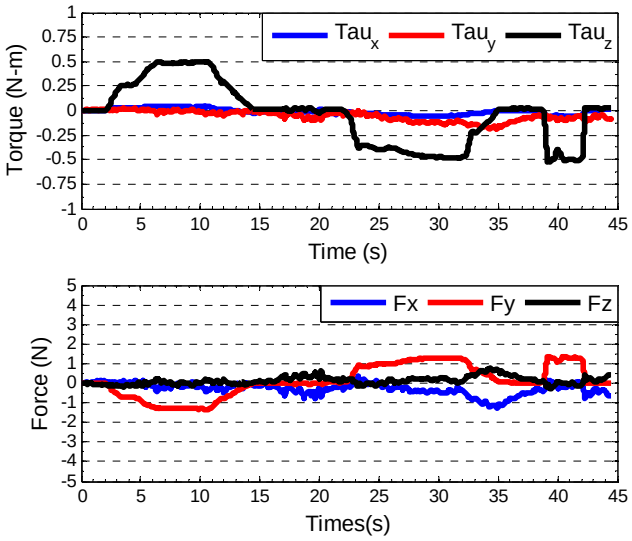

Figure V-12 Off-axis force/torque with 90° shaft bending under low input torque

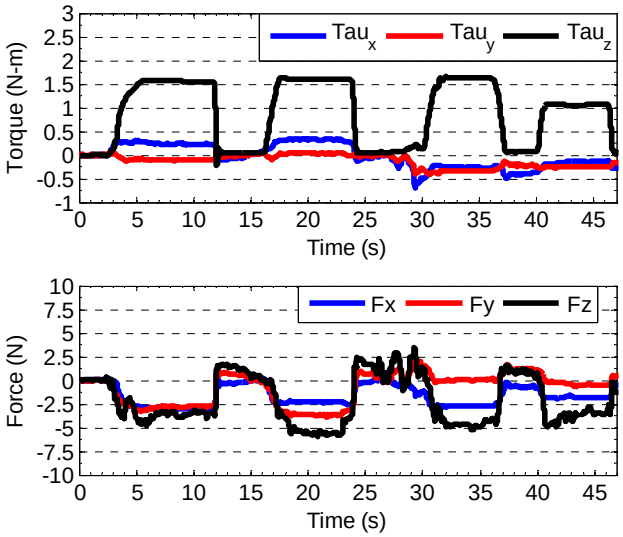

Figure V-13 Off-axis force/torque with 90° shaft bending under high torque

Strain Gage Torque Sensor Calibration

The strain gage torque measurement was calibrated with an external load cell (Figure V-14). In the calibration, torque was applied manually at one end of the shaft with strain gage attached; the other end of the shaft was connected to a 6-axis load cell. The output voltage signal of the strain gage and the torque measured by the load cell were plotted together for the calibration. The calibration results in Figure V-15 showed that the strain gage torque measurement was highly linear ($R^2 > 0.999$) with negligible hysteresis (RMS error = 0.0083 Nm).

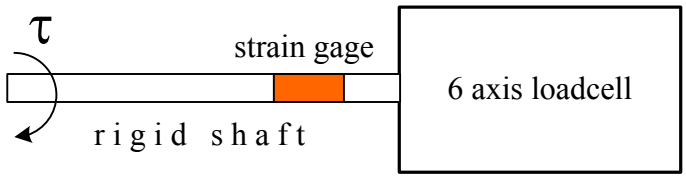

Figure V-14 Strain Gage Torque Sensor Calibration Setup

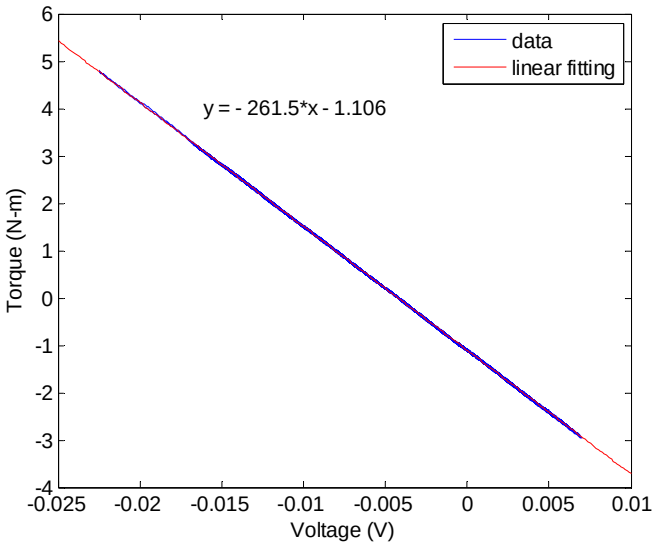

Figure V-15 Strain Gage Torque Measurement Calibration

Potentiometer Calibration

The potentiometer was calibrated with an encoder (Figure V-16). In the calibration, the shaft was manually rotated in both the clockwise and the counterclockwise directions for 10 times. The output voltage signal of the potentiometer and the rotating angle measured by the encoder were plotted together for the calibration Figure V-17. The calibration results showed that the strain gage torque measurement was highly linear ($R^2 > 0.999$) with minimal measurement inaccuracy. (RMS error = 0.215°).

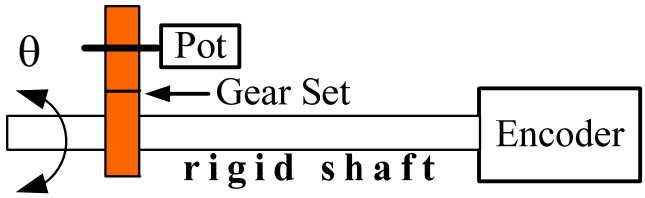

Figure V-16 Potentiometer Calibration Setup

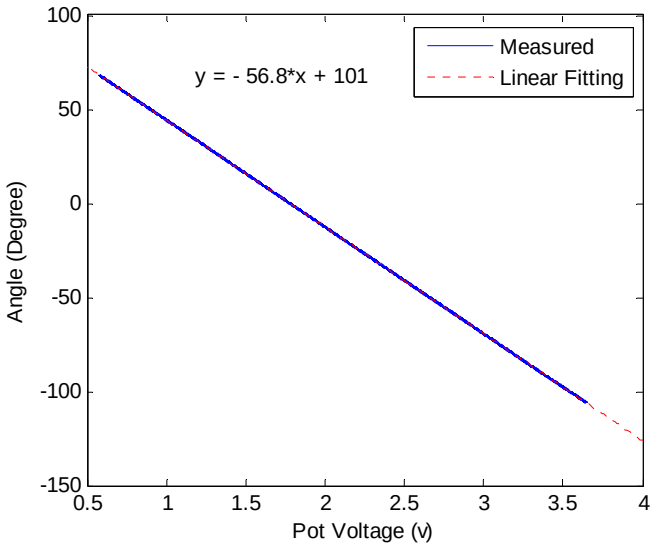

Figure V-17 Potentiometer Calibration

Performance Testing and Experimental Results

In this section, we present results of the experiments conducted to test the kinematic and kinetic performance of the ATX. For readability, we use J1, J2, J3, J4 and J5 as short for CMC F/E, CMC Ab/Ad, MCP F/E, MCP Ab/Ad and IP F/E, respectively.

Kinematic Performance Testing

Experiments were conducted to perform closed-loop joint position control with PI controllers on an artificial thumb. This artificial thumb has 5 DOF, corresponding to the human thumb DOF. For testing purpose, the axes of rotation of artificial thumb are orthogonal. The feedback signal to the PI controller was the joint angle of the thumb computed from the joint angle of the ATX, as measured with the potentiometer. The ATX was actuated by DC motors.

Ramp Trajectory Tracking

The first experiment was to examine the ability of the ATX to track a ramp trajectory for each individual joint. One joint was tested at a time. Table V-4 shows the parameters of the desired trajectory for each joint in these trials.

Table V-4 Parameters of Desired Ramp Trajectories

Joint	J1	J2	J3	J4	J5
Starting Position	0	0	0	0	0
End Position	30°	30°	45°	10°	30°
Velocity	30°/s	30°/s	25°/s	8°/s	25°/s

The experimental results of each joint in the trials are shown in Figure V-18. The tracking performance was good for all 5 joints. The root mean square (RMS) errors at

steady state were 0.098°, 0.105°, 0.124°, 0.118° and 0.140° from J1 to J5, respectively. Response delay was observed in the experiment ranging from 0.08 to 0.2 second.

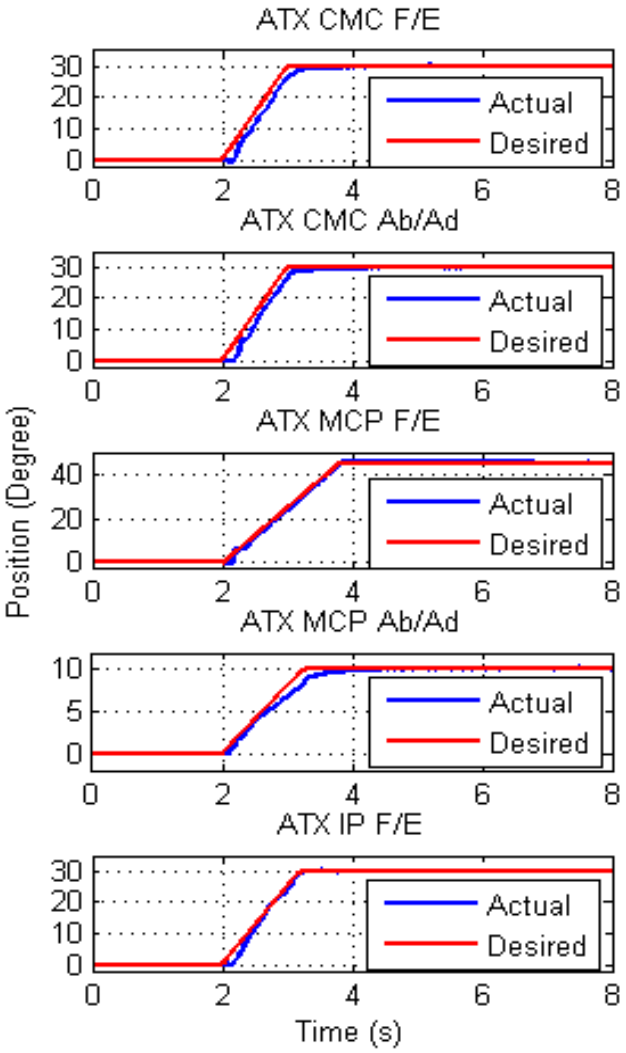

Figure V-18 Tracking of ramp trajectory for individual joint. Each joint was tested separately in different trials.

Velocity Capacity Testing

The second experiment was to examine the capability of the ATX to provide high instantaneous velocity at each joint. A smooth trajectory with maximum instant velocity of 1000°/s or more was created for each joint to track. One joint was tested at a time.

Figure V-19 shows the position and velocity trajectories for each joint in the trials. The maximum velocities observed were 450°/s, 550°/s, 650°/s, 520°/s and 900°/s from J1 to J5, respectively.

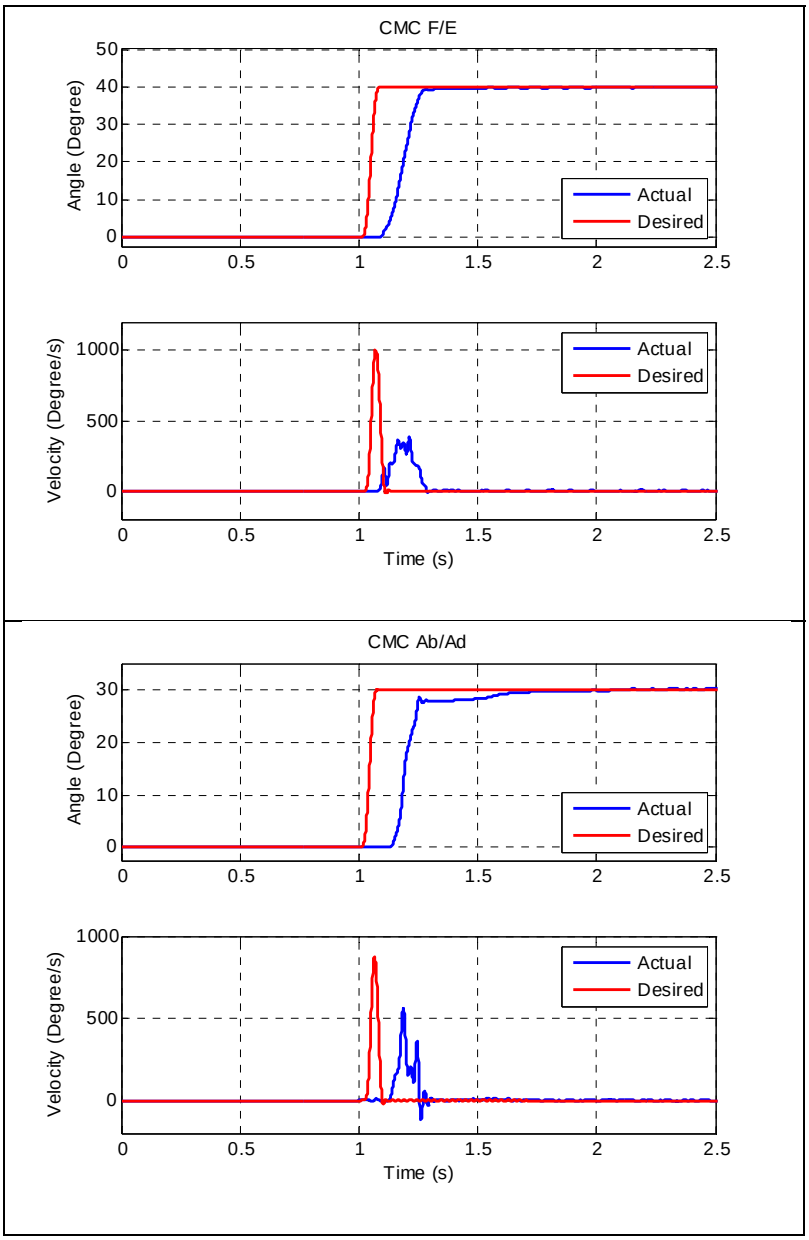

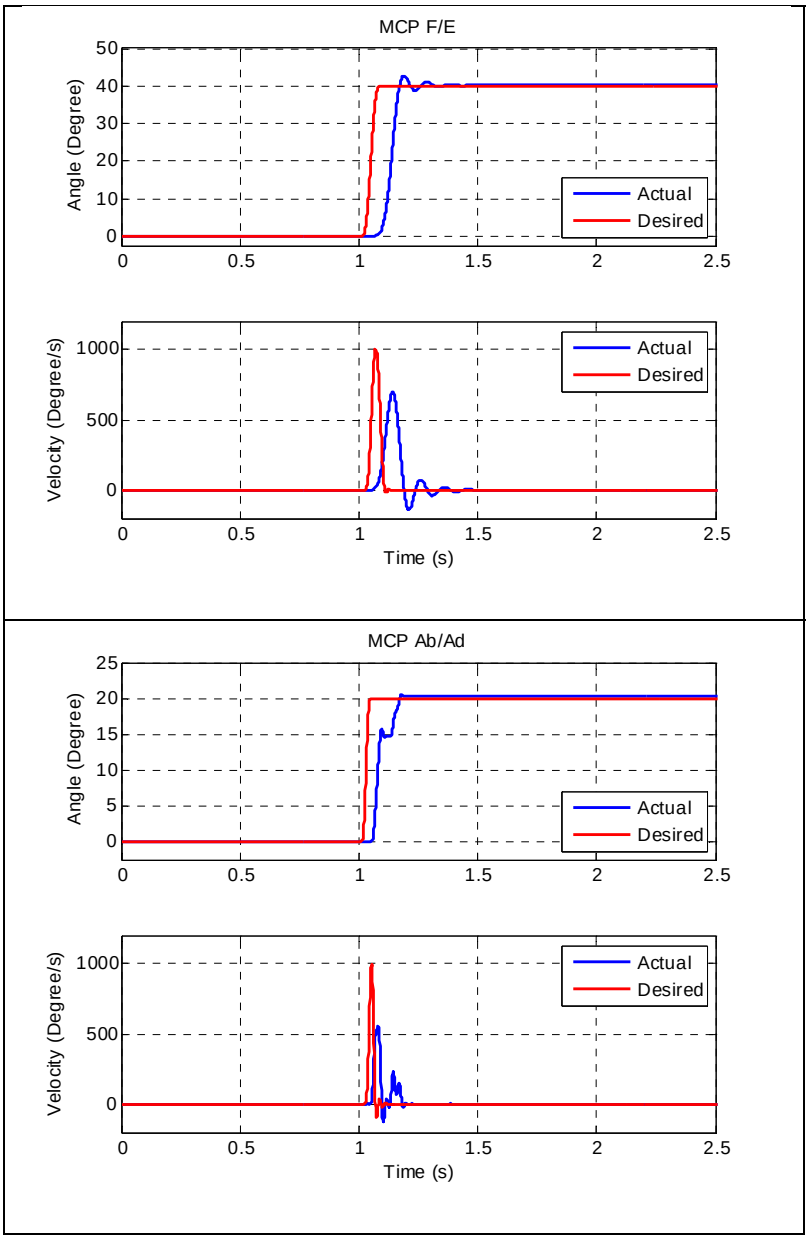
MCP F/E
Angle (Degree)
50
40
30
20
10
0
0
0.5
1
1.5
2
2.5
Actual
Desired
Velocity (Degree/s)
1000
500
0
Time (s)
MCP Ab/Ad
25
20
15
10
5

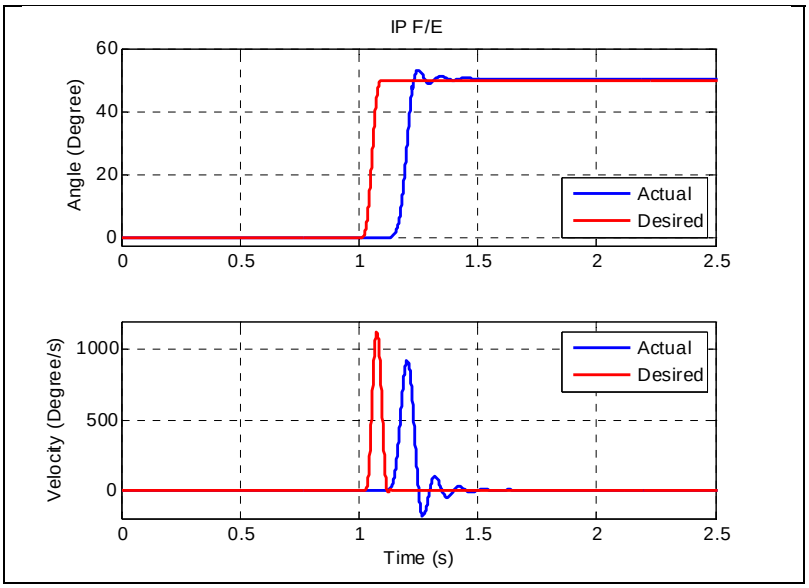

Figure V-19 Examination of peak instantaneous velocity at individual joint

Sinusoidal Trajectory Tracking

The third experiment was to examine the ability of the ATX to track a sinusoidal trajectory for each joint. The desired trajectories were sinusoidal trajectories with the amplitude of 10° (Figure V-20). The frequency of the sinusoids was 2 Hz for all joints expect for the CMC Ab/Ad, which was 1.5 Hz. Response delay of 0.05 to 0.08 seconds was observed in the experiment.

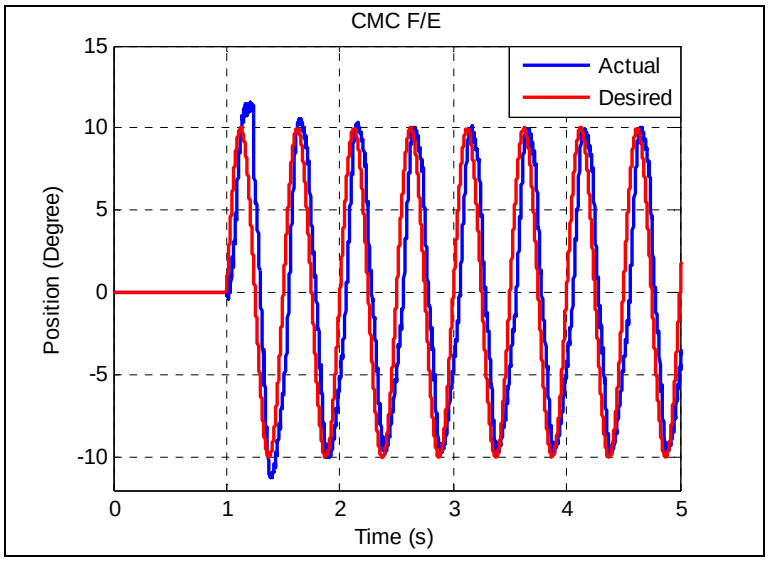

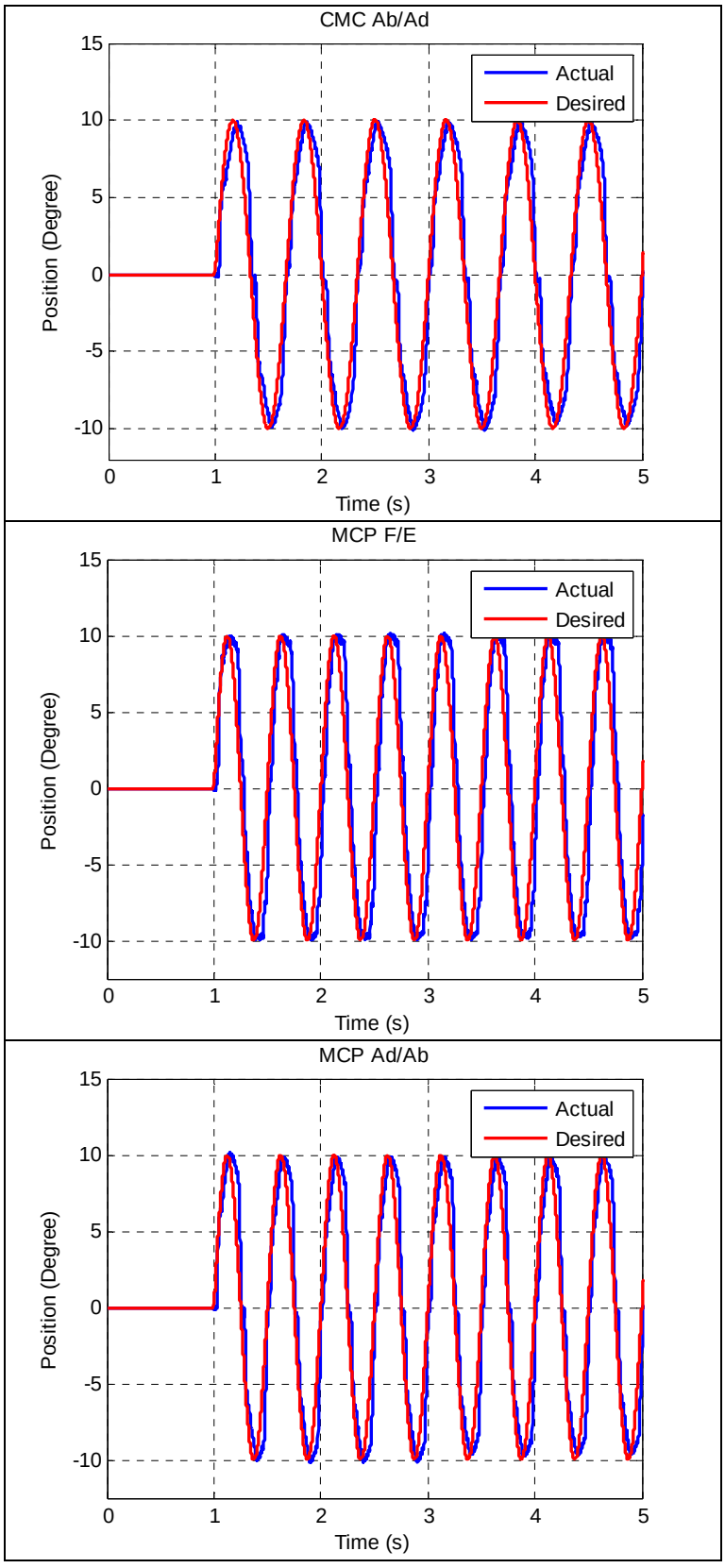
CMC Ab/Ad
Actual
Desired
Position (Degree)
Time (s)
MCP F/E
Actual
Desired
Position (Degree)
Time (s)
MCP Ad/Ab
Actual
Desired
Position (Degree)
Time (s)

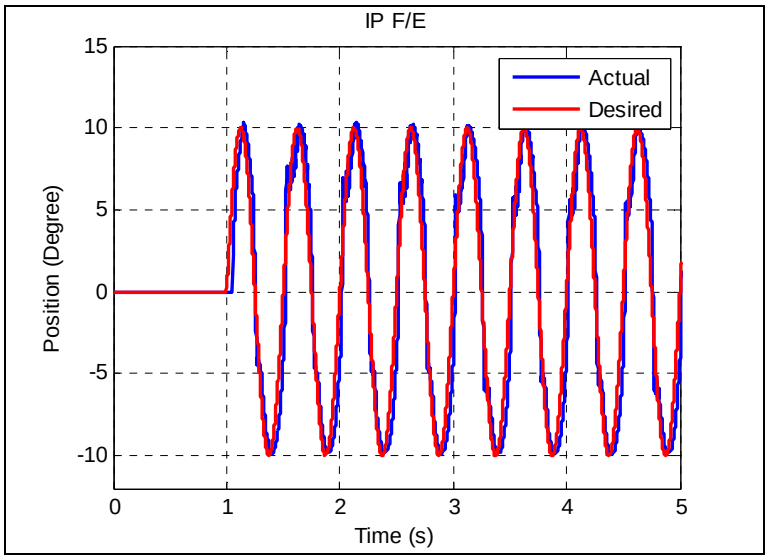

Figure V-20 Tracking of sinusoidal trajectory at individual joint

Multiple Joint Position Control

The next experiment was to control multiple joints to track different desired trajectories simultaneously. In the first trial, all three F/E joints were controlled to track different ramp trajectories. The Ab/Ad joints were passive in this trial with no motor actuation. The experimental results showed that all three F/E joints were able to track the desired trajectories. At the same time, the Ab/Ad joints were not affected by the motion of the F/E joints (Figure V-21). The RMS errors at steady state were 0.254°, 0.127° and 0.328° for J1, J3 and J5, respectively. The RMS variation in J2 and J4 were 0.037° and 0.171°, respectively.

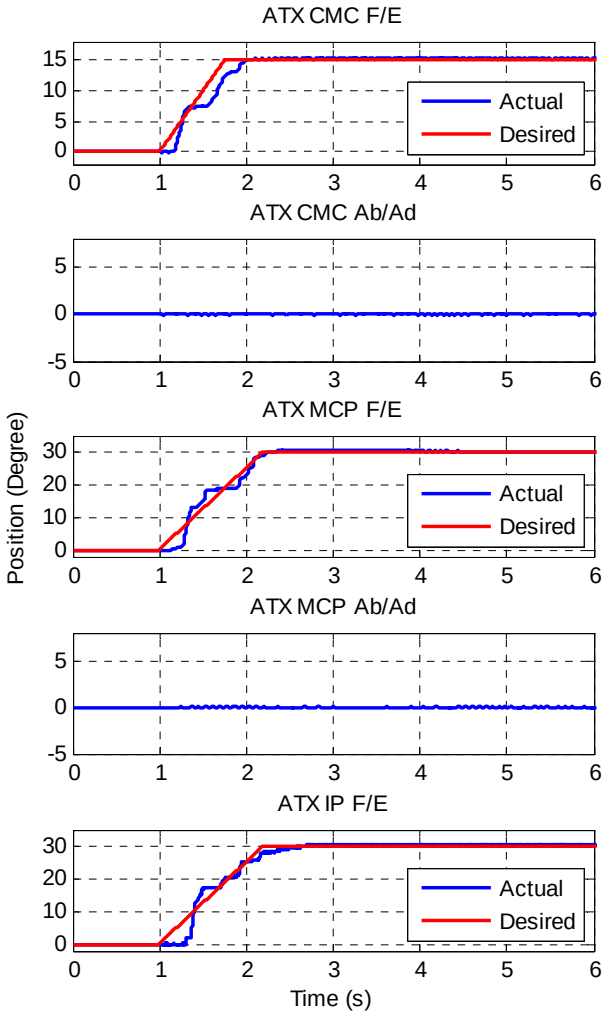

Figure V-21 Tracking of ramp trajectories at all F/E joints

In the second trial, the two Ab/Ad joints were controlled to track different ramp trajectories, while the F/E joints were passive in this trial with no motor actuation. The experimental results showed that both Ab/Ad joints were able to track the desired trajectories (Figure V-22). The F/E joints at MCP and IP were not affected by the motion of the Ab/Ad joints and the F/E joint at CMC showed motion (8° of flexion) when it was passive. This motion could be minimized (less than 1°) when the CMC F/E joint was

actively controlled. The RMS errors at steady state were 0.169° and 0.263° for J2 and J4, respectively. The RMS variation in J3 and J5 were 0.097° and 0.043°, respectively.

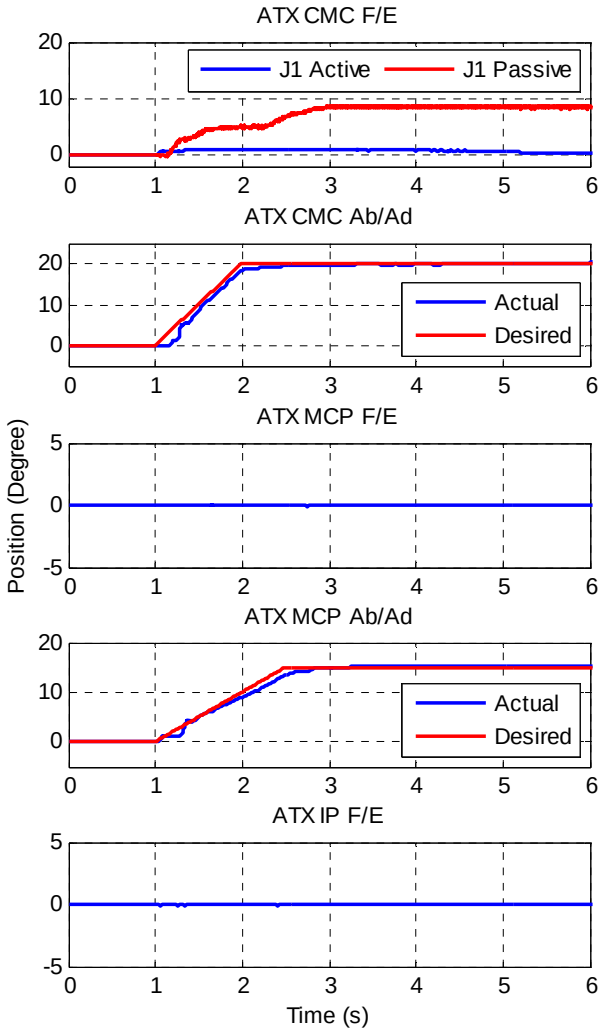

Figure V-22 Tracking of ramp trajectories at all Ab/Ad joints

In the third trial, all 5 joints of the ATX were controlled to track different ramp trajectories simultaneously. The starting configuration of the ATX was at 0° position for all 5 joints and the final configuration was at (15°, 20°, 30°, 12°, 30°) position from J1 to

J5. The experimental results are shown in Figure V-23. The RMS errors at steady state were 0.110°, 0.298° 0.303°, 0.114° and 0.148° from J1 to J5, respectively.

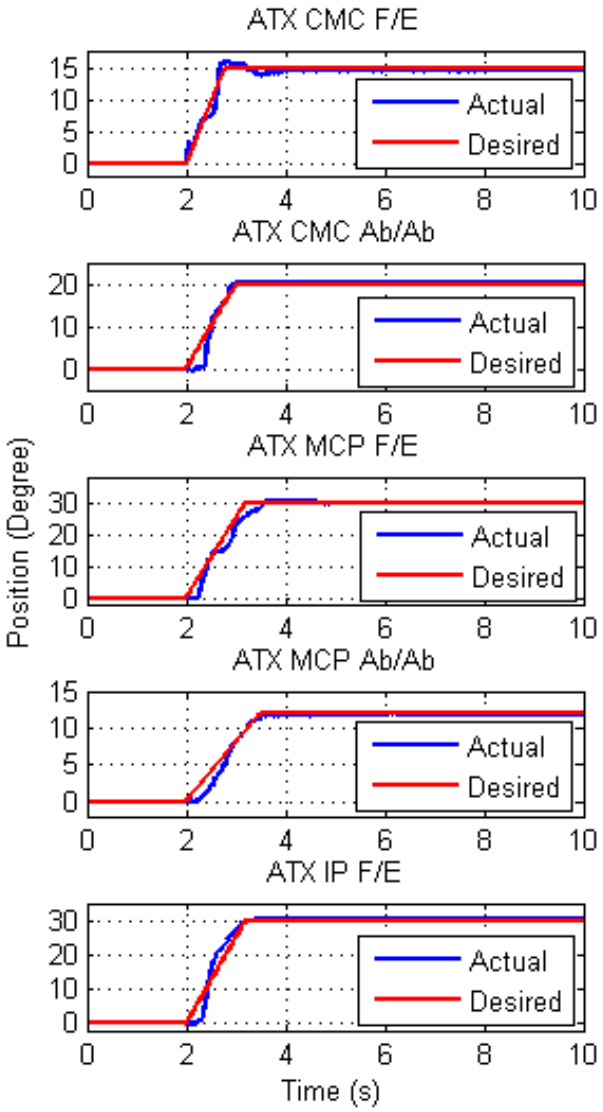

Figure V-23 Control of all 5 joints from one configuration to another

Kinetic Performance Testing

Joint torque control performance was also evaluated in experiments. The desired torque was 0.5 Nm for J1 and J2 joints, and 0.4 Nm for all other three joints. The

experimental results are shown in Figure V-24, all 5 joints were able to provide the desired torque accurately. The errors at steady state were minimal (under 0.005 Nm).

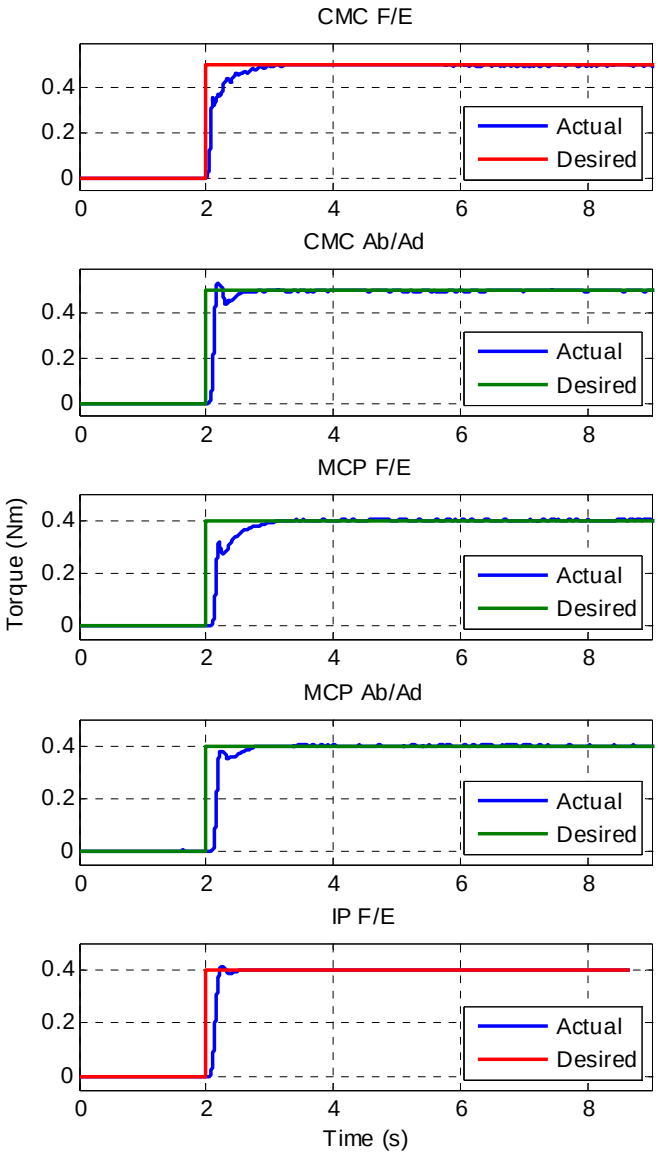

Figure V-24 Experimental results for individual joint torque control

In the next experiment, the F/E joints were controlled to apply a 0.2 Nm torque simultaneously. The actual joint torque are shown in Figure V-25 and the resulting contact force was shown in Figure V-26.

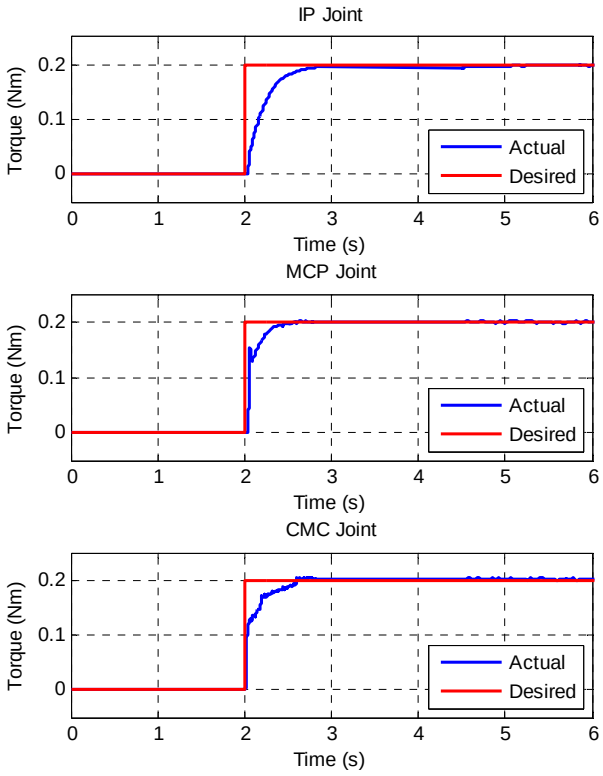

Figure V-25 Experimental Results on Multiple Joint Torque Control

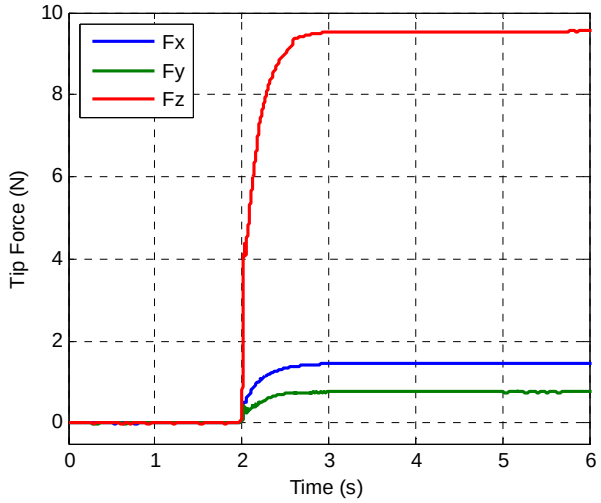

Figure V-26 Thumb-tip Force Measured by Loadcell in Multiple Joint Torque Control

The torque capacity was tested in an open loop experiment. The output command to the motor was gradually increased and the torque applied on the CMC F/E joint of the ATX was recorded by the strain gages. The torque trajectory is shown in Figure V-27. It should be noted that after about 8 second, the flexible shaft started to show observable helixing, which would severely degrade the transmission performance of the flexible shaft and produce excessive off-axis force and torque.

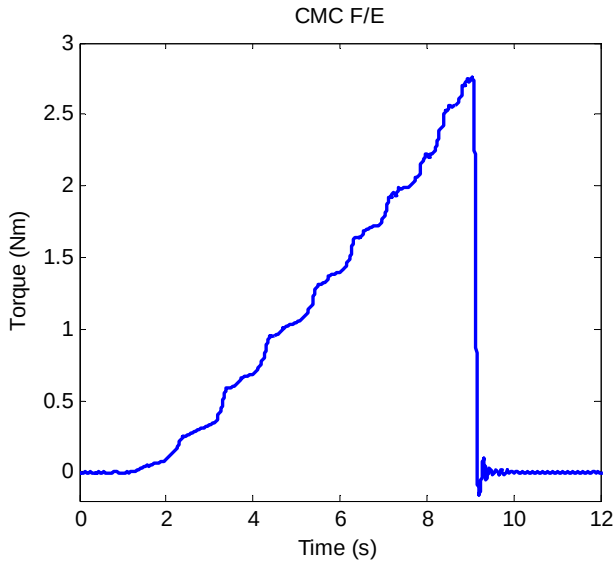

Figure V-27 Torque Capacity Testing at CMC F/E Joint

Discussion

In this work, we design an actuated thumb exoskeleton that provides independent actuation of each thumb DOF with the potential to serve as a general test-bed to implement various rehabilitation strategies and motor learning paradigms for the thumb. The joint range of motion provided by the ATX is able to cover the full ranges of motion of each joint for general sized human thumb.

To reduce the load on the user' thumb, the ATX is actuated by DC motors located remotely from the thumb exoskeleton. These motors are supported by an external platform. This is made possible by the use of flexible shafts to transmit motor torque to the ATX. The flexible shaft can transmit rotary motion between the motors and the exoskeleton, while still is able to change shape to accommodate variations in distance between the motor and the exoskeleton as the digit moves. This flexibility makes the system backdrivable. As the flexible shaft provides rigid couplings between the motor

shaft and the driving shaft of the ATX, it can rotate the joint in either the clockwise or the counter-clockwise direction, and thus, only one motor is needed for each DOF.

Kinematic and kinetic transmission performance of the flexible shaft was tested in our experiments. Transmission loss in motion was not observed under low torque while it did exist when the torque load went beyond 0.5 Nm. Transmission loss in torque was also observed as the torque went up. These observations confirmed the need to measure the joint position and joint torque directly at the exoskeleton joint by potentiometer and strain gages, respectively. The potentiometer and strain gages were calibrated for all joints and showed strong linearity and minimal hysteresis.

We also examined the off-axis forces and torques produced by the flexible shaft at its distal attachment. In addition to the desired torque that was transmitted about the z-axis, small residual moments were present about other axes and small forces were produced as well, with magnitudes dependent upon the shaft configuration. These residual forces and moments could be mitigated by placing an outer casing around the shaft to reduce the helixing of the shaft. Note that the relatively high torque is only needed when the user applies force on an object or has exceptionally high stiffness in the thumb joint. In such cases, the effect of off-axis forces and moments will be minimized due to the structural rigidity of the thumb. Moreover, the structure of the exoskeleton is designed to reject some of these unwanted moments/forces. The pin joints only allow rotation about the desired axis and strong coupling between the ATX and the hand resists the small off-axis forces. We tested our prototype on several subjects and they were largely unaware of any off-axis moments or forces.

The kinematic performance of the ATX was examined in a set of experiments including: the tracking of a ramp trajectory, examination of peak instantaneous velocity and tracking of sinusoidal trajectory for each individual joint, and the tracking of different ramp trajectories for multiple joints simultaneously.

The tracking of the ramp trajectory for individual joint was successful for all 5 joints. The RMS error at steady state was under 0.33° for all 5 joints. As the minimum displacement for perception of movement by human is 1° [47], this level of accuracy is sufficient. There was, however, a delay in the kinematic response. This might result from the flexible shaft having to undergo an initial winding up before beginning to transmit movement. The static friction in the transmission would also cause some delay and this effect could be reduced by adding friction compensation in the control loop.

The tracking of trajectories with high instantaneous velocity was also tested. The maximum velocities observed were 450°/s, 550°/s, 650°/s, 520°/s and 900°/s from J1 to J5, respectively. These joint velocities together will be sufficient to produce the angular velocity at the thumb-tip at the level of 1000°/s, which meets our design requirement. Moreover, in the next experiment, the ATX was able to track sinusoidal trajectories with angular frequency of 4π (2 Hz) for J1, J3, J4 and J5, and 3π (1.5 Hz) for J2. These two experiments demonstrate the high speed and response capacity of the ATX.

The tracking of different ramp trajectories for multiple joints showed some impressive results. In the trial of controlling all F/E joints, all active F/E joints were able to track the desired trajectories while no motion was observed at the passive Ab/Ad joints. On the other hand, in the trial of controlling all Ab/Ad joints, all active Ab/Ad joints were able to track the desired trajectories while no motion was observed at the passive F/E joints of

MCP and IP. Although the CMC F/E joint showed 8° degree of flexion, it is reasonable as this joint took the overall load of the ATX. This motion could be minimized by actively control the CMC F/E joint. These results indicate the F/E and the Ab/Ad motion of the ATX is independent and minimal off-axis force/torque is produced in the flexible shaft transmission. In the next trial, all 5 joints were controlled to track different ramp trajectories. The results show that the ATX can produce independent position control at each joint simultaneously.

The kinetic performance of the ATX was also examined in our experiments. All 5 joints were able to produce the desired torque accurately. The torque capacity tested at CMC F/E joint showed that the ATX was able to produce 2.5 Nm torque. However, due to the helixing observed in the experiment, the maximum torque transmitted by the current flexible shaft should not exceed 2 Nm to avoid excessive off-axis force caused by the helixing. In this case, the torque capacity of this joint is 20% lower than our goal of torque capacity. But the 2.0 Nm torque capacity is still much more than those reported by other devices. Moreover, as the CMC F/E joint is the first joint and is supported by the external platform, we can choose a thicker flexible shaft with higher torque rating to provide the 2.5 Nm torque.

From the experimental results and analysis, we believe that the current design comes close to our design requirements and is able to provide controllable independent actuation to each thumb joint with high speed and torque capacities. These capabilities, which exceed those of other current exoskeletons in power, speed, and actuated DOF, will permit careful evaluation of the motor control of stroke survivors and of different rehabilitation strategies. For example, the high achievable speeds will permit assessment

of spasticity [48] and isokinetic strength and power. The large torque capabilities and individual actuation of each DOF will be able to overcome the coactivation in the affected thumb and permit evaluation of peak strength.

Conclusion and Future Work

This work presents the design and performance testing of an actuated thumb exoskeleton (ATX) that permits independent bi-directional actuation in each of the 5 DOF of the thumb using a mechanism that has 5 active DOF and 3 passive DOF. The transmission system using flexible shaft is able to transmit considerable joint torques to the user while still allowing backdrivability. Independent control of each thumb joint and the ability to provide sufficient torque to overcome the excessive coactivation and increased stiffness in the affected thumb are important criteria in designing a general platform to implement thumb rehabilitation therapies and motor learning paradigms. Experiments of closed-loop position and torque control were conducted and the results showed that both the position and torque control performance was satisfying.

In the future work, we will implement different rehabilitation strategies on the ATX, e.g., low-impedance, force perturbation, passive, active and assist-as-needed strategies. A high-level supervisory controller will be developed to coordinate these rehabilitation strategies. Further, the ATX will be coupled with an actuated finger exoskeleton (AFX) [49] that we have developed for the index finger to implement rehabilitation strategies in restoring control of pinch movements following stroke.

References

[1] American Heart Association: Heart and Stroke Statistical Update, http://www.Americanheart.org/statistics/stroke.htm, 2009.

[2] R. Bonita, Steward, A, Beaglehole, R, "International trends in stroke mortality: 1970-1985," Stroke, vol. 21, pp. 989-992, 1990.

[3] J. P. Broderick, S. J. Phillips, J. P. Whisnant, W. M. O'Fallon, and E. J. Bergstralh, "Incidence rates of stroke in the eighties: the end of the decline in stroke?," Stroke, vol. 20, pp. 577-582, 1989.

[4] C. S. Gray, J. M. French, D. Bates, N. E. Cartlidge, 0. F. James, and G. Venables, "Motor recovery following acute stroke," Age Ageing, vol. 19, pp. 179-84, 1990.

[5] H. Nakayama, H. S. Jorgensen, H. 0. Raaschou, and T. S. Olsen, "Recovery of upper extremity function in stroke patients: The Copenhagen Stroke Study," Arch Phys Med Rehabilitation, vol. 75, pp. 394-398, 1994.

[6] V. M. Parker, D. T. Wade, and R. Langton Hewer, "Loss of arm function after stroke: measurement, frequency, and recovery." Int. Rehab Med, vol. 8, pp. 69-73, 1986.

[7] C. A. Trombly, "Stroke," in Occupational Therapy for Physical Dysfunction, Baltimore: Williams and Wilkins, 1989, pp. 454-471.

[8] D. Wade, "The epidemiologically based needs assessment reviews." Health Care Needs Assessment, Volume I, J. Raftery, Ed., 1994, pp. 111-255.

[9] S. L. Wolf, S. Blanton, H. Baer, J. Breshears, and A. J. Butler, "Repetitive task practice: a critical review of constraint-induced movement therapy in stroke," Neurologist, vol. 8, pp. 325-3 8, 2002.

[10] C. J. Winstein, D. K. Rose, S. M. Tan, R. Lewthwaite, H. C. Chui, and S. P. Azen, "A randomized controlled comparison of upper-extremity rehabilitation strategies in acute stroke: A pilot study of immediate and long-term outcomes," Arch Phys Med Rehab, vol. 85, pp. 620-8, 2004.

[11] S. J. Page, S. Sisto, P. Levine, and R. E. McGrath, "Efficacy of modified constraint-induced movement therapy in chronic stroke: a single-blinded randomized controlled trial," Arch Phys Med Rehab, vol. 85, pp. 14-8, 2004.

[12] T. A. Jones, C. J. Chu, L. A. Grande, and A. D. Gregory, "Motor skills training enhances lesion-induced structural plasticity in the motor cortex of adult rats," JNeurosci, vol. 19, pp. 10153-63, 1999.

[13] J. A. Kleim, T. A. Jones, and T. Schallert, "Motor enrichment and the induction of plasticity before or after brain injury," Neurochem Res, vol. 28, pp. 1757-69, 2003.

[14] T. A. Jones and T. Schallert, "Use-dependent growth of pyramidal neurons after neocortical damage," JNeurosci, vol. 14, pp. 2140-52, 1994.

[15] J. Liepert, H. Bauder, W. H. R. Miltner, E. Taub, and C. Weiller, "Treatment-induced cortical reorganization after stroke in humans," Stroke, vol. 31, pp. 1210-1216, 2000.

[16] J. Liepert, W. H. R. Miltner, H. Bauder, M. Sommer, C. Dettmers, E. Taub, and C. Weiller, "Motor cortex plasticity during constraint-induced movement therapy in stroke patients," Neurosci Letters, vol. 250, pp. 5-8, 1998.

[17] L. R. Macclellan, D. D. Bradham, J. Whitall, B. Volpe, P. D. Wilson, J. Ohlhoff, C. Meister, N. Hogan, H. I. Krebs, and C. T. Bever, Jr., "Robotic upper-limb neurorehabilitation in chronic stroke patients," J Rehabil Res Dev, vol. 42, pp. 717-22, 2005.

[18] M. Ferraro, J. J. Palazzolo, J. Krol, H. I. Krebs, N. Hogan, and B. T. Volpe, "Robot-aided sensorimotor arm training improves outcome in patients with chronic stroke," Neurology, vol. 61, pp.1604-7, 2003.

[19] D. J. Reinkensmeyer, L. E. Kahn, M. Averbuch, A. McKenna-Cole, B. D. Schmit, and W. Z. Rymer, "Understanding and treating arm movement impairment after chronic brain injury: progress with the ARM guide," J Rehabil Res Dev, vol. 37, pp. 653-62, 2000.

[20] P. S. Lum, C. G. Burgar, P. C. Shor, M. Majmundar, and M. Van der Loos, "Robot-assisted movement training compared with conventional therapy techniques for the rehabilitation of upperlimb motor function after stroke," Arch Phys Med Rehabil, vol. 83, pp. 952-9, 2002.

[21] Gupta, A., O'Malley, M. K., Patoglu, V. and Burgar, C., “Design, control and performance of RiceWrist: a force feedback wrist exoskeleton for rehabilitation and training” The International Journal of Robotics Research, 27, 233-251, 2008.

[22] B. T. Volpe, H. I. Krebs, N. Hogan, 0. L. Edelstein, C. Diels, and M. Aisen, "A novel approach to stroke rehabilitation: robotaided sensorimotor stimulation," Neurology, vol. 54, pp. 1938- 44, 2000.

[23] L. E. Kahn, M. L. Zygman, W. Z. Rymer, and D. J. Reinkensmeyer, "Effect of robot-assisted and unassisted exercise on functional reaching in chronic hemiparesis," presented at 23rd Annual IEEE Engineering in Medicine and Biology Conference, Istanbul, Turkey, 2001.

[24] J. L. Patton, M. E. Stoykov, M. Kovic, and F. A. Mussa-Ivaldi, "Evaluation of robotic training forces that either enhance or reduce error in chronic hemiparetic stroke survivors," Exp Brain Res, vol. 168, pp. 368-83, 2006.

[25] S. Hesse, C. Werner, M. Pohl, S. Rueckriem, J. Mehrholz, and M. L. Lingnau, "Computerized arm training improves the motor control of the severely affected

arm after stroke: a single-blinded randomized trial in two centers," Stroke, vol. 36, pp. 1960-6, 2005.

[26] Sergei V Adamovich, Gerard G Fluet, Abraham Mathai, Qinyin Qiu, Jeffrey Lewis and Alma S Merians, “Design of a complex virtual reality simulation to train finger motion for persons with hemiparesis: a proof of concept study”, Journal of NeuroEngineering and Rehabilitation 2009, 6:28.

[27] D. Jack, R. Boian, A. S. Merians, M. Tremaine, G. C. Burdea, S. V. Adamovich, M. Recce, and H. Poizner, "Virtual realityenhanced stroke rehabilitation," IEEE Trans Neural Syst Rehabil Eng, vol. 9, pp. 308-18, 2001.

[28] C. D. Takahashi, L. Der-Yeghiaian, V. Le, R. R. Motiwala, and S. C. Cramer, "Robot-based hand motor therapy after stroke," Brain, vol. 131, pp. 425-37, Feb 2008.

[29] L. Dovat, O. Lambercy, R. Gassert, T. Maeder, T. Milner, T. C. Leong, and E. Burdet, "HandCARE: a cable-actuated rehabilitation system to train hand function after stroke," IEEE Trans Neural Syst Rehabil Eng, vol. 16, pp. 582-91, Dec 2008.

[30] A. Wege and G. Hommel, "Development and control of a hand exoskeleton for rehabilitation of hand injuries," IEEE/RSJ International Conference on Intelligent Robots and Systems, Edmonton, Canada, 2005.

[31] I. Sarakoglou, N. G. Tsagarakis, and D. G. Caldwell, "Occupational and physical therapy using a hand exoskeleton based exerciser," presented at IEEE/RSJ International Conference on Intelligent Robots and Systems, Sendai, Japan, 2004.

[32] M. DiCicco, L. Lucas, and Y. Matsuoka, "Strategies for an EMG-controlled orthotic exoskeleton for the hand," IEEE International Conference on Robotics and Automation, New Orleans, USA, 2004.

[33] Kawasaki H, Ito S, Ishigure Y, Nishimoto Y, Aoki T, Mouri H, et al. “Development of a hand motion assist robot for rehabilitation therapy by patient self-motion control”. IEEE 10th Intl Conf Rehab Rob. Noordwijk, The Netherlands, 2007: 234-240.

[34] Giurintano DJ, Hollister AM, Buford WL, Thompson DE, Myers LM. “A virtual five-link model of the thumb”, Med Eng Phys 1995; 17: 297-303.

[35] Hollister AM, Buford WL, Myers LM, Giurintano DJ, Novick A. “The axes of rotation of the thumb carpometacarpal joint”, J Orthop Res 1992; 10: 454-460.

[36] Hollister A, Giurintano DJ, Buford WL, Myers LM, Novick A. “The axes of rotation of the thumb interphalangeal and metacarpophalangeal joints.”, Clin Orthop Relat Res. 1995 Nov;(320):188-93.

[37] Santos VJ, Valero-Cuevas FJ. “Reported anatomical variability naturally leads to multimodal distributions of Denavit-Hartenberg parameters for the human thumb”, IEEE Trans Biomed Eng 2006; 53: 155-63.

[38] D. G. Kamper and W. Z. Rymer, "Impairment of voluntary control of finger motion following stroke: role of inappropriate muscle coactivation," Muscle Nerve, vol. 24, pp. 673-81, May 2001.

[39] D. H. Saunders, et al., "Association of activity limitations and lower-limb explosive extensor power in ambulatory people with stroke," Arch Phys Med Rehabil, vol. 89, pp. 677-83, Apr 2008.

[40] W. P. Cooney, 3rd, M. J. Lucca, E. Y. Chao, and R. L. Linscheid, "The kinesiology of the thumb trapeziometacarpal joint," J Bone Joint Surg Am, 1981, vol. 63, pp. 1371-81.

[41] Buchholz B., Armstrong TJ., "A kinematic model of the human hand to evaluate its prehensile capabilities", J Biomech 1992 Feb; 25(2):149-62.

[42] J. A. Katarincic, "Thumb kinematics and their relevance to function," Hand Clin, 2001, vol. 17, pp. 169-74.

[43] Gutnik, B., Hudson, G., Ricacho, G., Skirius, J., "Power of Performance of the Thumb Adductor Muscles: Effect of Laterality and Gender", Medicina (Kaunas), 2006, 42(8), 654-656.

[44] Vikash Gupta, "Kinematic analysis of a thumb-exoskeleton system for post stroke rehabilitation", Thesis (M.S. in Mechanical Engineering), Vanderbilt University, Aug. 2010.

[45] Gowland C, Stratford P, Ward M, Moreland J, Torresin W, Van Hullenaar S, Sanford J, Barreca S, Vanspall B, Plews N. Measuring physical impairment and disability with the chedoke-mcmaster stroke assessment. Stroke. 1993;24:58-63

[46] xPC target, Mathworks, http://www.mathworks.com/help/toolbox/xpc/

[47] Gandevia, S.C., et al., Proprioceptive sensation at the terminal joint of the middle finger. J Physiol, 1983. 335: p. 507-17.

[48] D. G. Kamper and W. Z. Rymer, "Quantitative features of the stretch response of extrinsic finger muscles in hemiparetic stroke," Muscle Nerve, vol. 23, pp. 954-61, Jun 2000.

[49] C. Jones, F. Wang, et al, "Control and Kinematic Performance Analysis of an Actuated Finger Exoskeleton for Hand Rehabilitation Following Stroke", IEEE International Conference on Biomedical Robotics and Biomechatronics, Tokyo, Japan, 2010.

Appendix

Inverse Kinematics of the Artificial Thumb

The artificial thumb can be modeled as a 5 DOF manipulator connected by revolute joints. The D-H parameters of the artificial thumb is

i	α_{i-1} (Degree)	a_{i-1} (Inch)	θ_i	d_i
1	0	0	θ_1	0
2	90	0.55	θ_2	0
3	-90	2	θ_3	0
4	90	0.375	θ_4	0
5	-90	1.275	θ_5	0
6	0	1.25	0	0

Transformation Matrix

$$ {}^{i-1}_{i}T = \begin{bmatrix} \cos(\theta_i) & -\sin(\theta_i) & 0 & a_{i-1} \\ \sin(\theta_i)\cos(\alpha_{i-1}) & \cos(\theta_i)\cos(\alpha_{i-1}) & -\sin(\alpha_{i-1}) & -\sin(\alpha_{i-1})d \\ \sin(\theta_i)\sin(\alpha_{i-1}) & \cos(\theta_i)\sin(\alpha_{i-1}) & \cos(\alpha_{i-1}) & \cos(\alpha_{i-1})d \\ 0 & 0 & 0 & 0 \end{bmatrix} $$

$$ {}^{0}_{6}T = {}^{0}_{1}T\,{}^{1}_{2}T\,{}^{2}_{3}T\,{}^{3}_{4}T\,{}^{4}_{5}T\,{}^{5}_{6}T $$

The thumb-tip position is,

$$ \vec{P} = \begin{bmatrix} Px \\ Py \\ Pz \end{bmatrix} = {}^{0}_{6}T(1:3,4) = \vec{f}_{3\times1}(\vec{\theta}_i), \quad i = 1,2,3,4,5 \qquad \text{(a1)} $$

The inverse kinematics of the thumb model can be obtained by solving θ_i in Equation (a1). However, this equation is highly nonlinear and difficult to solve the analytical solutions. Instead, we solve inverse kinematics at the velocity level using the Jacobian matrix.

Differentiate Equation (a1) once, we get,

$$\vec{V} = \begin{bmatrix} \dot{P}x \\ \dot{P}y \\ \dot{P}z \end{bmatrix} = \begin{bmatrix} \frac{\partial Px}{\partial \vec{\theta}_i} \\ \frac{\partial Px}{\partial \vec{\theta}_i} \\ \frac{\partial Px}{\partial \vec{\theta}_i} \end{bmatrix} \frac{d\vec{\theta}_i}{dt} = J \cdot \dot{\vec{\theta}}, \tag{a2}$$

where,

$$J = \begin{bmatrix} \frac{\partial Px}{\partial \vec{\theta}_i} \\ \frac{\partial Px}{\partial \vec{\theta}_i} \\ \frac{\partial Px}{\partial \vec{\theta}_i} \end{bmatrix}_{3\times 5}$$ is the Jacobian matrix of the thumb model.

Thus, the velocity of each of the thumb joint is,

$$\dot{\vec{\theta}} == J^{-1} \cdot \vec{v} \tag{a3}$$

This is the inverse kinematics of the thumb model at velocity level. Note, the Jacobian matrix J is a non-square matrix, so J^{-1} in Euqation (a3) is the pseudoinverse of the Jacobian matrix.

Mapping of Joint Position between ATX and Thumb

In Section III, we present that the ATX and the thumb has a unique mapping in joint position. Now we will analyze the mapping of joint position of the ATX and the artificial thumb in detail.

The CMC F/E and Ab/Ad joints of the ATX are aligned with the corresponding joints of the thumb, so the joint positions of these two joints are the same for both the ATX and the thumb.

The IP joint has only 1 DOF of the F/E, so the motion of the ATX and the thumb is always in the same plane (Figure V-28). The mapping of IP joint angle between the ATX and the thumb can be solved by trigonometric equation. The joint angle of the thumb (alpha) versus the ATX (theta) is shown in Figure V-29. This curve matches well with the angle manually measured on the artificial thumb and the ATX. The RMS error of measured theta angles from the theta angles computed from the same alpha angles is only 0.192°.

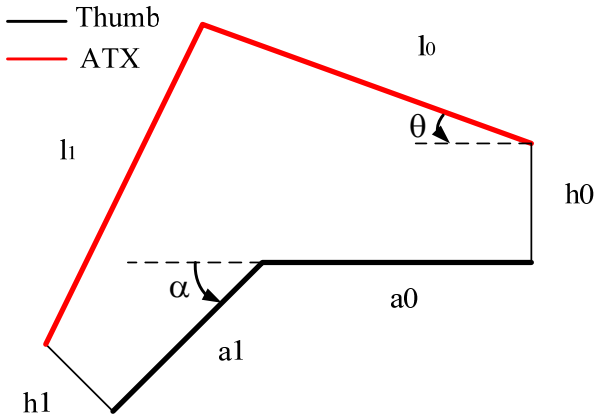

Figure V-28 Schematics of IP Joint Mapping

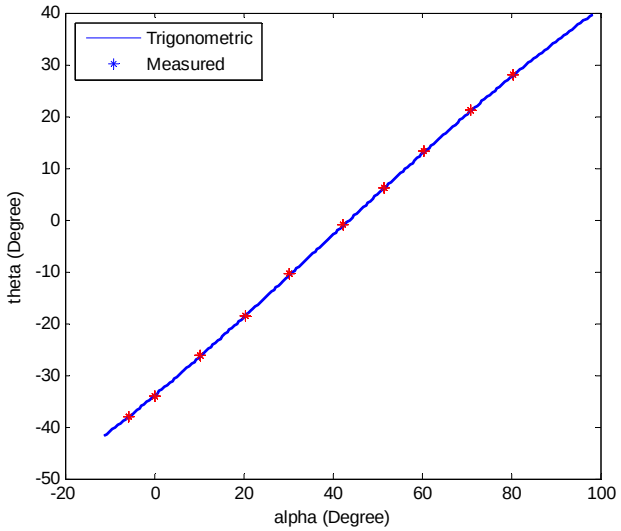

Figure V-29 Thumb versus ATX at IP F/E joint

The MCP joint of the artificial thumb has two 2 DOF, F/E and Ab/Ad, while the MCP joint of the ATX has 2 active DOF and 2 passive DOF. As the artificial thumb has no axial rotation, the passive joint for axial rotation of the ATX will have no motion, either. So the coupled system of the thumb and the ATX can be modeled as shown in Figure V-30.

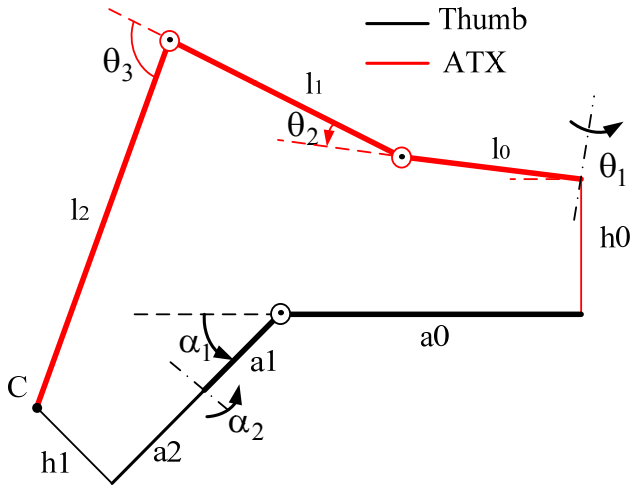

Figure V-30 Schematics of the MCP Joint Mapping. In this coupled system, h0 is considered part of the MCP of the ATX and h1 is considered part of the MCP of the artificial thumb.

The D-H parameters for the MCP joint of the artificial thumb is,

Table V-5 D-H Parameters for MCP joint of Artificial Thumb

i	α_{i-1} (Degree)	a_{i-1} (Inch)	θ_i	d_i
1	0	a_0	α_1	0
2	90	a1	α_2	0
3	-90	a2	90	0
4	0	h1	0	0

The transformation matrix for the MCP joint of the artificial thumb is,

$$T_{thumb} = {}^{1}_{0}T_t \cdot {}^{2}_{1}T_t \cdot {}^{3}_{2}T_t \cdot {}^{4}_{3}T_t \qquad \text{(a4)}$$

The D-H parameters for the MCP joint of the ATX from θ_1 is,

Table V-6 D-H Parameters for MCP joint of the ATX

i	α_{i-1} (Degree)	a_{i-1} (Inch)	θ_i	d_i
1	90	0	θ_1	0
2	-90	l_0	θ_2	0
3	0	l_1	θ_3	0
4	0	l_2	0	0

The transformation matrix for the MCP joint of the ATX is,

$$T_{ATX} = D_y(h_0) \cdot R_z(10°) \cdot {}^1_0T_x \cdot {}^2_1T_x \cdot {}^3_2T_x \cdot {}^4_3T_x \tag{a5}$$

The endpoint positions of both transformation matrices are identical as the two models are connected at C,

$$\begin{aligned} &\vec{P}_t = T_{thumb}(1:3,4); \quad \vec{P}_x = T_{ATX}(1:3,4) \\ &\vec{P}_t = \vec{P}_x \end{aligned} \tag{a6}$$

The mapping between α and θ needs to be solved at velocity level as the Equation (a6) is highly nonlinear. Differentiate (a6) once,

$$\begin{aligned} &\vec{v}_t = \vec{J}_t \cdot \dot{\vec{\alpha}}; \quad \vec{v}_x = \vec{J}_x \cdot \dot{\vec{\theta}}; \quad \vec{v}_t = \vec{v}_x \\ &\vec{J}_t \cdot \dot{\vec{\alpha}} = \vec{J}_x \cdot \dot{\vec{\theta}} \end{aligned} \tag{a7}$$

Thus, the mapping of angular velocities of the MCP Joint for the ATX and the artificial thumb is

$$\dot{\vec{\theta}} = \vec{J}_x^{-1} \cdot \vec{J}_t \cdot \dot{\vec{\alpha}} \tag{a8}$$

From the discussion above, the complete mapping of all joint positions is established between the ATX and the artificial thumb. For a given set of joint-space trajectories of

the artificial thumb and initial configuration of the artificial thumb and the ATX, the corresponding joint-space trajectories of the ATX will be obtained, and vice versa.

CHAPTER VI

CONTRIBUTIONS AND FUTURE WORK

Contributions

The research work presented in this dissertation focuses in the area of robot-assisted upper extremity rehabilitation following stroke. We have worked towards improving robot-assisted upper extremity rehabilitation in three different approaches: enhancement of existing robotic systems, implementation and evaluation of novel rehabilitation training strategies, and design and development of new robotic systems. The main contributions of this work are:

1) Design of a high-level supervisory controller for the existing rehabilitation robotic system to automatically adjust the rehabilitation therapy according to the user's verbal feedback. This high-level supervisory controller monitors the task execution and safety, and makes task adjustment according to the recognized verbal feedback from the user during the task execution to impart effective therapy an automated manner. This enhancement allows the user-robot direct interaction, and reduces the intervention and workload of the therapists.

2) Evaluation of the impact of the integrated training method of assist-as-needed and visual error augmentation in upper limb rehabilitation. A new training strategy is proposed which integrates the assist-as-needed and visual error augmentation strategies. This new strategy is implemented in the existing robotic system. A crossover study with 20 subjects is designed to assess the impact of the integrated training method of these two

strategies on robot-assisted upper limb rehabilitation. Statistical analysis of the experimental results has demonstrated the proposed integrated training strategy has the potential to improve the efficacy of the robot-assisted upper limb rehabilitation.

3) Control of an actuated finger exoskeleton (AFX). The real-time control system is developed for the AFX with position and torque control. The position and force controller is PI controller with friction compensation and feedforward compensation. A planner is designed to distribute the control command to the appropriate motor in the motor pair. Experimental results show the AFX has independent actuation of each joint with full range of finger motion, high backdrivability, high speed and torque capacities that will facilitate the scientific research of finger rehabilitation and motor control of stroke survivors.

4) Design and development of an actuated thumb exoskeleton (ATX). An ATX that has 5 active degree-of-freedoms (DOF) and 3 passive DOF is designed to provide independent actuation for each DOF of the human thumb. Sensory, actuation and control systems are developed to permit real-time control. The ATX is tested in experiments and the performance comes close to all the design goals. The ability to provide independent actuation of each DOF of the thumb with high torque and speed capacity will allow the ATX to serve as a test bed to facilitate the thumb rehabilitation and motor control study.

Future Work

The future work remains focused on improving the robot-assisted rehabilitation. Building on the results in this dissertation, there are many exciting research directions that will promote this research area and benefit the stroke population as follows:

1) Implementation and evaluation of various rehabilitation strategies and motor control paradigms for the hand with the AFX and ATX. The capabilities of the AFX and ATX permit the implementation of various rehabilitation strategies and motor control paradigms. Systematically experiments on human subjects will demonstrate the differences in efficacy of these strategies in improving hand rehabilitation, thus help therapist find the more efficient way to conduct rehabilitation.

2) Coordinated control of the AFX and ATX. With both the AFX and ATX being controlled separately, the next step is to coordinately control these two devices to conduct practical hand tasks, e.g., pinching and rolling tasks. A high-level supervisory controller will be needed to coordinate the two separate devices and generate reference task for both devices.

3) Design of a full hand exoskeleton for all four fingers and the thumb. The human hand has 21 DOF in total, namely, 4 DOF for each finger and 5 DOF for the thumb. A full hand exoskeleton will be able to provide rehabilitation therapies to each digits of the hand and retrain the full hand function of the stroke survivors. This exoskeleton can also facilitate research in sensorimotor control, especially as it relates to integration of proprioception. This kinesthetic sense is fundamental to control of movement, and could be further incorporated into user control of assistive technology, such as robotic or prosthetic hands or neuromuscular stimulation systems.